Copyright
by
Sonia Hernandez
2014

The Dissertation Committee for Sonia Hernandez
certifies that this is the approved version of the following dissertation:

Low-Thrust Trajectory Design Techniques with a Focus on Maintaining Constant Energy

Committee:

Maruthi Akella, Supervisor

Ryan P. Russell

Glenn Lightsey

Behcet Acikmese

Jacob Englander

Low-Thrust Trajectory Design Techniques with a Focus on Maintaining Constant Energy

by

Sonia Hernandez, B.S.AS.E; M.S.

DISSERTATION

Presented to the Faculty of the Graduate School of

The University of Texas at Austin

in Partial Fulfillment

of the Requirements

for the Degree of

DOCTOR OF PHILOSOPHY

THE UNIVERSITY OF TEXAS AT AUSTIN

August 2014

To my father,

who gave me the desire to know everything about the universe.

"Caminante, son tus huellas
el camino y nada más;
Caminante, no hay camino,
se hace camino al andar.
Al andar se hace el camino,
y al volver la vista atrás
se ve la senda que nunca
se ha de volver a pisar.
Caminante no hay camino
sino estelas en la mar."

Antonio Machado

Acknowledgments

As Dr. Seuss said it, "How did it get so late so soon? It's night before it's afternoon. December is here before it's June. My goodness how the time has flewn. How did it get so late so soon?" I have spent the last five years in Austin, and it almost seems like it was yesterday that I walking through the hallways of WRW for the first time. I have lived many experiences here, good ones and not so good ones; but from all of them I have learned and will cherish all of them.

First of all, I would like to thank my advisor, Dr. Maruthi Akella. Our time working together has been short, but I have greatly enjoyed the two and a half years working with him. I admire his way of mathematically working through any problem at hand. Everybody has a different ideal for an advisor, and Dr. Akella has definitely fit my ideal. I enjoy sitting down with him and working through the problems together with pen and paper. I also like the fact that he knows how to give me the space when necessary for me to do my work. I have learned a lot from him and I am very pleased with the problems we have solved for my dissertation together.

Besides my advisor, I have been privileged to have several mentors throughout the Ph.D. process. Dr. Cesar Ocampo, who is an incredibly brilliant person, was a big part of my early graduate school career at UT. Celestial

Mechanics was my favorite and most challenging class that I ever took. He also taught me most of my trajectory design and optimization techniques I know and use now. It was thanks to Brent Barbee's encouragement and passion for astrodynamics that I initially moved to UT Austin to pursue a Ph.D. He has given me the chance to work with him on many exciting projects, such as Near-Earth asteroid missions, and it is thanks to him that I had the chance to spend several summers at NASA Goddard. All my mentors have shaped me into a strong researcher, and mission designer; which has helped start of my career in my ideal place, JPL, where I will be moving next.

I am so thankful to have such an amazing family. I am grateful to my mother, who is an amazing loving person and is always supportive of every decision I make. My father, who has instilled in me his love for the academic career. Without him I would not be at the brinks of becoming a doctor. And my sister, who always knows how to bring a smile to my face.

Lastly, I am incredibly thankful to all my friends here. They have been my family and support in Austin, and have made the last few years a fun and exciting roller coaster. I mention here some of the ones I am most thankful to

Ricardo my research partner, tennis partner, and a lot of other experiences in Austin

Walter my favorite musician

Hana mi mejor amiga de ricitos para nuestras aventuras

Zrinka my coffee shop partner

Michele the best yogi partner

Bonnie who was there when I needed her the most

Petar my favorite two-step dancing partner

Low-Thrust Trajectory Design Techniques with a Focus on Maintaining Constant Energy

Publication No. _____

Sonia Hernandez, Ph.D.
The University of Texas at Austin, 2014

Supervisor: Maruthi Akella

Analytical solutions to complex trajectory design problems are scarce, since only a few specific cases allow for closed-form solutions. The main purpose of this dissertation is to design simple algorithms for trajectory design using continuous thrust, with a focus on low-thrust applications. By "simple" here we seek to achieve algorithms that either admit an analytical solution, or require minimal input by the user and minimal computation time. The three main contributions of this dissertation are: designing Lyapunov-based closed-loop guidance laws for orbit transfers, finding semi-analytical solutions using a constant magnitude thrust, and perturbation theory for approximate solutions to low-thrust problems. The technical aspect that these problems share in common is that they all use, fully or partially, a thrusting model in which the energy of the system is kept constant. Many orbit transfer problems are shown to be solved with this thrusting protocol.

Table of Contents

Acknowledgments **v**

Abstract **vii**

List of Tables **xii**

List of Figures **xiii**

Chapter 1. Introduction **1**

1.1 Problem Motivation 1

1.1.1 Lyapunov-Based Guidance (Chapters 2 and 3) 2

1.1.2 Perturbation Theory for a Low-Thrust Model (Chapter 4) 5

1.1.3 Analytical Solution for Constant Acceleration Thrust (Chapter 5) 6

1.2 Dynamical Model 8

1.2.1 Regularized Perturbed Two-Body Model 8

1.3 Contributions 11

1.4 Outline 13

Chapter 2. Lyapunov-Based Guidance for Planar Orbit Transfers in Levi-Civita Coordinates **15**

2.1 Levi-Civita Equations of Motion 18

2.1.1 Unperturbed Equations of Motion 22

2.1.2 Finite Thrust Maneuvers 23

2.2 Matching Semi-Major Axis 24

2.2.1 Upper-Bound on Total Transfer Time 27

2.2.2 Example 29

2.3 Orbit Transfer Problem 31

2.3.1 Elliptical to Circular Orbit Transfer 31

2.3.2 Elliptical to Elliptical Orbit Transfer 39
2.4 Final Remarks 43

Chapter 3. Lyapunov-Based Guidance for Orbit Transfers in KS Variables 47
3.1 KS Equations of Motion 49
3.1.1 Unperturbed Equations of Motion 53
3.1.2 Defining the Thrust Vector **F** 53
3.2 Convergence on Energy: Targeting Semi-Major Axis 55
3.2.1 Planar Low-thrust Circle-to-Circle Transfer 58
3.3 In-Plane Transfers by Holding Energy Constant 59
3.3.1 Targeting Circular Orbits ($e^* = 0$) 61
3.3.2 Targeting Eccentric Orbits ($0 \leq e^* < 1$) 66
3.4 Out-of-Plane Transfers by Holding Energy Constant 69
3.4.1 Transfer to a Circular Equatorial Orbit of Specified Radius 70
3.4.2 Targeting Angular Momentum Vector 78
3.4.3 Targeting Angular Momentum and Eccentricity Vectors 83
3.5 Final Remarks 87

Chapter 4. Perturbation Theory in Levi-Civita Coordinates with Constant Energy 92
4.1 Governing Differential Equation 94
4.2 Taylor Expansion About Acceleration Magnitude 98
4.2.1 Solving for the Expansion Coefficients 102
4.3 Analytical Solution for Initial Circular Orbits 104
4.3.1 Example: Spacecraft Initial Location on Positive x-Axis 105
4.4 Final Remarks 110

Chapter 5. Energy Conserved Planar Spacecraft Motion with Constant Thrust Acceleration 114
5.1 Introduction 114
5.2 Equations of Motion 117
5.2.1 Equations of Motion in Cartesian Coordinates 118
5.2.2 Equations of Motion in a Body-Fixed Frame 120

5.3 Trajectory Solution Starting From a Circular Orbit 124
5.3.1 Example Trajectories 125
5.3.2 Semi-Analytical Solution to the Dynamical System . . . 128
5.3.3 Orbital Elements as a Function of Position Magnitude . 131
5.4 Comparison with the Radial Thrust Problem 136
5.5 Periodic Motion 140
5.6 Final Remarks 146

Chapter 6. Dissertation Summary **150**
6.1 Future Work 154

Appendices **155**

Appendix A. Nonlinear Control (Chapters 2 and 3) **156**
A.1 Stability of Autonomous Systems 158

Appendix B. Analytical Expression for the Switching Functions (Chapter 2) **163**
B.1 Switching Function S_1 for Circular Orbit Transfers 163
B.2 Switching Function S_2 for General Orbit Transfers 164

Appendix C. Guidance Scheme in Cartesian Coordinates (Chapter 3) **166**

Appendix D. Technical Obstacles with Lyapunov-Based Guidance for Rendezvous **170**
D.1 Rendezvous Using Cartesian Coordinates 170
D.2 Rendezvous Design in Fictitious Time Using KS Variables: Equivalent to an Orbit Transfer 172
D.3 Rendezvous Design in Real Time Using KS Variables 175

Appendix E. Perturbation Theory (Chapter 4) **179**

Appendix F. Time-Varying Coefficients (Chapter 4) **183**
F.1 Coefficients of the example in Section 4.3.1 183
F.2 Coefficients for any initial condition on the circle 185

References **188**

Vita **198**

List of Tables

2.1 Initial and final orbital parameters for the example in Figure 2.3 38
2.2 Initial and final orbital parameters for the example in Figure 2.4 43

3.1 Initial and final orbital parameters for the example in Figure 3.1 59
3.2 Comparison of a low-thrust solution orbit transfer, where the results are shown in Figure 3.1. 61
3.3 Initial and final orbital parameters for examples in Section 3.3 67
3.4 Final mass and transfer time for example in Figure 3.3 67
3.5 Propellant used and flight time for the example in Figure 3.6 . 77
3.6 Initial and final orbital parameters for the examples in Section 3.4 77
3.7 Summary of guidance schemes 90

5.1 Periodic bounded orbit conditions when firing in for $n_{min} \leq n \leq 24$. 145
5.2 Initial conditions for periodic orbits in Fig. 5.10 146

C.1 Summary of guidance schemes in normal cartesian coordinates 169

List of Figures

1.1 Motivation example for regularized two-body model. 9
1.2 Story of Alice in Wonderland. 10

2.1 Relation between x-y and u_1-u_2 coordinates. 19
2.2 Semi-major axis matching using control (2.23), where $DU = a^* = 10,000$ km and $MU = 1,000$ kg. 30
2.3 Eccentricity matching using control (2.23) and the switching scheme (2.33–2.34) with initial and final conditions in Table 2.1. 37
2.4 Orbit transfer using control (2.23) and the switching scheme (2.44–2.45) with parameters in Table 2.2. 46

3.1 Comparison of algorithm using control (3.22) with Edelbaum's analytical low-thrust optimal solution, where the initial conditions are given in Table 3.1. 60
3.2 Schematic of the switching function S_e, defined in Eq. (3.30). . 66
3.3 Semi-major axis and eccentricity matching with parameters in Table 3.3. 68
3.4 Comparison of integration time between using KS model and "normal" (cartesian) model, using parameters in Table 3.3. . . 70
3.5 Representation of the vector $\mathbf{q}_i$ and its components. 74
3.6 Orbit transfer to a circular equatorial orbit with initial parameters in Table 3.6 76
3.7 Orbit transfer to a circular equatorial orbit with initial parameters in Table 3.6. 79
3.8 Orbit transfer to a circular equatorial orbit with initial parameters in Table 3.6. 80
3.9 Semi-major axis and angular momentum matching around Ceres ($\mu = 63.1$ km^3/s^2), with parameters in Table 3.6. 84
3.10 Full orbit transfer with initial parameters in Table 3.6. 88
3.11 Full orbit transfer with initial parameters in Table 3.6. 89

4.1 Initial conditions of a spacecraft on a circular orbit, with initial conditions in Eq. (4.43). 106
4.2 Comparison of "True" solution and "Analytical" solution with an acceleration magnitude $\varepsilon = 0.642$, when firing inwards ((a),(c),(e)) and firing outwards ((b),(d),(f)). 111
4.3 Comparison of "True" solution and "Analytical" solution with an acceleration magnitude $\varepsilon = 0.193$. 112
4.4 Comparison of "True" solution and "Analytical" solution with an acceleration magnitude $\varepsilon = 1.285$. 113

5.1 Spacecraft motion with vel-normal thrust. 119
5.2 Spacecraft motion in inertial and body-fixed frame. 120
5.3 Trajectory solution integrated firing in, to a perigee distance $r_p = 0.1$ for four revolutions, using $a_T = 1.5878$. 126
5.4 Trajectory solution integrated firing out, to an apogee distance $r_a = 1.9$ for four revolutions, using $a_T = 0.2160$. 127
5.5 Perigee/Apogee radius reached versus acceleration magnitude a_T when starting in an initial circular orbit of radius $r = 1$. . 129
5.6 Symmetry properties of angular displacement and period of an orbit after one revolution. 132
5.7 Eccentricity, its time-derivative and second time-derivative for two different examples. 135
5.8 Comparison between vel-normal thrust and radial thrust when firing inwards. 138
5.9 Comparison between vel-normal thrust and radial thrust when firing outwards. 139
5.10 Periodic orbits for different a_T values, and n revolutions. . . . 148
5.11 Poincare surface of sections corresponding to different a_T values for firing inwards (blue) and outwards (red). 149

A.1 Example of the stability of an autonomous system. 159

F.1 ε^0 analytical results for any initial location. 186
F.2 ε^1 analytical results for any initial location. 186
F.3 ε^2 analytical results for any initial location. 187

Chapter 1

Introduction

1.1 Problem Motivation

The problem of trajectory design involves complex dynamical systems and has been studied for centuries. Many efforts have been made to provide analytical solutions, but very few have actually been found. The main purpose of this dissertation is to design simple algorithms for trajectory design using continuous thrust, with a focus on low-thrust applications. By "simple" here we seek to achieve algorithms that either a) admit an analytical solution, or b) require minimal input by the user and minimal computation time.

With this aim in mind, several problems have been addressed. Each problem studied led to new ideas and new problems to solve (as generally happens with basic research problems). Therefore, this dissertation is a combination, in chronological order, of the problems that motivated its author toward finding simple closed-form solutions to different trajectory design problems. The three main focus areas are: designing Lyapunov-based guidance laws, finding semi-analytical solutions using a constant magnitude thrust, and perturbation theory for approximate solutions to low-thrust problems. The feature that these problems have in common is that they all use (fully or partially)

a thrusting model in which the energy of the system remains constant. Many orbit transfer problems are shown to be solved with this thrusting protocol.

1.1.1 Lyapunov-Based Guidance (Chapters 2 and 3)

Historically, the problem of computing finite thrust orbit transfers and rendezvous has been studied extensively in the literature [12, 15, 18, 35, 36, 42–44, 51, 54, 56, 66]. Much work has concentrated on optimal transfers using both direct and indirect methods [22, 30, 41, 63, 67]. Low-thrust orbit transfers have been a topic of research interest for many decades, and have achieved increasing attention with the recent success of several missions. For example *SMART-1* used Hall ion thrusters to transfer from GTO to lunar orbit in 2003 [50]. Also, *Dawn* has successfully used ion thrusters to explore the asteroid Vesta, and is currently on its way to the dwarf planet Ceres [21]. Some of the earliest work regarding many-revolution orbit transfers was performed in Ref. [15], with an optimal analytical solution for circle-to-circle low-thrust transfers. Since then, most of the work has concentrated on optimal transfers using both direct and indirect methods [22, 52, 58, 67]. More recently, adding evolutionary algorithms has increased the ability to converge to optimal solutions [17]. The drawback to many of these types of methods is that they often do not result in a closed-form solution, they are computationally expensive, and convergence can be challenging without a good initial guess.

To ease the burden of the computation time, a heuristic approach is used to achieve orbit transfers where closed-loop feedback control laws are

designed based on candidate Lyapunov functions. These controllers not only require significantly lower computation time, but, because they only require knowledge of the current state of the spacecraft, they permit easy onboard (closed-loop) implementation. Previous work on this topic has mostly used singular perturbation theory in conjunction with Lagrange's variational equations to establish suitable guidance laws [14, 29, 32, 40, 47, 55]. These methods have the drawback of becoming singular when either the eccentricity or inclination are zero and proof of convergence is only available in very limited settings [40]. A closed-loop solution for full orbit transfers based on targeting the angular momentum and eccentricity vectors is given in [14], with a detailed convergence proof. However, this method does not allow for targeting a subset of orbital elements. A detailed summary of the different Lyapunov-based guidance laws that exist to date is found in Ref. [23].

Even though there are drawbacks to the current guidance schemes designed, it is worth noting the Q-law [37, 47], which is an extensive algorithm to perform any general orbit transfer for low-thrust applications. In this work, the Lyapunov functions are created based on expressions for the maximum rate of change of the orbital elements. The guidance scheme is designed so as to provide the steepest descent to the target orbit, by allowing for time-varying gains based on the desired orbital elements. Even though any heuristic approach will most likely not be equal to an optimal solution, this algorithm allows for close to optimal results. However, one of the main drawbacks is that the algorithm becomes singular at zero eccentricity or inclination, and proof

of convergence is not shown (mainly due to the complexity in the time-varying gains).

In Chapters 2 and 3 of this dissertation, Lyapunov theory is used to design guidance laws for closed orbit transfers; however, the results presented are quite novel since singularities are avoided, a subset of desired orbital elements can be targeted, and full proof of convergence is shown. Chapter 2 deals with planar orbit transfers and Chapter 3 allows for out-of-plane transfers. Designing these algorithms involves formulating a candidate Lyapunov function (i.e., quadratic function) that is always monotonic (i.e., non-increasing), and minimum at our desired final state. A rudimentary background on Lyapunov-based control theory is given in Appendix A. The orbit transfer design is performed in two steps by using a constant thrust engine. The first step involves converging the spacecraft orbit to the desired semi-major axis (or equivalently, the desired energy), by using a Lyapunov analysis that gives rise to an asymptotically stabilizing control law. Once the energy has been met, to within any pre-specified tolerance bound, the second step involves converging the remaining subset of desired orbital elements (by holding energy constant). Rigorous proof is given to show that any orbital element can be targeted by holding energy constant, albeit non-optimally, which is one of the major contributions to the dissertation.

Another interesting application of the proposed Lyapunov-based design approach, not included in this dissertation, but is worth noting is Ref. [61, 62]. A novel decentralized cooperative control protocol is designed for the

convergence of an autonomous spacecraft swarm to a common circular orbit using finite thrust. In these publications, guidance and consensus algorithms are designed and implemented in a decentralized fashion to drive agents to an orbit of prescribed semi-major axis and zero eccentricity, with the plane of orbital motion determined through consensus. The thrust limited guidance and consensus schemes are designed separately and then readily combined to obtain asymptotic stability of the overall closed-loop system. Through rigorous convergence analysis, it is shown that the multi-agent system arrives on a common orbit with the desired eccentricity and semi-major axis when the communication topology is given by a connected and undirected tree or ring graph. Numerical simulation studies are presented for a spacecraft formation around Earth, as well as for a formation with planet Ceres as the primary body to highlight all the novel aspects of this work.

1.1.2 Perturbation Theory for a Low-Thrust Model (Chapter 4)

Because nonlinear differential equations tend to be fairly complex, exact analytical solutions are often not possible to find. In general, numerical methods are necessary to solve the differential equations, as is the case of most optimization schemes and closed-loop control algorithms (as the ones derived in Chapters 2 and 3). For this reason, we explore what are known as *asymptotic methods* to find approximate analytical solutions, which involve a Taylor series expansion.

In Chapter 2, a guidance scheme is designed to match any desired orbit

in the plane, by first matching the desired energy, and then matching the remaining orbital elements. An upper bound for the transfer time to reach the desired energy of the orbit is derived. However, no estimate is given on how long the remaining part of the transfer takes. One of the motivating elements behind Chapter 4 is to provide approximate analytical solutions (to within an order of magnitude) of the transfer schemes designed in previous chapters, to provide an estimate of the entire transfer time. This perturbation work involves performing a Taylor series expansion about the acceleration magnitude, which is assumed to be constant and of small magnitude, consistent with low-thrust applications.

1.1.3 Analytical Solution for Constant Acceleration Thrust (Chapter 5)

The problem of continuous thrusting in the two-body problem has been studied in many different ways for a vast number of spacecraft applications. Only in a few specific situations does this problem have an analytical solution. For example, some of the earliest work was done by Tsien studying circumferential thrust to solve the problem of escaping from an initial circular orbit [65]. The classical problem of spacecraft motion subject to a constant radial thrust has been extensively investigated and allows for analytical solutions [2, 3, 5, 8, 49]. The problem of tangential thrust acceleration also allows for some partial analytical solutions [9, 48], as well as an exponential sinusoid approximation for many revolution transfers and interplanetary trajectories [47]. Therefore, the problem of thrusting radially (in the position

direction), circumferentially (perpendicular to the position), and tangentially (in the velocity direction) have been studied fairly extensively. The problem that has not yet been explored sufficiently is thrusting in the direction perpendicular to the velocity, which is the focus of Chapter 5.

Chapter 5 is related to the work performed in the previous chapters in that all the thrusting protocols are designed by thrusting perpendicular to the velocity. The reason for this is that, when thrusting perpendicular to the velocity, there is one integral of motion in the system, since the energy of the system is conserved. This is because the energy is only changed by a perturbation acceleration along the velocity direction. The fact that there is one integral of motion is reminiscent of the constant radial thrust problem, in which the angular momentum of the system is conversed rather than the energy. In the radial thrust acceleration problem there is one additional integral of motion, and therefore, the problem is fully solved analytically [2]. However, a full analytical solution is not possible in the problem of thrusting normal to the velocity, since there is only one integral of motion. Several techniques are studied to find semi-analytical solutions to this dynamical system.

Before diving in to a detailed explanation of the contributions to this dissertation, a brief explanation of the dynamical model used throughout the dissertation follows.

1.2 Dynamical Model

All of the work in this dissertation uses a perturbed two-body model, in which a spacecraft, assumed to be massless, is under the influence of a spherical mass of constant mass distribution, with gravitational parameter μ. The perturbation comes from a spacecraft that is thrusting, with a (variable) acceleration magnitude a_T. Denoting the position of the spacecraft with respect to the gravitating body as $\mathbf{r}$ and its two-norm as r, its acceleration is given by

$$\ddot{\mathbf{r}} = -\frac{\mu}{r^3}\mathbf{r} + a_T\hat{\mathbf{u}} \tag{1.1}$$

where $\hat{\mathbf{u}}$ is a unit vector in the direction of the thrust.

Eq. (1.1) is used literally as-is in the work of Chapter 5. However, a transformed perturbed two-body model is used in Chapters 2, 3, and 4. Some background about the motivation to use this model is outlined below.

1.2.1 Regularized Perturbed Two-Body Model

Originally, the regularization problem was developed in celestial mechanics for collision avoidance-type problems [1, 7, 34, 38]. A collision between two bodies occurs when the distance between them approaches zero, which corresponds to a singularity in Eq. (1.1). The goal was to transform the singular differential equations into regular ones, such that the model would still be numerically well defined even as $r \to 0$ (see Figure 1.1). Since the regular equations were developed, they have been mostly used to deal with close encounter-type problems, but has been relatively underexplored for orbit

transfer problems [64]. One of the main goals for this dissertation is to investigate whether there are advantages to using a regularized perturbed model, rather than the usual equations of motion in Eq. (1.1), for trajectory design problems.

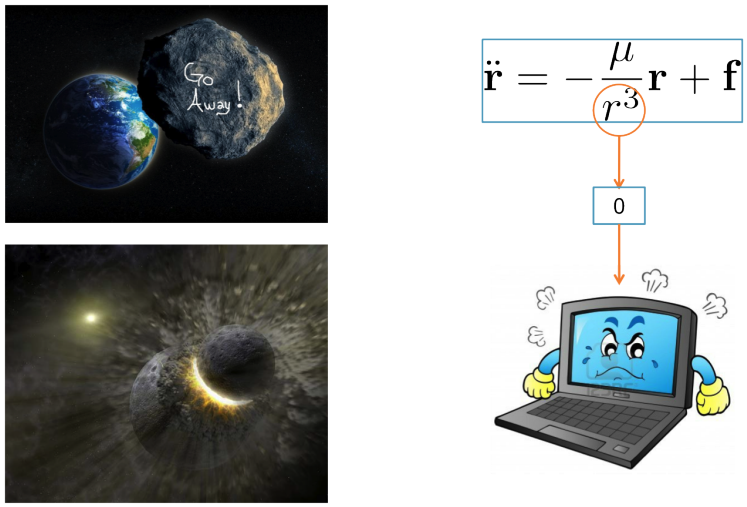

Figure 1.1: Motivation example for regularized two-body model.

The standard technique of regularization theory involves three main steps:

1. Change of coordinates.
2. Time transformation, in order to avoid an infinite velocity at the singularity.
3. Use of conservation of energy, to transform the singular equations of motion into the regularized equations.

An interesting article [13], which gives a basic introduction of regulation theory, compares the three steps to obtain the regular equations of motion to the story by L. Carrol "Alice's adventures in wonderland". I will use this great analogy explained by Celletti. The change of coordinates is analogous to when Alice begins her dream by falling in through the hole, and steps into a new world (see Figure 1.2(1)). The introduction of a new time variable happens when the white rabbit appears in the story claiming that he is running out of time (Figure 1.2(2)). Finally, Alice undergoes changes in her size during the story, from becoming very tiny to becoming a giant (Figure 1.2(3)). However, she ends up awakening back to her normal size, the same way that the regular equations of motion are able to preserve the form of the original two-body model.

Figure 1.2: Story of Alice in Wonderland.

The regularized equations of motion in the plane are known as the Levi-Civita model [7], and in three-dimensions as the Kustaanheimo-Stiefel model [34]. The full derivation of these equations is outlined at the beginning of Chapter 2 (in the plane) and the beginning of Chapter 3 (for out-of-plane

motion).

1.3 Contributions

The three topics outlined in Section 1.1 are divided into four chapters in the dissertation.

Chapter 2 considers planar orbit transfers around a central body using Lyapunov stability theory. The model used is the Levi-Civita transformation of the planar two-body problem. One of the advantages of working in these transformed coordinates is that the solution to the unperturbed equations of motion is that of a simple harmonic oscillator, where the frequency of oscillation is a function of a, the semi-major axis of the orbit. Therefore, during any coast phase, the analytical solution is explicitly characterized. A closed-loop guidance scheme is designed for orbit transfers from any initial elliptical orbit to any final elliptical orbit utilizing a spacecraft with thrust-coast capabilities. The proposed Lyapunov functions give rise to asymptotically stabilizing control laws. The control scheme is performed in two phases: first, a matching of the semi-major axis of the target orbit; and second, a matching of the eccentricity and argument of periapsis by holding energy constant. The algorithms designed are robust to initial and final conditions, as well as to perturbations; they are also computationally fast and can be used for both low- and high-thrust problems.

The results in Chapter 2 are extended to three-dimensional orbit transfers in Chapter 3. The design is performed in the Kustaanheimo-Stiefel (KS)

model, which is the three-dimensional equivalent of the Levi-Civita model. The KS model aids in the design of the guidance schemes, but the new guidance solutions can be explicitly characterized in the regular two-body model. The control scheme covers two main phases: first, a matching of the semi-major axis of the target orbit; and second, a matching of the remaining desired orbital elements by holding energy constant. No constraint is imposed on the magnitude of the thrust; however, an emphasis is placed on low-thrust examples, since they compare well with results from optimal control.

Using the second part of the guidance scheme derived in Chapter 2 (in which energy is held constant), and assuming a constant magnitude acceleration, a Taylor series expansion is performed about the acceleration magnitude in Chapter 4. This is performed using the Levi-Civita equations of motion in order to find an analytical solution to the equations of motion for small accelerations. It is found that an analytical solution only exists when the spacecraft is initially in a circular orbit, and in fact provides a reasonably accurate approximation of the solution. Any other closed orbit (with some eccentricity) involves equations that, up to now, we have not been able to solve.

The fact that in Chapter 4 an approximate analytical solution is found for initial conditions beginning on a circular orbit, when thrusting continuously and in a direction such that the energy remains constant, led to study this problem even further. In Chapter 5, planar two-body orbital motion of spacecraft under the action of constant thrust acceleration in the direction perpendicular to the velocity is studied. It is shown that thrusting in this

manner maintains constant energy of the orbit. A spacecraft starting in an initial circular orbit will obtain a minimum (perigee) radius along an *inbound* trajectory. If the thrust is maintained, the spacecraft returns to the initial circular orbit in an outbound trajectory. A maximum (apogee) radius is obtained when starting in a circular orbit along an *outbound* trajectory, after which the vehicle will return again to the initial circular orbit. A full analytical solution to this problem does not exist; however, an analytical solution to the flight direction angle, that is, the angle between the position and velocity vectors, is found. This new solution leads to several important insights on the problem, such as obtaining analytical expressions on a valid range of acceleration magnitudes for bounded motion, as well as proving periodicity of the position magnitude in time. Periodic orbits are also found in this system for different values of acceleration, and their stability is studied.

1.4 Outline

The dissertation is organized as follows. In Chapter 2, we design Lyapunov-based guidance laws for any planar orbit transfer using the regularized Levi-Civita model. The control algorithms are extended to three-dimensional orbit transfers in Chapter 3 using the KS model. Using the planar model and guidance scheme from Chapter 2, perturbation theory about the acceleration magnitude is performed in Chapter 4 to find an analytical solution to any initial circular orbit. Orbital motion of spacecraft under the action of constant thrust acceleration in the direction perpendicular to the velocity is

studied in Chapter 5. Concluding remarks are presented in Chapter 6.

Chapter 2

Lyapunov-Based Guidance for Planar Orbit Transfers in Levi-Civita Coordinates

[1] Most trajectory design problems for orbit transfers and rendezvous involve solving optimal transfers using both direct and indirect methods [22, 30, 41, 42, 51, 67]. These solutions are computationally expensive and do not often result in closed-form solutions. Heuristic models have been used in the past to achieve orbit transfers where feedback control laws are designed based on candidate Lyapunov functions [14, 29, 47, 55]. These methods use mostly Lagrange's variational equations to establish suitable guidance laws. Similar methods to rendezvous a spacecraft with a target have been studied as well [39, 68]. In this chapter, advantage of Lyapunov theory is used to design guidance laws for closed orbit transfers. The resulting new controllers require significantly lower computation time to permit easy onboard implementation.

We take on a new approach to the problem of finite-thrust orbit transfers by working in a transformed model to design Lyapunov-based control laws. The model we use is the classical Levi-Civita regularization transformation of

[1]The work presented in this chapter has been published in Ref. [25]: S. Hernandez and M. R. Akella. Lyapunov-based guidance for orbit transfers and rendezvous in levi-civita coordinates. AIAA Journal of Guidance, Control, and Dynamics, 37(4):1170-1181, 2014, doi:10.2514/1.62305. M. R. Akella is the supervisor.

the planar two-body problem [1, 5, 38]. The main idea behind regularization is to transform both the position coordinates and time coordinates to a new model. One of the main advantages of working in these transformed coordinates is that the solution to the unperturbed equations of motion is that of a simple linear harmonic oscillator, where the frequency of oscillation is a function of a, the semi-major axis of the orbit. Therefore, during any coast phase, the analytical solution is explicitly characterized by a linear combination of sines and cosines. Additionally, this model is advantageous for propagating highly eccentric orbits [6]. This is due to the time transformation, where an orbit segmented into equal time steps becomes segmented equally in position by using this model. Since small time steps present an issue when propagating Keplerian orbits, this transformation is useful to provide better resolution near periapsis.

The major contribution of this chapter is to perform arbitrary planar orbit transfers among closed orbits. This requires matching three desired parameters: semi-major axis a^*, eccentricity e^*, and argument of periapsis ω^*. The idea is to design the control laws by using Lypaunov stability theory. This involves forming a candidate Lyapunov function (i.e., quadratic function) that is always monotonic (i.e., non-increasing), and minimum at our desired final state. Note that while the guidance schemes are designed in the transformed regularized coordinates, the results can be explicitly characterized in the original coordinates; the transformation procedure merely acts as an enabler for the design. The algorithms designed are robust to any initial and final con-

ditions, computationally fast, and can be used for both low- and high-thrust problems.

A closed-loop guidance scheme is designed for a coplanar orbit transfer from any initial closed orbit (with semi-major axis a_0, eccentricity $0 \leq e_0 < 1$, and argument of periapsis ω_0), to any final closed orbit with a specified a^*, $0 \leq e^* < 1$, and ω^*, utilizing a spacecraft with thrust-coast capabilities. The convergence to the desired orbit is performed in two steps. The first step involves converging the spacecraft orbit to the desired semi-major axis a^* by continuously thrusting, even though the eccentricity and orientation at this stage may not be the desired ones, by using a Lyapunov analysis that gives rise to an asymptotically stabilizing control law. Once a^* has been reached to within a specified tolerance, the second step of the algorithm involves matching the desired eccentricity and argument of periapsis (while always maintaining the specified target a^*), using exactly the same control law as before, but with an added on/off switching mechanism for coasting during certain intervals. A special case of the transfer problem is also addressed, in which we desire to transfer to a circular orbit ($e^* = 0$). In this case, only two orbital parameters are required to be matched, since the argument of periapsis is undefined for a circular orbit.

The chapter is organized as follows. Section 2.1 begins by deriving the Levi-Civita equations of motion of a spacecraft which is allowed to thrust in a two-body force model. The next section deals with designing a guidance scheme to target only one orbital parameter: the semi-major axis a^*. This

serves as a motivating example to solve the orbit transfer problem. We are able to show in Section 2.3 that by allowing the spacecraft to have thrust-coast capabilities, we can perform any planar closed-orbit transfer problem. Several examples are shown for all the problems discussed. The last section summarizes the chapter and discusses future work.

2.1 Levi-Civita Equations of Motion

The transformation into a regularized model begins by looking at the planar perturbed two-body model. The equations of motion are

$$\ddot{\mathbf{r}} = -\frac{\mu}{r^3}\mathbf{r} + \mathbf{f} \iff \begin{bmatrix} \ddot{x} \\ \ddot{y} \end{bmatrix} = -\frac{\mu}{r^3}\begin{bmatrix} x \\ y \end{bmatrix} + \begin{bmatrix} f_1 \\ f_2 \end{bmatrix} \tag{2.1}$$

The vector $\mathbf{r} = [x,\ y]^T$ has magnitude $r = \sqrt{x^2 + y^2}$, and $\mathbf{f} = [f_1,\ f_2]^T \in \mathbb{R}^2$.

As was stated in the Introduction, the main idea behind regularization is to transform both the position coordinates and time coordinates to a new model [1, 7, 57]. There are three steps to convert Eq. (2.1) into the regularized model, following the notation in Ref. [1].

1. *Change of position coordinates (Levi-Civita coordinates):*

   The following transformation is introduced,

   $$\begin{aligned} x &= u_1^2 - u_2^2 \\ y &= 2u_1u_2 \end{aligned} \iff \begin{aligned} u_1 &= \sqrt{r}\cos(\theta/2) \\ u_2 &= \sqrt{r}\sin(\theta/2) \end{aligned} \tag{2.2}$$

   where the transformed position vector is $\mathbf{u} = [u_1\ u_2]^T$. The visual relationship between $\mathbf{r}$ and $\mathbf{u}$ is shown in Figure 2.1. Note,

   $$r^2 = x^2 + y^2 \iff r = \mathbf{u}\cdot\mathbf{u} = u_1^2 + u_2^2 \tag{2.3}$$

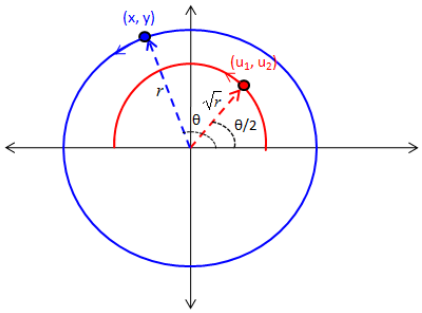

Figure 2.1: Relation between x-y and u_1-u_2 coordinates.

The transformation from $\mathbf{u}$ to $\mathbf{r}$ can be expressed in terms of the following linear operator

$$\mathbf{r} = \mathcal{L}(\mathbf{u})\mathbf{u} = \begin{bmatrix} u_1 & -u_2 \\ u_2 & u_1 \end{bmatrix} \begin{bmatrix} u_1 \\ u_2 \end{bmatrix} \tag{2.4}$$

The linear operator $\mathcal{L}(\mathbf{u})$ has the following properties [57]:

P1. $\mathcal{L}^T(\mathbf{u})\mathcal{L}(\mathbf{u}) = r\mathbf{I}$, where $\mathbf{I}$ is the identity matrix

P2. $\mathcal{L}'(\mathbf{u}) = \mathcal{L}(\mathbf{u}')$, where $'$ denotes the time derivative

P3. $\mathcal{L}(\mathbf{u})\mathbf{v} = \mathcal{L}(\mathbf{v})\mathbf{u}$

P4. $(\mathbf{u}\cdot\mathbf{u})\mathcal{L}(\mathbf{v})\mathbf{v} - 2(\mathbf{u}\cdot\mathbf{v})\mathcal{L}(\mathbf{u})\mathbf{v} + (\mathbf{v}\cdot\mathbf{v})\mathcal{L}(\mathbf{u})\mathbf{u} = \mathbf{0}$

2. *Introduce a fictitious time, by means of a velocity transformation:*

The second step in the derivation involves performing a Sundman transformation [59]

$$\dot{\mathbf{r}} = \frac{1}{r}\mathbf{r}' \iff \frac{d\mathbf{r}}{dt} = \frac{1}{r}\frac{d\mathbf{r}}{d\tau}$$

Note, that $\dot{(\,)} = \frac{d}{dt}(\,)$, denotes the time derivative in $\mathbf{r}$ coordinates, whereas $(\,)' = \frac{d}{d\tau}(\,)$ is the time derivative in $\mathbf{u}$ coordinates.

$$\frac{d}{dt} = \frac{1}{r}\frac{d}{d\tau} \tag{2.5}$$

$$\frac{d^2}{dt^2} = \frac{1}{r^2}\frac{d^2}{d\tau^2} - \frac{r'}{r^3}\frac{d}{d\tau} \tag{2.6}$$

Using properties 2 and 3 of the linear operator $\mathcal{L}(\mathbf{u})$, the first and second order derivative of $\mathbf{r}$ in terms of $\mathbf{u}$ coordinates are

$$\mathbf{r}' = \frac{d}{d\tau}\mathbf{r} = \frac{d}{d\tau}\left[\mathcal{L}(\mathbf{u})\mathbf{u}\right] = 2\mathcal{L}(\mathbf{u})\mathbf{u}' \tag{2.7}$$

$$\mathbf{r}'' = \frac{d}{d\tau}\mathbf{r}' = 2\mathcal{L}(\mathbf{u}')\mathbf{u}' + 2\mathcal{L}(\mathbf{u})\mathbf{u}'' \tag{2.8}$$

Using Eq. (2.6), the second time derivative of $\mathbf{r}$ can be written as

$$\ddot{\mathbf{r}} = \frac{1}{r^2}\mathbf{r}'' - \frac{r'}{r^3}\mathbf{r}'$$

which, when compared to Eq. (2.1), and solved for $\mathbf{r}''$ gives

$$\mathbf{r}'' = \frac{1}{r}\left[r'\mathbf{r}' - \mu\mathbf{r} + r^3\mathbf{f}\right] \tag{2.9}$$

Using the fact that $r = \mathbf{u}\cdot\mathbf{u}$, its time derivative is $r' = 2\mathbf{u}\cdot\mathbf{u}'$. Equating Eq. (2.8) and Eq. (2.9), and using Eq. (2.4) and Eq. (2.7),

$$2\mathcal{L}(\mathbf{u}')\mathbf{u}' + 2\mathcal{L}(\mathbf{u})\mathbf{u}'' = \frac{r'}{r}2\mathcal{L}(\mathbf{u})\mathbf{u}' - \frac{\mu}{r}\mathcal{L}(\mathbf{u})\mathbf{u} + r^2\mathbf{f}$$

Rearranging, and using property P4 of the linear operator $\mathcal{L}(\mathbf{u})$,

$$\mathbf{u}'' + \frac{\mu/2 - \mathbf{u}'\cdot\mathbf{u}'}{\mathbf{u}\cdot\mathbf{u}}\mathbf{u} = \frac{1}{2}(\mathbf{u}\cdot\mathbf{u})\mathcal{L}^T(\mathbf{u})\mathbf{f} \tag{2.10}$$

3. *Use the energy equation:*

   The third and final step in the transformation involves using the conservation of energy principle. Before, note that $\dot{\mathbf{r}} = \mathbf{r}'/r = 2\mathcal{L}(\mathbf{u})\mathbf{u}'/r$, and therefore, the norm of the velocity squared is

$$v^2 = \dot{\mathbf{r}}^T\dot{\mathbf{r}} = \frac{4}{r}\mathbf{u}' \cdot \mathbf{u}' \tag{2.11}$$

   where we have made use of property P1 of the linear operator. The energy of the two-body problem

$$E = \frac{v^2}{2} - \frac{\mu}{r} = \frac{1}{r}\left(2\mathbf{u}' \cdot \mathbf{u}' - \mu\right) \tag{2.12}$$

   which allows to simplify Eq. (2.10) such that the Levi-Civita equations of motion are obtained:

$$\mathbf{u}'' = \frac{E}{2}\mathbf{u} + \mathbf{f}_u \tag{2.13}$$

   where the perturbing acceleration in Levi-Civita coordinates

$$\mathbf{f}_u = \frac{1}{2}r\mathcal{L}^T(\mathbf{u})\mathbf{f} \tag{2.14}$$

   The energy E varies with time according to

$$E' = \frac{4}{r}\mathbf{u}' \cdot \mathbf{f}_u = 2\mathbf{u}' \cdot \mathcal{L}^T(\mathbf{u})\mathbf{f} \tag{2.15}$$

Lemma 2.1.1. *The quadratic potential*

$$C(\tau) = -\frac{E}{4}\left(\mathbf{u} \cdot \mathbf{u}\right) + \left(\mathbf{u}' \cdot \mathbf{u}'\right) = \frac{\mu}{2} \tag{2.16}$$

is an integral of motion of the perturbed equations of motion in (2.13) and (2.15).

Proof. Taking the time derivative of $C(\tau)$, and using Eq. (2.13) and Eq. (2.15), it is readily seen that $C'(\tau) = 0$, regardless of the value of the perturbing acceleration $\mathbf{f}$; and in fact $C(\tau) = C(\tau_0) = \mu/2 \; \forall \; \tau \geq \tau_0$. □

2.1.1 Unperturbed Equations of Motion

In the case when there is no perturbing acceleration acting on the spacecraft, that is, $\mathbf{f} = \mathbf{0}$, the equations of motion in Eq. (2.13) become de-coupled linear harmonic oscillators of the form

$$\mathbf{u}'' = -\mathcal{W}^2\mathbf{u} \tag{2.17}$$

where the frequency of oscillation is $\mathcal{W} = \sqrt{-E/2}$. Since, in this case, we are dealing with closed orbits, $E < 0$, and $E' = 0$ from Eq. (2.15). The analytical solution is therefore known and given by

$$\begin{aligned} u_1(\tau) &= u_{1_0}\cos(\mathcal{W}\tau) + \frac{u'_{1_0}}{\mathcal{W}}\sin(\mathcal{W}\tau) = A_{u_1}\cos(\mathcal{W}\tau + \Phi_{u_1}) \\ u_2(\tau) &= u_{2_0}\cos(\mathcal{W}\tau) + \frac{u'_{2_0}}{\mathcal{W}}\sin(\mathcal{W}\tau) = A_{u_2}\cos(\mathcal{W}\tau + \Phi_{u_2}) \end{aligned} \tag{2.18}$$

where

$$\begin{aligned} A_{u_1} &= \sqrt{u_{1_0}^2 + \left(u'_{1_0}/\mathcal{W}\right)^2} \text{ and } \Phi_{u_1} = \tan^{-1}\left(\frac{u'_{1_0}}{u_{1_0}\mathcal{W}}\right) \\ A_{u_2} &= \sqrt{u_{2_0}^2 + \left(u'_{2_0}/\mathcal{W}\right)^2} \text{ and } \Phi_{u_2} = \tan^{-1}\left(\frac{u'_{2_0}}{u_{2_0}\mathcal{W}}\right) \end{aligned}$$

and u_{1_0}, u_{2_0}, u'_{1_0}, and u'_{2_0} are the initial conditions at τ_0. Note, that in the case when the orbit is unbounded, that is $E \geq 0$, the analytical solution is also known, and its solution has an exponential form, with its exponents given by

the roots of its characteristic equation. Also note that the analytical solution is known in τ, and in order to obtain time t, an integration still needs to be performed.

2.1.2 Finite Thrust Maneuvers

Suppose that the perturbation now comes from a finite thrust engine, with constant thrust magnitude T, specific impulse I_{sp}, exhaust velocity $c = gI_{sp}$, and variable thrust angle ϕ (measured counter-clockwise from the positive x-axis), such that

$$\mathbf{f} = A \begin{bmatrix} \cos\phi \\ \sin\phi \end{bmatrix}$$

The acceleration magnitude $A = T/m$ and m is the mass of the spacecraft at any point in time, which varies according to $\dot{m} = -T/c$. In the Levi-Civita coordinates, this corresponds to

$$\mathbf{f}_u = \frac{Ar^{3/2}}{2} \begin{bmatrix} \cos(\phi - \theta/2) \\ \sin(\phi - \theta/2) \end{bmatrix} \tag{2.19}$$

For implementation purposes it is convenient to introduce a new parameter

$$\alpha = \frac{1}{a} \tag{2.20}$$

where a is the semi-major axis of the orbit. The parameter α is related to the energy E of an orbit through the relation $E = -\mu/(2a) = -(\mu/2)\alpha$ and its derivative $\alpha' = -(2/\mu)E'$. Combining this into Eq. (2.13) and (2.15) results in the new equations of motion

$$
\begin{aligned}
\mathbf{u}'' &= -\frac{\mu\alpha}{4}\begin{bmatrix} u_1 \\ u_2 \end{bmatrix} + \frac{Ar^{3/2}}{2}\begin{bmatrix} \cos(\phi - \theta/2) \\ \sin(\phi - \theta/2) \end{bmatrix} \\
\alpha' &= -\frac{4A}{\mu} r^{1/2}\sqrt{u_1'^2 + u_2'^2}\sin(\phi + \lambda - \theta/2) \\
m' &= -r\frac{T}{c} \\
t' &= u_1^2 + u_2^2
\end{aligned}
\tag{2.21}
$$

where the following has been defined

$$
\sin\lambda = \frac{u_1'}{\sqrt{u_1'^2 + u_2'^2}} \quad \text{and} \quad \cos\lambda = \frac{u_2'}{\sqrt{u_1'^2 + u_2'^2}}
$$

Note that the last equation in Eq. (2.21) is necessary in order to obtain the actual time t, since the integration is in transformed time τ.

2.2 Matching Semi-Major Axis

As a first step to performing orbit transfers, we will start with a motivating example. Suppose for now that we are interested in matching the semi-major axis of a target orbit, but do not take into account any other orbital elements. Let the semi-major axis of the target orbit be denoted as a^*, and therefore, its inverse is $\alpha^* = 1/a^*$. At any point in time (in τ coordinates) the spacecraft, whose motion is governed by Eq. (2.21), has a semi-major axis $a(\tau)$, and correspondingly $\alpha(\tau) = 1/a(\tau)$. The difference between the current $\alpha(\tau)$ and the target α^* is denoted by $e_\alpha = \alpha - \alpha^*$.

The quadratic candidate Lyapunov-like function

$$
V = \frac{1}{2}e_\alpha^2 \tag{2.22}
$$

is minimized when the semi-major axis of the spacecraft matches that of the desired orbit. The time-derivative of V (with respect to the τ variable) along solutions of (2.21) is given by

$$\begin{aligned} V' &= e_\alpha e'_\alpha = (\alpha - \alpha^*)\alpha' \\ &= -(\alpha - \alpha^*)\frac{4A\sqrt{r}\sqrt{u_1'^2 + u_2'^2}}{\mu}\sin(\phi + \lambda - \theta/2) \end{aligned}$$

Choosing

$$\phi = -\lambda + \theta/2 + \sin^{-1}(Ke_\alpha), \quad K = 1/|e_{\alpha_0}| > 0 \tag{2.23}$$

where $e_{\alpha_0} = e_\alpha(\tau_0)$, results in

$$V' = -\frac{4A\sqrt{r\left(u_1'^2 + u_2'^2\right)}}{\mu}Ke_\alpha^2 \leq 0 \tag{2.24}$$

which ensures that V is non-increasing.

Proposition 2.2.1. *Let a spacecraft with a constant available maximum thrust T and initial mass m_0 be on a closed orbit with initial semi-major axis $a(\tau_0) = a_0$. All solutions governed by the force model (2.21) with control (2.23) and $A = T/m$ converge to any prescribed final semi-major axis a^*.*

Proof. Due to the commanded thrust protocol for driving $\alpha(\tau)$ to some prescribed final value α^* (by Eq. (2.23)), $\alpha(\tau)$ becomes an exponential function of $e_\alpha(s)$, since

$$e'_\alpha = \alpha' = -K_1 A f(\mathbf{u}, \mathbf{u}')e_\alpha$$

where $K_1 = (4K)/\mu > 0$ and $f(\mathbf{u}(\tau), \mathbf{u}'(\tau)) = \sqrt{(u_1^2 + u_2^2)(u_1'^2 + u_2'^2)}$. We are guaranteed that $K_1 > 0$ and $A(\tau) = T/m(\tau) > 0$ (as long as $m(\tau) > 0$,

otherwise $A = 0$ by turning the thrusters off). Therefore, to show that we always converge to the desired α^*, it is necessary to show that $f(\mathbf{u}, \mathbf{u}')$ cannot become zero, and if it does, it cannot stay at zero indefinitely.

The signal $\alpha(\tau)$ is monotonic due to the control chosen in Eq. (2.23), i.e., $\alpha(\tau)$ is non-decreasing for the case $\alpha^* > \alpha_0$ and $\alpha(\tau)$ is non-increasing for the case $\alpha^* < \alpha_0$. Therefore, we are guaranteed that there exists some α_{min} and α_{max} such that $0 < \alpha_{min} \leq \alpha(\tau) \leq \alpha_{max}\ \forall\ \tau \geq \tau_0$. Specifically, $\alpha_{min} \doteq \min[\alpha(\tau_0), \alpha^*]$ and $\alpha_{max} \doteq \max[\alpha(\tau_0), \alpha^*]$.

The integral of motion $C(\tau) = C(\tau_0) \neq 0\ \forall\ \tau \geq \tau_0$ in Eq. (2.16) and, since it is a quadratic function of $\mathbf{u}$ and $\mathbf{u}'$, we can guarantee that both $r = (u_1^2 + u_2^2)$ and $(u_1'^2 + u_2'^2)$ cannot both simultaneously be at zero at the same time, which implies that they cannot perpetually stay at zero. Therefore, $f(\mathbf{u}, \mathbf{u}')$ cannot remain at zero, which means that there exits finite constants $\tau^* > 0$ and $\delta > 0$ such that $\int_{\tau}^{\tau+\tau^*} f[\mathbf{u}(\sigma), \mathbf{u}'(\sigma)]d\sigma \geq \delta\ \forall\ \tau \geq \tau_0$. We can then conclude that $e_\alpha(\tau) = e_\alpha(\tau_0)\exp^{-K_1 \int_{\tau_0}^{\tau} A(\sigma) f(\mathbf{u},\mathbf{u}')d\sigma} \rightarrow 0$ exponentially. □

It is interesting to note that we can lower-bound $f(\mathbf{u}, \mathbf{u}')$, by rewriting it as $f(\mathbf{u}, \mathbf{u}') = (rv)/2$. The angular momentum of an orbit $h = rv\cos\gamma$, where γ is the flight path angle, is an integral of motion of any unperturbed orbit. For a circular orbit, $\gamma = 0^o$ for the entire orbit, so $h = rv$, therefore, $f(\mathbf{u}, \mathbf{u}') = h/2$ for a circular orbit. For any elliptical orbit, $0 < \sin\gamma \leq 1$, and therefore, f is lower-bounded by $f(\mathbf{u}, \mathbf{u}') \geq h/2$, which again guarantees exponential convergence of $e_\alpha(\tau)$.

Because the guidance scheme is designed to match α^*, the thrust vector is always pointing in the velocity direction, until the desired value is reached. At this point, the thrust vector becomes perpendicular to the velocity, so that α does not vary (this comes as a consequence that by thrusting perpendicular to the velocity, the energy of the system does not vary, and is explained in detail in the following chapters).

Because we are guaranteed that $0 < \alpha_{min} \leq \alpha(\tau) \leq \alpha_{max}$, the eccentricity of the orbit $e(\tau) < 1 \ \forall \ \tau \geq \tau_0$, so the orbit during the transfer will always remain bounded. However, for implementation purposes, especially for high thrust problems, the eccentricity might get very close to the critical value of making the orbit unbounded, before the desired semi-major axis has been reached. This issue is dealt with in detail in Section 2.3 by ensuring that the eccentricity stays below a certain tolerance at all times.

In Subsection 2.2.1 an upper bound on the time taken by the system to achieve a prescribed error tolerance on the semi-major axis is derived. This is done to give the user a maximum possible transfer time. Subsection 2.2.2 follows, by a showing the results of the algorithm to reach a desired semi-major axis.

2.2.1 Upper-Bound on Total Transfer Time

An upper bound on the total propagation time τ_f to arrive at a prescribed semi-major axis error tolerance ϵ_α is outlined here. We achieve the desired tolerance when $e_\alpha(\tau_f) = \alpha(\tau_f) - \alpha^* = \epsilon_\alpha$. The procedure involves

analytically integrating the time-derivative of e_α and solving for time.

Since the control variable in Eq. (2.23) makes the time-derivative e'_α a direct function of e_α, by integrating e'_α, its solution over time is given by

$$e_\alpha(\tau) \;=\; e_\alpha(\tau_0)\,\exp\left[-K_1\int_{\tau_0}^{\tau} A(\sigma) f[\mathbf{u}(\sigma),\mathbf{u}'(\sigma)]d\sigma\right] \tag{2.25}$$

In order to integrate Eq. (2.25) and obtain an upper-bound on τ_f, and upper-bound on $A(\tau)$ and $f[\mathbf{u}(\tau),\mathbf{u}'(\tau)]$ needs to be established.

First, the position can be bounded by $r_{min} \leq r(\tau) \leq r_{max}$. The upper-bound is found by solving for the minimum perigee radius possible, $r_{min} = (1/\alpha_{max})(1 - e_{max})$. Recall $E = -(\mu/2)\alpha$, so the integral of motion in Eq. (2.16) is also written as

$$C(\tau) = \frac{\mu}{2} = \frac{\mu}{8}\alpha\left(u_1^2 + u_2^2\right) + \left(u_1'^2 + u_2'^2\right) \geq \frac{\mu}{8}\alpha_{min} r(\tau)\;\forall\;\tau \geq \tau_0$$

Therefore, the upper-bound on $r(\tau)$ is $r_{max} = 4/\alpha_{min}$. From the energy equation in (2.12) it can be established that $v \geq \sqrt{(2\mu)/r}$. Therefore, the function $f(\mathbf{u},\mathbf{u}')$ is upper-bounded by $f(\mathbf{u},\mathbf{u}') = \frac{1}{2}rv \geq \sqrt{(r\mu)/2} \geq \sqrt{(r_{min}\mu)/2}$ and the parameter $A(\tau) = T/m(\tau) \geq T/m_0\;\forall\;\tau \geq \tau_0$. With these two bounds and given a desired converged tolerance for α^*, $|e_\alpha(\tau_f)| = \epsilon_\alpha$, Eq. (2.25) can be integrated to find

$$\tau_f \leq \tau_0 + \frac{m_0}{KT}\sqrt{\frac{2}{r_{min}\mu}}\,[\;\ln[e_\alpha(\tau_0)] - \ln(\epsilon_\alpha)\;] \tag{2.26}$$

In fact, an even tighter bound can be found on τ_f by noting that the mass

varies according to $m' = -(T/c)r$. By integrating,

$$\begin{aligned} m(\tau) &= m_0 - \frac{T}{c}\int_{\tau_0}^{\tau} r(\sigma)d\sigma \\ &\leq m_0 - \frac{T}{c} r_{min}(\tau - \tau_0) \end{aligned}$$

Using this fact to integrate e'_α in Eq. (2.25) yields

$$\tau_f \leq \frac{1}{K_2}\left[\exp\left(\frac{K_1}{K_2}[\ln[e_\alpha(\tau_0)] - \ln(\epsilon_\alpha)]\right) - m_0\right] \tag{2.27}$$

where $K_1 = TK\sqrt{(\mu r_{min})/2}$ and $K_2 = -(T/c)r_{min}$. This is a powerful result since it ensures that the transfer time will never take longer than the result in Eq. (2.27); this in spite of the fact that our analysis is predominantly asymptotic in nature.

A similar approach can be taken to find a lower bound on the total fuel mass $m(\tau_f)$ by integrating m' with a bound on $r(\tau) \leq r_{max}$; but due to the extreme conservatism inherent with this bounding process, the utility of this estimate is not immediately obvious.

2.2.2 Example

An example trajectory under the gravitational pull of Earth ($\mu = 398,600$ km^3/s^2) using the control in Eq. (2.23), $T = 200$ N, and $I_{sp} = 400$ s is shown in Figure 2.2. A desired final semi-major axis $a^* = 10,000$ km is targeted from an initial circular orbit with $a_0 = 7,000$ km. The integration of Eq. (2.21) is performed in dimensionless units, in order to avoid build-up numerical errors caused by $e_\alpha = \alpha - \alpha^*$, which can be a very small number when working in units of km. The dimensionless units are distance unit

$DU = a^* = 10,000$ km, mass unit $MU = m_0 = 1,000$ kg, and time unit TU, chosen such that $\mu = 1\ DU^3/TU^2$. The trajectory in x, y coordinates is shown in Figure 2.2(a), which has been transformed using Eq. (2.4) from the u_1, u_2 results of the integration. The total transfer time is 4.36 hours, and a bound was found of 7.23 hours using Eq. (2.27). Note that the semi-major axis is met to within 1 km precision, which corresponds to $\epsilon_\alpha = 10^{-4}$, but the final eccentricity reaches a value of $e_f = 0.307$. This leads to the next section, which deals on how to target any desired orbit.

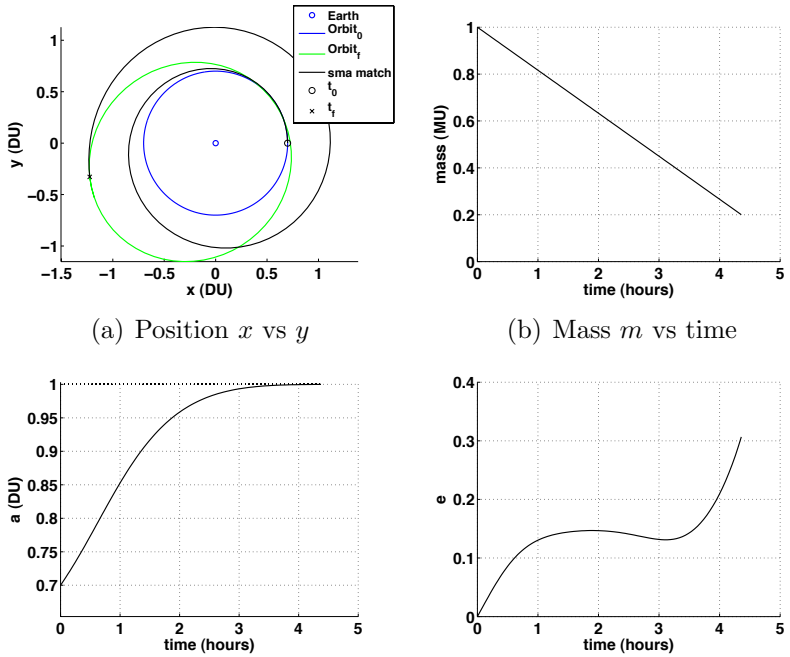

(a) Position x vs y

(b) Mass m vs time

(c) Semi-major axis a vs time

(d) Eccentricity e vs time

Figure 2.2: Semi-major axis matching using control (2.23), where $DU = a^* = 10,000$ km and $MU = 1,000$ kg.

2.3 Orbit Transfer Problem

As a motivation example, Section 2.2 dealt with a simple problem, in which a desired semi-major axis was the only parameter targeted. We now deal with a more complex and realistic problem, in which the goal is to perform an orbit transfer to any bounded orbit. We begin Section 2.3.1 by outlining the theory to perform an orbit transfer to any desired circular orbit and continue in Section 2.3.2 by explaining the general orbit transfer to any elliptical orbit, with any relative orientation. For both cases, the algorithm is performed in two-steps: first, a matching of the desired semi-major axis a^* by a constant thrust, followed by a matching of the remaining desired orbital elements, by means of a thrust/coast protocol. The beauty of the full designed algorithm is that the control law is exactly the same for both steps. However, one of the reasons for matching the semi-major axis first, is because when the transformation to the Levi-Civita model is performed, a very nice and compact dynamical equation for the time-evolution of α' is obtained, which facilitates enormously the derivation of the guidance law (see Section 2.2).

2.3.1 Elliptical to Circular Orbit Transfer

An orbit transfer to any circular orbit requires matching two orbital parameters: semi-major axis and eccentricity. The process of matching the semi-major axis has been explained in the previous section. In order to target a specified eccentricity $e^* = 0$ from any initial orbit with $0 \leq e_0 < 1$, the first step is to express the eccentricity in the Levi-Civita coordinates.

The angular momentum vector expressed in the direction $\hat{\mathbf{k}}$ normal to the orbit plane is $\mathbf{h} = \mathbf{r} \times \mathbf{v} = (x\dot{y} - y\dot{x})\,\hat{\mathbf{k}}$ and its magnitude is:

$$\begin{aligned} h &= \|\mathbf{h}\| = \begin{bmatrix} x \\ y \end{bmatrix}^T \begin{bmatrix} 0 & 1 \\ -1 & 0 \end{bmatrix} \begin{bmatrix} \dot{x} \\ \dot{y} \end{bmatrix} \\ &= [\mathcal{L}(\mathbf{u})\mathbf{u}]^T \begin{bmatrix} 0 & 1 \\ -1 & 0 \end{bmatrix} \left[\frac{2}{r}\mathcal{L}(\mathbf{u})\mathbf{u}'\right] \\ &= 2(u_1 u_2' - u_2 u_1') \end{aligned} \tag{2.28}$$

Recall that $\alpha = 1/a$ and the semi-latus rectum $p = a(1-e^2) = h^2/\mu$. Therefore, the eccentricity can be written as

$$e^2 = 1 - \frac{\alpha}{\mu}h^2 = 1 - 4\frac{\alpha}{\mu}(u_1 u_2' - u_2 u_1')^2 \tag{2.29}$$

The difference between the current eccentricity $e(\tau)$ and the desired one e^* is denoted by $e_e = e(\tau) - e^*$. The quadratic candidate Lyapunov-like function

$$W = V + W_1$$

where V is given by Eq. (2.22) and

$$W_1 = \frac{1}{2}e_e^2 = \left[\frac{1}{2} - 2\frac{\alpha}{\mu}\left(u_1 u_2' - u_2 u_1'\right)^2\right] \tag{2.30}$$

is minimized when the spacecraft is in a circular orbit, $e^* = 0$ and has the desired semi-major axis a^*. The time-derivative in τ-coordinates of W_1 along solutions of (2.21) is given by

$$\begin{aligned} W_1' &= ee' = -2\frac{\alpha'}{\mu}\left(u_1 u_2' - u_2 u_1'\right)^2 - 4\frac{\alpha}{\mu}(u_1 u_2' - u_2 u_1')\left[u_1 u_2'' - u_2 u_1''\right] \\ &= -\alpha'\frac{h^2}{2\mu} - \frac{h\alpha}{\mu}Ar^{3/2}\left[u_1 \sin(\phi - \theta/2) - u_2\cos(\phi - \theta/2)\right] \end{aligned}$$

Assume that a spacecraft in an initial orbit with semi-major axis a_0 and eccentricity $0 \leq e_0 < 1$ thrusts using the guidance scheme (2.23) from $0 \leq \tau \leq \tau_i$ until it reaches a desired semi-major axis $\alpha(\tau_i) \approx \alpha^*$ (to within a specified tolerance ϵ_α), but the eccentricity $e(\tau_i) \neq e^*$. At this point, the second part of the orbit transfer begins, from $\tau_i \leq \tau \leq \tau_f$, where the quadratic potential W_1 in Eq. (2.31) is again minimized when $e(\tau_f) = e^* = 0$. In our definition, convergence on eccentricity is met when $e_e = |e - e^*| \leq \epsilon_e$, Choosing the same control law as in Eq. (2.23), and since $e_\alpha \approx 0$,

$$\phi = -\lambda + \theta/2 + \sin^{-1}(Ke_\alpha) \approx -\lambda + \theta/2$$

The time derivative of W_1 with control (2.23) is

$$\begin{aligned} W_1' &= \frac{2AKh^2}{\mu^2}\sqrt{r(u_1'^2 + u_2'^2)}\,(\alpha - \alpha^*) + \frac{Ah\alpha r^{3/2}}{\mu\sqrt{u_1'^2 + u_2'^2}}\,[u_1u_1' + u_2u_2'] \\ &\approx \frac{Ah\alpha r^{3/2}}{\mu\sqrt{u_1'^2 + u_2'^2}}\,[u_1u_1' + u_2u_2'] \end{aligned} \tag{2.31}$$

W_1' is regulated to ensure that W_1 is non-increasing by choosing

$$S_1 = (u_1u_1' + u_2u_2') < 0 \tag{2.32}$$

where S_1 is defined as a switching function.

The orbit transfer is performed in the following way:

1. Semi-Major Axis Matching from $\tau_0 \leq \tau \leq \tau_i$:

$$A(\tau) = +T/m \qquad \text{while } \; |\alpha(\tau) - \alpha^*| > \epsilon_\alpha \tag{2.33}$$

2. Eccentricity Matching from $\tau_i \leq \tau \leq \tau_f$:

$$A(\tau) = \begin{cases} +T/m & \text{if } S_1 < 0 \\ 0 & \text{otherwise} \end{cases} \qquad \text{while } \; |e(\tau) - e^*| > \epsilon_e \quad (2.34)$$

Note, that the approximation of $\phi \approx -\lambda + \theta/2$ is used only to define the switching function S_1, which determines when to thrust or coast. However, in the algorithm, the full expression for ϕ, defined in Eq. (2.23), is used. This ensures not only that $W_1' \leq 0$, but in fact $W' \leq 0$, so α will also approach the desired α^* even during the eccentricity matching routine.

In some cases S_1 can be small in magnitude, and, because of the approximation that $e_\alpha \approx 0$, importance still needs to be given to W_1' (*before* the approximation was made in Eq. (2.31)). When transferring to an orbit with a lower semi-major axis than the initial one, $(\alpha - \alpha^*) \leq 0 \; \forall \; \tau \geq \tau_0$; therefore we ensure $W_1' < 0$ as long as $S_1 < 0$. However, when transferring to a higher semi-major axis, $(\alpha - \alpha^*) \geq 0$, so it is necessary to ensure that the first term in W_1' never becomes larger in magnitude than the second one, which is ensured as long as $\alpha - \alpha^* > \frac{2r}{2-r\alpha}|S_1|$, when $S_1 < 0$.

Also, when performing the semi-major axis matching, especially if using a high enough thrust, the eccentricity might become large enough to where the orbit is unbounded. This can be addressed by adding a check point, where, during the semi-major axis matching section, the eccentricity is not allowed to get larger than a specified $e_{max} < 1$. If at some point in time $\tau = \tau_{temp}$, the eccentricity $e(\tau_{temp}) = e_{max}$, the second part of the algorithm will circularize the orbit by temporarily freezing the desired semi-major axis

term to $\alpha^* = \alpha(\tau_{temp})$. Once the orbit has been circularized ($e \approx 0$), the scheme in Eq. (2.33–2.34) can be restarted again, until the desired convergence is met in both α^* and e^*.

Proposition 2.3.1. *Let a spacecraft with a constant available maximum thrust T and initial mass m_0 be on a closed orbit with a semi-major axis a_0 and an eccentricity $0 \leq e_0 < 1$. All solutions governed by the force model (2.21) with control (2.23) and switching algorithm (2.33–2.34), with a specified e_{max} constraint, converge to a final circular orbit with semi-major axis a^* and eccentricity $e^* = 0$.*

Proof. The first part of the algorithm involves matching a desired semi-major axis, which occurs once $\alpha(\tau_i) \approx \alpha^*$. This has been proven in Proposition 2.2.1. The eccentricity convergence occurs because the quadratic potential in (2.31) is radially unbounded, decrescent and its time-derivative $W_1' \leq 0$ by the choice of control ϕ and switching scheme (2.34). The proof is based on the fact that due to the thrust protocol, W_1 becomes a convergent sequence, that will inevitably make $e_e \to 0$ as time progresses.

Suppose $S_1(\tau) < 0 \ \forall \ \tau \geq \tau_i$. In this case, $W_1' < 0 \ \forall \ \tau \geq \tau_0$, which leads to $W_1 \to 0$ as $\tau \to \infty$. For our convergence definition, this is met at a finite value τ_f when $e_e(\tau_f) \leq \epsilon_e$. Suppose on the other hand that $S_1(\tau) > 0$ for some $\tau_i \leq \tau < \tau_1$, in which case thrusting is turned off by choosing $A = 0$ and the analytical solution is given by the sinusoidal function in Eq. (2.18), with a frequency of oscillation $\mathcal{W} = \sqrt{(\mu\alpha^*)/4}$. The function S_1, which is a product

of the analytical position and velocity solutions, also becomes a sinusoidal function; so it cannot remain above zero for an indefinite amount of time; (in fact this amount of time has been computed and is given in Appendix B). During this process, the potential function $W_1(\tau_i) = W_1(\tau_1)$ because $W_1' = 0$. When $S(\tau_1) < 0$, the thruster is turned back on by $A = T/m$, until S_1 crosses the origin again at time τ_2, at which point $W_1(\tau_2) < W_1(\tau_1)$. The coast/thrust process is repeated again as many times as necessary to reach the desired convergence tolerance ϵ_e; therefore, $W_1(\tau_i) = W_1(\tau_1) > W_1(\tau_2) = W_1(\tau_3) > W_1(\tau_4) > \ldots > W_1(\tau_f) = \frac{1}{2}\epsilon_e^2$. □

It is interesting to note that a different guidance law can be designed to match both the semi-major axis a^* and eccentricity e^* in just one step, rather than in two steps as is designed here. This can be achieved by coupling the candidate Lyapunov functions for both the semi-major axis and eccentricity, $W = V + W_1$, and designing the control law ϕ to make $W' \leq 0$. Even though this solution seems to give more feasible results in terms of fuel, we have designed the guidance scheme in two steps because we are able to utilize the *same* control law that matches the semi-major axis to match any circular orbit (or even to match any general orbit, as will be shown in the next subsection). To better quantify the performance of different guidance schemes, a detailed example is shown in Chapter 3.

The orbital parameters of the example transfer shown in Figure 2.3 are given in Table 2.1. The convergence is performed using the guidance scheme (2.23) and switching function (2.33–2.34). The initial spacecraft mass

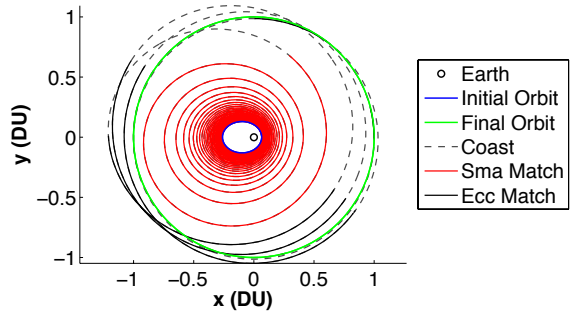

(a) x vs. y

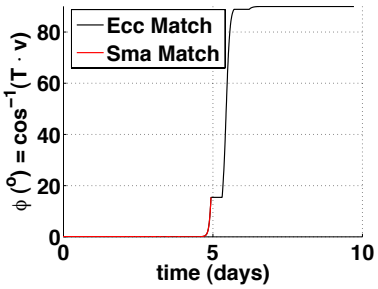

(b) ϕ vs time

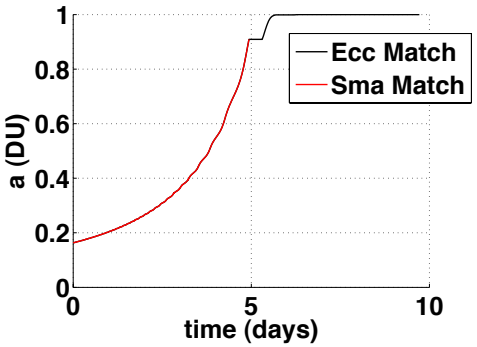

(c) a vs time

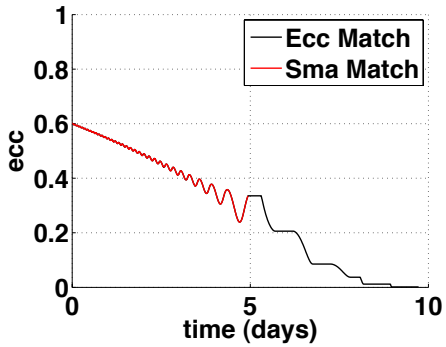

(d) e vs time

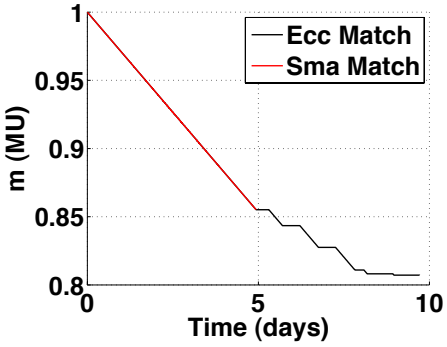

(e) m vs time

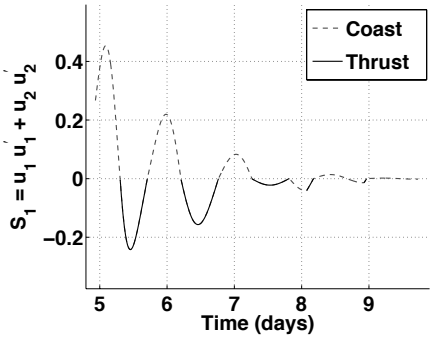

(f) S_1 vs time during e match

Figure 2.3: Eccentricity matching using control (2.23) and the switching scheme (2.33–2.34) with initial and final conditions in Table 2.1.

Table 2.1: Initial and final orbital parameters for the example in Figure 2.3

	Initial Orbit	Final Orbit
Semi-Major Axis (km)	6,878	42,164
Eccentricity	0.6	0.0
Mass (kg)	1,000	807.1
Time of Flight (days)	–	9.72

is $m_0 = 1,000$ kg, the engine parameters are $T = 10$ N and $I_{sp} = 3,000$ s. The results have been scaled using $DU = a^*$ and $MU = m_0$. The transfer takes 9.72 days and consumes 193 kg of its mass in fuel (Figure 2.3(e)). Note, that the tolerance at which the semi-major axis matching is stopped is $\epsilon_\alpha = 0.1$, at which point it is clear that $a \neq a^*$; however, during the eccentricity matching, the semi-major axis continues to converge to the desired value, due to the fact that the exact same guidance control is used for this section. The time history of the thrust direction is shown in Figure 2.3(b): it is tangential to the velocity during the first part of the transfer, and becomes perpendicular to the velocity as the orbit becomes circularized. The switching function S_1 in Eq. (2.32) is shown in Figure 2.3(f) beginning at time $t = 4.94$ days, once the eccentricity matching portion begins. Note that at this time, $S_1 > 0$ and therefore, a coasting phase begins. Around day 8 of the transfer, the switching function S_1 gets close to zero and its time-derivative become small. When this occurs, it is convenient to coast (even if $S_1 < 0$), until S_1 reaches a minimum, at which point the thrust is turned back on. This is done to avoid chattering

Once the amplitude of S_1 is within a small tolerance ($amp(S_1) \leq \epsilon_{S_1}$), any infinitesimal change in time τ results in a change of sign $S_1(\tau)$. This leads

to chattering, and therefore, full convergence will take an infinite amount of time to integrate. A viable and effective solution is to implement the switching function by allowing for coast arcs *even* when $S_1(\tau) < 0$, but only *once* the magnitude of the error in the velocity is below a specified tolerance. The continuation of the guidance scheme in Eq. (2.34) is written as

2i. Avoid Chattering: If $amp(S_1) \leq \epsilon_{S_1}$ for $\tau_i \leq \tau \leq \tau_f$

$$A(\tau) = \begin{cases} T/m & \text{if } S_1(\tau) < 0 \text{ and increasing} \\ 0 & \text{otherwise} \end{cases} \tag{2.35}$$

The full algorithm is now given by Eq. (2.33), (2.34), and (2.35).

2.3.2 Elliptical to Elliptical Orbit Transfer

In this section, we discuss the process to target any desired elliptical orbit, with a specified semi-major axis a^*, eccentricity $0 \leq e^* < 1$, and argument of periapsis (AOP) w^*. Without loss of generality, targeting these three orbital elements, is equivalent to targeting a^* and the two components of the eccentricity vector $\mathbf{e}^* = [e_x^*,\ e_y^*]^T$.

The eccentricity vector [4] in Levi-Civita coordinates is given by

$$\begin{aligned} \mathbf{e} &= \frac{1}{\mu}\left[\left(v^2 - \frac{\mu}{r}\right)\mathbf{r} - (\mathbf{r}\cdot\mathbf{v})\,\mathbf{v}\right] \\ &= \frac{1}{\mu r}\left[(4\mathbf{u}'\cdot\mathbf{u}' - \mu)\,\mathcal{L}(\mathbf{u})\mathbf{u} - 4\,(\mathbf{u}\cdot\mathbf{u}')\,\mathcal{L}(\mathbf{u})\mathbf{u}'\right] \end{aligned} \tag{2.36}$$

which can be simplified even further by components to

$$e_x = \frac{1}{r}\left[\frac{4}{\mu}\left(u_1^2 u_2'^2 - u_2^2 u_1'^2\right) - \left(u_1^2 - u_2^2\right)\right] \tag{2.37}$$

$$e_y = -\alpha u_1 u_2 - \frac{4}{\mu} u_1' u_2' \tag{2.38}$$

Their respective time-derivatives can be algebraically found to be (after extensive simplification)

$$e'_x = \frac{4A\sqrt{r(u_1'^2+u_2'^2)}}{\mu}\left[u_1^2\sin(\phi+\lambda-\theta/2) - r\sin\lambda\cos(\phi-\theta/2)\right] \quad (2.39)$$

$$e'_y = \frac{2A\sqrt{r(u_1'^2+u_2'^2)}}{\mu}\left[2u_1u_2\sin(\phi+\lambda-\theta/2) - r\cos(\phi-\lambda-\theta/2)\right] \quad (2.40)$$

The quadratic potential $W = V + W_2$, where V is given by Eq. (2.22) and

$$W_2 = \frac{1}{2}\left(\mathbf{e}-\mathbf{e}^*\right)^T\left(\mathbf{e}-\mathbf{e}^*\right) \quad (2.41)$$

is minimized when the semi-major axis and both components of the eccentricity vector are matched. In our definition, convergence on eccentricity is met when $e_{e_x} = |e_x - e_x^*| \leq \epsilon_e$ and $e_{e_y} = |e_y - e_y^*| \leq \epsilon_e$.

Again, assume that the semi-major axis matching portion occurs from $\tau_0 \leq \tau \leq \tau_i$, until $e_\alpha = |\alpha(\tau_i) - \alpha^*| \leq \epsilon_\alpha$, specified by the user. Choosing the same control law as in Eq. (2.23), and since $(\alpha - \alpha^*) \approx 0$,

$$\phi = -\lambda + \theta/2 + \sin^{-1}\left(Ke_\alpha\right) \approx -\lambda + \theta/2$$

The time-derivative of the Lyapunov-like function W_2 is

$$\begin{aligned} W_2' &= e_x'(e_x - e_x^*) + e_y'(e_y - e_y^*) \\ &= \frac{2Ar^{1/2}\sqrt{\mathbf{u}'\cdot\mathbf{u}'}}{\mu}\left[2Ku_1\left(u_1e_{e_x}+u_2e_{e_y}\right)e_\alpha - \frac{r}{\mathbf{u}'\cdot\mathbf{u}'}\left(2u_1'u_2'e_{e_x}+\left(u_2'^2-u_1'^2\right)e_{e_y}\right)\right] \\ &\approx -\frac{2Ar^{3/2}}{\mu\sqrt{\mathbf{u}'\cdot\mathbf{u}'}}\left[2u_1'u_2'e_{e_x} + \left(u_2'^2 - u_1'^2\right)e_{e_y}\right] \end{aligned} \quad (2.42)$$

The convergence to the desired e_x^* and e_y^* to ensure $W_2' \leq 0$ is performed by thrusting with an acceleration magnitude $A = T/m$ when

$$S_2 \;=\; 2(e_x - e_x^*)u_1' u_2' + (e_y - e_y^*)\left(u_2'^2 - u_1'^2\right) > 0 \tag{2.43}$$

The full orbit transfer is performed in the following way

1. Semi-Major Axis Matching from $\tau_0 \leq \tau \leq \tau_i$:

$$A(\tau) = +T/m \;\text{ while }\; |\alpha(\tau) - \alpha^*| > \epsilon_\alpha \tag{2.44}$$

2. Eccentricity and AOP Matching from $\tau_i \leq \tau \leq \tau_f$:

$$A(\tau) = \begin{cases} +T/m & \text{if } S_2 > 0 \\ 0 & \text{otherwise} \end{cases} \tag{2.45}$$

The same e_{max} constraint is placed on this algorithm, as was done in Section 2.3.1, to ensure that the orbit does not become unbounded.

Proposition 2.3.2. *Let a spacecraft with a constant available maximum thrust T and initial mass m_0 be on a closed orbit with a semi-major axis a_0, eccentricity $0 \leq e_0 < 1$, and argument of periapsis ω_0. All solutions governed by the force model (2.21) with control (2.23) and switching function (2.44–2.45), with an e_{max} constraint, converge to a final orbit with semi-major axis a^*, eccentricity $0 \leq e^* < 1$, and argument of periapsis ω^*.*

Proof. The proof follows identically as in Proposition 2.3.1; the only difference being that the switching scheme is now given by S_2 in (2.43), and the coast time is again analytically solved for in Appendix B. □

An example orbit transfer about Earth is shown in Figure 2.4 using control (2.23) and the switching scheme (2.44–2.45), with $T = 50$ N, $I_{sp} = 1,000$ s, and initial and final orbital parameters given by Table 2.2. The results have been scaled using $DU = a^*$ and $MU = m_0 = 1,000$ kg. The trajectory in x-y coordinates is shown in Figure 2.4(a), which has been transformed using Eq. (2.4) from the $\mathbf{u}$ results of the integration (shown in Figure 2.4(b)). The time history of the thrust direction is shown in Figure 2.4(c): it is tangential to the velocity during the first part of the transfer, and becomes perpendicular to the velocity as convergence to the desired orbit is achieved. The semi-major axis a, eccentricity e, and argument of periapsis ω over time are shown in Figure 2.4(f–h).

To emphasize the different coasting/thrusting phases, a plot of the switching function S_2 in Eq. (2.43) over time is shown, beginning at the time when the eccentricity (Ecc) and argument of periapsis (AOP) matching section begins. Notice that as the orbital parameters converge closer to the desired ones, $S_2 \to 0$, and careful attention needs to be given on when to thrust or coast. The assumption was made that $e_\alpha \approx 0$; however, as S_2 becomes smaller in magnitude, the approximation in Eq. (2.42) might not be not valid anymore to ensure $W_2' < 0$ during the thrusting phase. Therefore, once $|S_2| \leq \epsilon$, it is necessary to ensure that thrusting happens only when the bracketed term *before* the approximation was made in W_2' is negative.

Table 2.2: Initial and final orbital parameters for the example in Figure 2.4

	Initial Orbit	Final Orbit
Semi-Major Axis (km)	10,000	20,000
Eccentricity	0.3	0.6
AOP(^{o})	0.0	90.0
Mass (kg)	1,000	447.4
Time of Flight (days)	–	2.28

2.4 Final Remarks

In this chapter a new approach is taken to solve the problem of orbit transfers by working in a transformed model to design Lyapunov-based control laws. The model we use is the classical Levi-Civita regularization transformation of the planar two-body problem. The advantage of working in these transformed coordinates is that the solution to the unperturbed equations of motion is that of a simple linear harmonic oscillator, where the frequency of oscillation is a function of a, the semi-major axis of the orbit.

We design a closed-loop guidance scheme for a coplanar orbit transfer from any initial elliptical orbit to any final specified elliptical orbit utilizing a spacecraft with thrust-coast capabilities. The convergence to the desired formation is performed in two steps. The first step involves converging the spacecraft orbit to the desired semi-major axis a^*, even though no other parameters reach their desired values, by using a Lyapunov analysis that gives rise to an asymptotically stabilizing control law. Once a^* has been reached to within a specified tolerance, the second step of the algorithm involves matching the other desired orbital parameters, using the same control law as before,

but with an added on/off switching mechanism for coasting during certain intervals. Another advantage of working in the Levi-Civita coordinates is that since the analytical solution is known during the coast phases, using Lyapunov stability it is possible to determine analytically the exact time (in τ) at which the thrusters should be turned back on. The algorithms designed are robust, computationally fast, and can be used for both low- and high-thrust problems, though fuel or time-optimality is not guaranteed. Several examples are given for various initial and final parameters as well as different engine capabilities for the orbit transfer problem.

One of the powerful results of this work is that the guidance law is designed based *only* on matching the desired semi-major axis. With the same control law that matches semi-major axis, we are able to match any desired orbit by adding thrust/coast arcs. However, the two convergence sections may indeed be combined by virtue of selecting a different Lyapunov candidate function and re-designing the control law. This option will be studied in our future work, since we are interested in designing control laws that are likely to be closer to the fuel optimal solution. Also, we would like to determine at which point during the orbit it is optimal to begin thrusting. One of the possible answers is to examine the time-derivative of the candidate Lyapunov functions, and determine at which point their slope is maximum, which will aid in converging to closer optimal solutions.

The next major step is to expand the orbit transfer algorithms to the three-dimensional model using the Kustaanheimo-Stiefel (KS) coordinate

transformation, which transforms the state vector from cartesian space into a four-dimensional space, similar to the Levi-Civita model, which is the the topic of the next chapter.

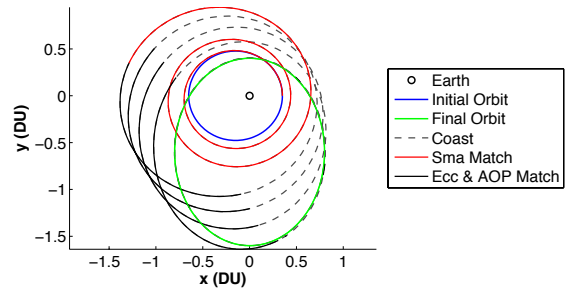

(a) x vs. y

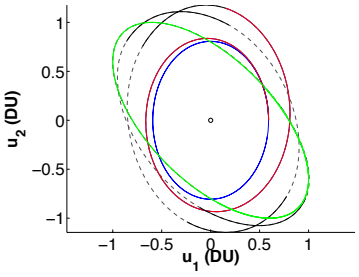

(b) u_1 vs. u_2

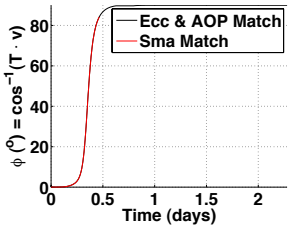

(c) ϕ vs time

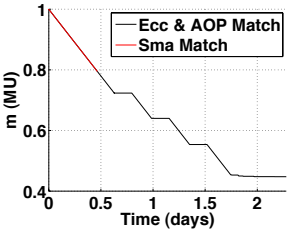

(d) m vs time

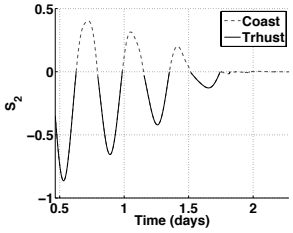

(e) S_2 vs time during e and ω match

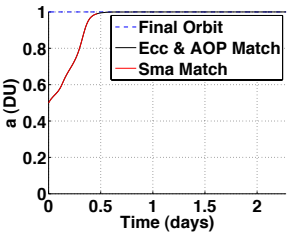

(f) a vs time

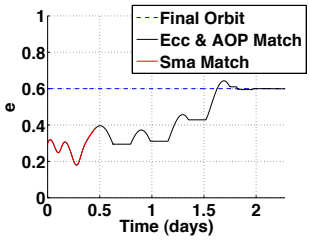

(g) e vs time

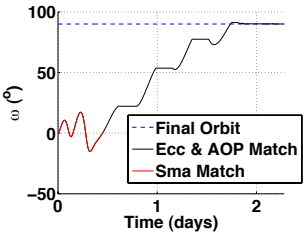

(h) ω vs time

Figure 2.4: Orbit transfer using control (2.23) and the switching scheme (2.44–2.45) with parameters in Table 2.2.

Chapter 3

Lyapunov-Based Guidance for Orbit Transfers in KS Variables

[1]In order to allow for out-of-plane maneuvers, we now move to the three-dimensional perturbed two-body equations of motion. We are again interested in regularizing these equations of motion. Note that the transformation in two-dimensions to the regular model involves a mapping of the form $\mathbf{r} \in \mathbb{R}^2 \rightarrow \mathbf{u} \in \mathbb{R}^2$ (as we saw in Chapter 2). However, in three-dimensions it is not possible to find a mapping into $\mathbb{R}^3$ to obtain a regularized model. Kustaanheimo and Stiefel worked around this issue by creating a four-dimensional formulation to arrive at the regularized model (known as the KS transformation) [34].

The idea is to design the control laws by using Lyapunov stability theory. The orbit transfer is performed in two steps by using a constant thrust engine. The first step involves converging the spacecraft orbit to the desired semi-major axis a^* (or equivalently, the desired energy), by using a Lyapunov analysis that gives rise to an asymptotically stabilizing control law. Once the energy has been met, to within any pre-specified tolerance bound, the second step involves converging the remaining subset desired orbital elements

[1]The work presented in this chapter is in Ref. [26].

(by holding energy constant). We are able to rigorously show that any orbital element can be targeted by holding energy constant, which is one of the major contributions to this chapter. The algorithms designed are robust to any initial and final conditions, computationally fast, and can be theoretically used for both low- and high-thrust problems (although our numerical studies suggest closer to optimal results are usually obtained for low-thrust engines). Also, the effectiveness of the guidance scheme in a dynamical environment where unmodeled perturbations are present is shown via numerical simulation. We show the validity of this by adding J_2 perturbations to an example.

This chapter is organized as follows. We begin Section 3.1 by reviewing and deriving the KS equations of motion of a spacecraft which is allowed to thrust in a two-body force model. The next section deals with designing a guidance scheme to target *only* the desired semi-major axis a^*, which fixes the energy of the orbit for the remainder of the orbit transfer design. By holding energy constant, we are able to then target different subsets of orbital elements by thrusting in-plane in Section 3.3 and out-of-plane in Section 3.4, with the final capability of performing a full orbit transfer by targeting all orbital elements at the end of Section 3.4. Note that while the guidance schemes are designed in the transformed regularized coordinates, the results can be explicitly characterized in the original coordinates; the transformation procedure merely acts as an enabler for the design. The algorithms are written out in the original coordinates in Appendix C.

Even though this chapter is focused on performing orbit transfers, an

extensive study on the possibility of designing guidance schemes to perform a full rendezvous (by matching both position and velocity coordinates) was performed. Unfortunately, there are many technical issues encountered with performing rendezvous by using a Lyapunov approach, and all the findings are detailed in Appendix D.2.

3.1 KS Equations of Motion

The equations of motion of a spacecraft in a perturbed two-body model are

$$\ddot{\mathbf{r}} = -\frac{\mu}{r^3}\mathbf{r} + \mathbf{f} \tag{3.1}$$

where μ is the gravitational parameter of the central body, the position vector

$$\mathbf{r} = [r_1 \;\; r_2 \;\; r_3]^T$$

where r_1, r_2, and r_3 are, respectively, the x, y, and z components in a fixed coordinate frame. The vector $\mathbf{r}$ has magnitude $r = \sqrt{r_1^2 + r_2^2 + r_3^2}$, and $\mathbf{f} \in \mathbb{R}^3$ is the perturbing acceleration.

The derivation of the equations of motion follows similarly to the Levi-Civita equations in Section 2.1, by making two transformations to convert Eq. (3.1) into the regularized model. First, a change of position coordinates, second, a time transformation. Following the notation in [1], we begin with the first step.

1. *Change of position coordinates:*

Let the position vector in the KS model be

$$\mathbf{u} = [u_1 \;\; u_2 \;\; u_3 \;\; u_4]^T \;\; \in \mathbb{R}^4 \tag{3.2}$$

and define an expanded position vector

$$\mathbf{R} = \begin{bmatrix} \mathbf{r} \\ r_4 \end{bmatrix} = \begin{bmatrix} r_1 \\ r_2 \\ r_3 \\ r_4 \end{bmatrix} \;\; \in \mathbb{R}^4 \tag{3.3}$$

where $r_4 = 0$ acts merely a fictitious variable. The transformation from $\mathbf{u}$ to $\mathbf{R}$ can be expressed in terms of the following linear operator

$$\mathcal{L}(\mathbf{u}) = \begin{bmatrix} u_1 & -u_2 & -u_3 & u_4 \\ u_2 & u_1 & -u_4 & -u_3 \\ u_3 & u_4 & u_1 & u_2 \\ u_4 & -u_3 & u_2 & -u_1 \end{bmatrix} \tag{3.4}$$

such that

$$\mathbf{R} = \mathcal{L}(\mathbf{u})\mathbf{u} \tag{3.5}$$

The magnitude of the position vector is

$$r = \|\mathbf{r}\| = (\mathbf{r} \cdot \mathbf{r})^{1/2} \quad \Longleftrightarrow \quad r = \|\mathbf{R}\| = \mathbf{u} \cdot \mathbf{u} \tag{3.6}$$

The linear operator $\mathcal{L}(\mathbf{u})$ satisfies

$$\mathcal{L}^T(\mathbf{u})\mathcal{L}(\mathbf{u}) = \mathcal{L}(\mathbf{u})\mathcal{L}^T(\mathbf{u}) = r\mathbf{I}, \tag{3.7}$$

where $\mathbf{I}$ is the identity matrix. The same P1$-$P4 properties outlined in Section 2.1 are also satisfied here.

2. *Perform Sundman transformation to change the time variable*

The second step in the derivation involves introducing a velocity transformation by performing a Sundman transformation [59],

$$\dot{\mathbf{R}} = \frac{1}{r}\mathbf{R}' \iff \frac{d\mathbf{R}}{dt} = \frac{1}{r}\frac{d\mathbf{R}}{d\tau}$$

Note, that $\dot{(\,)} = \frac{d}{dt}(\,)$, denotes the time derivative in $\mathbf{R}$ coordinates, whereas $(\,)' = \frac{d}{d\tau}(\,)$ is the time derivative in $\mathbf{u}$ coordinates. The derivative of $\mathbf{R}$ in terms of $\mathbf{u}$ coordinates is in Eq. (2.7), but will be restated here for completeness,

$$\mathbf{R}' = \frac{d}{d\tau}\mathbf{R} = \frac{d}{d\tau}\left(\mathcal{L}(\mathbf{u})\mathbf{u}\right) = 2\mathcal{L}(\mathbf{u})\mathbf{u}' \tag{3.8}$$

such that

$$\mathbf{u}' = \frac{1}{2}\mathcal{L}^T(\mathbf{u})\dot{\mathbf{R}} \quad \iff \quad \dot{\mathbf{R}} = \frac{2}{r}\mathcal{L}(\mathbf{u})\mathbf{u}' \tag{3.9}$$

By following the same steps as in the derivation of the planar regularized model, which is outlined in Section 2.1, the perturbed two-body equations of motion in Eq. (3.1) in the regularized form are

$$\mathbf{u}'' = \frac{E}{2}\mathbf{u} + \frac{1}{2}r\mathcal{L}^T(\mathbf{u})\mathbf{F} \tag{3.10}$$

where the augmented perturbing acceleration vector is

$$\mathbf{F} = \begin{bmatrix} \mathbf{f} \\ 0 \end{bmatrix} \in \mathbb{R}^4 \tag{3.11}$$

and E is the energy of the orbit, which varies according to $E' = 2\mathbf{u}' \cdot \mathcal{L}^T(\mathbf{u})\mathbf{F}$. Using the definition of the inverse of the semi-major axis α in Eq. (2.20), it

is related to the energy E of an orbit through the relation $E = -(\mu/2)\alpha$ and its derivative $\alpha' = -(2/\mu)E'$. Combining this into Eq. (3.10), results in the complete equations of motion

$$\begin{aligned} \mathbf{u}'' &= -\frac{\mu\alpha}{4}\mathbf{u} + \frac{1}{2}r\mathcal{L}^T(\mathbf{u})\mathbf{F} \\ \alpha' &= -\frac{4}{\mu}\mathbf{u}' \cdot \mathcal{L}^T(\mathbf{u})\mathbf{F} \\ t' &= \mathbf{u} \cdot \mathbf{u} \end{aligned} \tag{3.12}$$

where the last equation is necessary to obtain true time t, since the variable of integration is the fictitious time τ.

Note, that one of the components of $\mathbf{u}$ is arbitrary, since the transformation involves a transformation from $\mathbb{R}^3$ to $\mathbb{R}^4$. Therefore, there is some freedom in the choice of initial conditions, when transforming from $\mathbf{r}(t_0)$ to $\mathbf{u}(\tau_0)$[1].

If $r_{1_0} \geq 0$			If $r_{1_0} < 0$		
u_{4_0}	=	0	u_{3_0}	=	0
u_{1_0}	=	$\left[\frac{1}{2}\left(r_{1_0} + r_0\right)\right]^{1/2}$	u_{2_0}	=	$\left[\frac{1}{2}\left(r_0 - r_{1_0}\right)\right]^{1/2}$
u_{2_0}	=	$\frac{1}{2}\left(\frac{r_{2_0}}{u_{1_0}}\right)$	u_{1_0}	=	$\frac{1}{2}\left(\frac{r_{2_0}}{u_{2_0}}\right)$
u_{3_0}	=	$\frac{1}{2}\left(\frac{r_{3_0}}{u_{1_0}}\right)$	u_{4_0}	=	$\frac{1}{2}\left(\frac{r_{3_0}}{u_{2_0}}\right)$

The integral of motion found in the Levi-Civita coordinates in Eq. (2.16), holds as well in the four-dimensional KS variables. We will restated here for completeness:

Lemma 3.1.1. *The quadratic potential*

$$C(\tau) = -\frac{E}{4}\|\mathbf{u}\|^2 + \|\mathbf{u}'\|^2 = \frac{\mu}{2} \tag{3.13}$$

is an integral of motion of the perturbed equations of motion in (3.10).

Proof. Taking the time derivative of $C(\tau)$, and using Eq. (3.10), it is readily seen that $C'(\tau) = 0$, regardless of the value of the perturbing acceleration $\mathbf{F}$. □

3.1.1 Unperturbed Equations of Motion

In the case when there is no perturbing acceleration acting on the spacecraft, that is, $\mathbf{F} = \mathbf{0}$, the equations of motion in Eq. (3.12) become de-coupled linear harmonic oscillators

$$\mathbf{u}'' = -\frac{\mu\alpha}{4}\mathbf{u} \qquad \text{and} \qquad \alpha' = 0 \tag{3.14}$$

The analytical solution is known, with a frequency of oscillation $\mathcal{W} = \sqrt{\mu\alpha/4}$. Therefore, during any coast phase, the analytical solution is always known and given by

$$\mathbf{u}(s) = \mathbf{u}_0 \cos(\mathcal{W}s) + \frac{\mathbf{u}_0'}{\mathcal{W}} \sin(\mathcal{W}s) \tag{3.15}$$

3.1.2 Defining the Thrust Vector F

Suppose that the perturbation $\mathbf{f}$ in Eq. (3.1) now comes from a finite thrust engine, with constant thrust magnitude T. The acceleration magnitude $\|\mathbf{f}\| = T/m$ and m is the mass of the spacecraft at any point in time, which varies according to $\dot{m} = -T/c$, such that

$$m' = -r\frac{T}{c} \tag{3.16}$$

where $c = gI_{sp}$, $g = 9.81$ m/s^2, and I_{sp} is the specific impulse of the engine. We choose the acceleration vector direction to be defined in a body-fixed frame of the spacecraft, with two spherical variable angles β and δ, such that

$$\mathbf{f} = \frac{T}{m}\left[\sin\beta\hat{\mathbf{r}}' + \cos\beta\cos\delta\hat{\mathbf{p}} + \cos\beta\sin\delta\hat{\mathbf{h}}\right] \in \mathbb{R}^3 \tag{3.17}$$

where the unit vectors $\hat{\mathbf{r}}'$, $\hat{\mathbf{p}}$, and $\hat{\mathbf{h}}$ form a basis in the body-frame and are defined as

$$\begin{aligned}
\hat{\mathbf{r}}' &= \mathbf{r}'/\|\mathbf{r}'\| \\
\hat{\mathbf{h}} &= \mathbf{h}/\|\mathbf{h}\|, \text{ where } \mathbf{h} = \mathbf{r}\times\dot{\mathbf{r}} = (\mathbf{r}/\|\mathbf{r}\|)\times\mathbf{r}' \\
\hat{\mathbf{p}} &= \hat{\mathbf{r}}'\times\hat{\mathbf{h}}
\end{aligned}$$

where $\hat{\mathbf{r}}'$ points in the velocity direction, $\hat{\mathbf{h}}$ points in the direction perpendicular to the orbit plane, and $\hat{\mathbf{p}}$ completes the right-handed frame (and lies in the plane of the orbit). Note that usually $\mathbf{f}$ is expressed in the radial, circumferential, and angular momentum direction (e.g. Gauss's form of the variational equations). However, for ease in our design purposes, we have chosen to express $\mathbf{f}$ in a slightly different frame; but, by means of a matrix transformation, the thrust vector can always be expressed in any desired frame. Furthermore, as will be discussed subsequently, selecting the coordinate frame in this manner results in a natural decoupling of the guidance to match semi-major axis.

The augmented acceleration vector $\mathbf{F}$ implemented in Eq. (3.12) is then defined as

$$\mathbf{F} = \begin{bmatrix} \mathbf{f} \\ 0 \end{bmatrix} = \frac{T}{m}\left[\sin\beta\hat{\mathbf{R}}' + \cos\beta\cos\delta\hat{\mathbf{P}} + \cos\beta\sin\delta\hat{\mathbf{H}}\right] \tag{3.18}$$

where

$$\hat{\mathbf{R}}' = \begin{bmatrix} \hat{\mathbf{r}}' \\ 0 \end{bmatrix}, \hat{\mathbf{P}} = \begin{bmatrix} \hat{\mathbf{p}} \\ 0 \end{bmatrix}, \text{ and } \hat{\mathbf{H}} = \begin{bmatrix} \hat{\mathbf{h}} \\ 0 \end{bmatrix}$$

Note that by fixing the thrust magnitude and defining the thrust vector in spherical coordinates, this allows for *only* two degrees of freedom to our design problem: the two time-varying angles $-180^o \leq \delta \leq 180^o$ and $-90^o \leq \beta \leq 90^o$. These are now the only design control inputs we have control over. The remaining portion of the chapter will be focused on designing β and δ such that we are *guaranteed* via rigorous mathematical proof to converge to the desired orbital parameters.

3.2 Convergence on Energy: Targeting Semi-Major Axis

Suppose that the desired semi-major axis is given by a^*, and therefore, its inverse is $\alpha^* = 1/a^*$. At any point in time (in τ coordinates) the spacecraft, whose motion is governed by Eq. (3.12), has a semi-major axis $a(\tau)$, and correspondingly $\alpha(\tau) = 1/a(\tau)$. The difference between the current $\alpha(\tau)$ and the desired α^* is denoted by

$$e_\alpha = \alpha - \alpha^* \tag{3.19}$$

The quadratic candidate Lyapunov function

$$V_\alpha = \frac{1}{2} e_\alpha^2 \tag{3.20}$$

is minimized when the semi-major axis of the chaser spacecraft matches the semi-major axis of the target. The time-derivative of V_α along solutions of

Eq. (3.12) is given by

$$\begin{aligned} V'_\alpha &= e_\alpha e'_\alpha = e_\alpha \alpha' \\ &= -\frac{4}{\mu} e_\alpha \mathbf{u}' \cdot \mathcal{L}^T(\mathbf{u})\mathbf{F} \\ &= -\frac{2}{\mu}\frac{T}{m} e_\alpha \mathbf{R}'^T \left[\sin\beta \hat{\mathbf{R}}' + \cos\beta\cos\delta\hat{\mathbf{P}} + \cos\beta\sin\delta\hat{\mathbf{H}}\right] \\ &= -\frac{2}{\mu}\frac{T}{m} e_\alpha \|\mathbf{R}'\| \sin\beta \end{aligned}$$

Recall that the vectors $\hat{\mathbf{R}}'$, $\hat{\mathbf{H}}$, and $\hat{\mathbf{P}}$ form an orthogonal basis, and therefore, $\hat{\mathbf{R}}' \cdot \hat{\mathbf{H}} = \hat{\mathbf{R}}' \cdot \hat{\mathbf{P}} = \mathbf{0}$. Note, the angle δ does not play a role in matching semi-major axis; this angle can have any value, and it will not affect the semi-major axis. This in fact verifies that the semi-major axis is changed by thrusting only along the velocity direction, which is observed by looking at the time-derivative of the inverse of the semi-major axis.

$$\alpha' = -\frac{4}{\mu}\mathbf{u}' \cdot \mathcal{L}^T(\mathbf{u})\mathbf{F} = -\frac{2}{\mu}\mathbf{R}' \cdot \mathbf{F} \Longleftrightarrow \dot{\alpha} = -\frac{2}{\mu}\dot{\mathbf{r}} \cdot \mathbf{f} \tag{3.21}$$

By choosing

$$\beta = \sin^{-1}(K e_\alpha) \quad \text{where} \quad K = 1/\|e_{\alpha_0}\| \tag{3.22}$$

results in

$$\alpha' = -\frac{2}{\mu}\frac{T}{m}\|\mathbf{R}'\| K e_\alpha \tag{3.23}$$

which ensures that V_α is non-increasing

$$V'_\alpha = -\frac{2}{\mu}\frac{T}{m} K e_\alpha^2 \leq 0 \tag{3.24}$$

Note that we have freedom in the choice of the gain $K > 0$. Even though we have suggested a value $K = 1/\|e_{\alpha_0}\|$, K could be initialized to any positive number, and could even be designed to be time-varying, such as to make the time-derivative of the Lyapunov function as negative as possible. However, there should always be caution in choosing K "too" large, so that saturation does not occur. For simulation purposes it is at times convenient to chose $\beta = \sin^{-1}(\tanh(Ke_\alpha))$, which is slightly different from the definition in Eq. (3.22), but has no impact on the convergence analysis.

Proposition 3.2.1. ***Targeting Semi-Major Axis:*** *Let a spacecraft with a constant available thrust T and initial mass m_0 be on a closed orbit with initial semi-major axis $a(\tau_0) = a_0$. All solutions governed by the force model in Eq. (3.12) with thrust vector in Eq. (3.18) and mass varying according to Eq. (3.16), converge to any prescribed final semi-major axis a^*, with control angle β defined in Eq. (3.22), regardless of the choice of control angle δ.*

Proof. Due to the commanded thrust protocol for driving $\alpha(\tau)$ to α^* (by Eq. (3.22)), $\alpha(\tau)$ becomes an exponential function of $e_\alpha(\tau)$, since

$$e'_\alpha = \alpha' = -K_1 A f(\mathbf{u}, \mathbf{u}') e_\alpha$$

where $K_1 = (2K)/\mu > 0$, $A(\tau) = T/m(\tau) > 0$, and $f(\mathbf{u}(\tau), \mathbf{u}'(\tau)) = \|\mathbf{R}'\| > 0$. Therefore $e_\alpha(\tau) \to 0$ exponentially. Detailed convergence proof follows identically to the proof in Chapter 2, Section 2.2.

□

3.2.1 Planar Low-thrust Circle-to-Circle Transfer

A low-thrust solution is shown in Figure 3.1. In this case, the simulation is a circle-to-circle transfer from $a_0 = 6,978$ km to $a^* = 42,164$ km using $T = 1$ N and $I_{sp} = 3,000$ s. In this guidance solution the only required control is to match the desired semi-major axis, since the thrust is low and the eccentricity and inclination stay relatively unchanged throughout the transfer. This solution is compared to Edelbaum's approximate fuel-optimal analytical solution for circle-to-circle transfers [16], which is derived assuming a constant acceleration magnitude and a low eccentricity ($e << 0.1$) during the transfer. The initial and final orbital parameters are listed in Table 3.1. For this simulation $\delta = 0$ (since it plays no role in the change in semi-major axis), $\beta = \sin^{-1}(\tanh(Ke_\alpha))$, where $K = 50$. The integration of Eq. (3.12) is performed in dimensionless units, in order to avoid build-up of numerical errors caused by $e_\alpha = \alpha - \alpha^*$, which can be a very small number when working in units of km. The dimensionless units are distance unit $DU = a^* = 42,164$ km, mass unit $MU = m_0 = 1,000$ kg, and time unit TU, chosen such that $\mu = 1\ DU^3/TU^2$. [1] The stopping tolerance was $\epsilon_\alpha = 10^{-2}$. The trajectory in x, y coordinates is shown in Figure 3.1(a), which has been transformed using Eq. (3.5) form the $\mathbf{u}$ results of the integration. The thrust angle with respect to the velocity vector is shown in Figure 3.1(b), which is purely in the velocity direction, until convergence to the desired semi-major axis, at which point the

[1] The remaining simulations shown in the chapter are performed in dimensionless units, by setting $DU = a^*$, $MU = m_0$, and $\mu = 1\ DU^3/TU^2$.

thrust angle become purely perpendicular. The semi-major axis and eccentricity over time compared to Edelbaum's solution are shown in Figure 3.1(c),(d). The total transfer time is 48.50 days, which is slightly faster than Edelbaum's result of 51.89 days (see Table 3.2). The total propellant used is 142.38 kg, compared to the fuel-optimal solution of 141.34 kg. Therefore, the proposed solution in this chapter is in fact extremely close to a fuel-optimal solution. This example shown is a planar transfer, which can also be performed with the guidance scheme derived in Chapter 2, by choosing the out-of-plane angle $\delta = 0$, and equivalent results are obtained.

We also use the algorithm in this example to show that a perturbed model due to J2 [60] is still robust (see comparison in Table 3.2). As expected, the perturbed model takes longer and uses more propellant; however, because the control law is updated based on the current state, it still converges to the desired orbit.

Table 3.1: Initial and final orbital parameters for the example in Figure 3.1

	a (km)	e	i (^{o})	T (N)	m_0 (kg)	I_{sp} (s)
Initial Orbit	6978	0.0	0.00	1	1000	3000
Final Orbit	42164	$<< 0.1$	free			

3.3 In-Plane Transfers by Holding Energy Constant

We begin Section 3.3.1 by discussing planar transfers to circular orbits of prescribed radius (this involves targeting semi-major axis a^* and zero eccentricity $e^* = 0$). The control δ is designed to match the desired eccen-

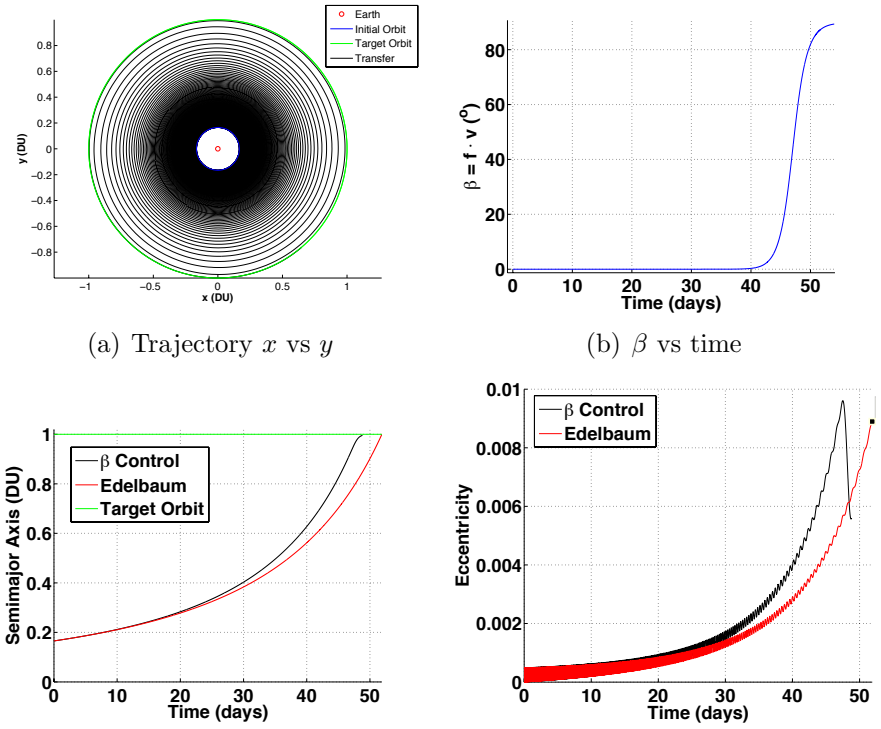

(a) Trajectory x vs y

(b) β vs time

(c) Semi-major axis a vs time

(d) Eccentricity e vs time

Figure 3.1: Comparison of algorithm using control (3.22) with Edelbaum's analytical low-thrust optimal solution, where the initial conditions are given in Table 3.1.

tricity by holding energy constant; that is, the circularization begins once the semi-major axis has reached the target value. In Section 3.3.2, we extend the results to achieve any desired eccentricity value ($0 \leq e^* < 1$). Note that we do not discuss targeting a specific orientation of the orbit, since extensive studies were done in Chapter 2.

Table 3.2: Comparison of a low-thrust solution orbit transfer, where the results are shown in Figure 3.1.

	"Optimal" [16]	β Control (Lyapunov)	β Control (J_2 Pert.)
Transf. Time (days)	51.89	48.50	48.86
Propellant Used (kg)	141.34	142.38	142.91
Final Eccentricity	0.0091	0.0056	0.0059

3.3.1 Targeting Circular Orbits ($e^* = 0$)

The eccentricity e of an orbit expressed in KS variables is [1]

$$e^2 = (1 - r\alpha)^2 + \frac{4}{\mu}\alpha(\mathbf{u} \cdot \mathbf{u}')^2 \tag{3.25}$$

where the following relations with the eccentric anomaly $\mathcal{E}$ have been used

$$\begin{aligned} e\cos\mathcal{E} &= 1 - r/a \\ e\sin\mathcal{E} &= (\mathbf{r} \cdot \dot{\mathbf{r}})/\sqrt{\mu a} \end{aligned}$$

To target a circular orbit $e^* = 0$, a Lyapunov-candidate function (which is minimum when $e = 0$) is

$$V_e = \frac{1}{2}(e - e^*)^2 = \frac{1}{2}e^2 \geq 0 \tag{3.26}$$

Note $r' = 2\mathbf{u} \cdot \mathbf{u}'$. The time derivative of V_e along solutions of Eq. (3.12)

is

$$\begin{aligned} V_e' &= \frac{1}{2}\frac{d}{d\tau}e^2 \\ &= r\alpha^2(\mathbf{u}\cdot\mathbf{u}') + \left[-r(1-r\alpha) + \frac{2}{\mu}(\mathbf{u}\cdot\mathbf{u}')^2\right]\alpha' + \frac{4}{\mu}\alpha(\mathbf{u}\cdot\mathbf{u}')[\mathbf{u}\cdot\mathbf{u}''] \\ &= 2r\frac{\alpha}{\mu}(\mathbf{u}\cdot\mathbf{u}')\left(\mathcal{L}(\mathbf{u})\mathbf{u}\right)\cdot\mathbf{F} + \frac{4}{\mu}\left[r(1-r\alpha) - \frac{2}{\mu}(\mathbf{u}\cdot\mathbf{u}')^2\right]\left(\mathcal{L}(\mathbf{u})\mathbf{u}'\right)\cdot\mathbf{F} \\ &= 2r\frac{\alpha}{\mu}(\mathbf{u}\cdot\mathbf{u}')\mathbf{R}\cdot\mathbf{F} + \frac{2}{\mu}\left[r(1-r\alpha) - \frac{2}{\mu}(\mathbf{u}\cdot\mathbf{u}')^2\right]\mathbf{R}'\cdot\mathbf{F} \end{aligned} \tag{3.27}$$

This result is conclusive with the known fact that eccentricity is changed by the in-plane components of the thrust (or perturbing acceleration $\mathbf{F}$), that is, in the position $\mathbf{R}$ and velocity direction $\mathbf{R}'$. We now use the fixed-thrust control law $\mathbf{F}$ in Eq. (3.18). The time-derivative of V_e simplifies to

$$\begin{aligned} V_e' &= \frac{2}{\mu}\frac{T}{m}\|\mathbf{R}'\|\left[2\left(\frac{r^2\alpha}{\|\mathbf{R}'\|^2} - \frac{1}{\mu}\right)(\mathbf{u}\cdot\mathbf{u}')^2 + r(1-r\alpha)\right]\sin\beta \\ &\quad + \frac{2}{\mu}\frac{T}{m}r\alpha(\mathbf{u}\cdot\mathbf{u}')(\mathbf{R}\cdot\hat{\mathbf{P}})\cos\beta\cos\delta \end{aligned} \tag{3.28}$$

Since the control angle β has already been designed to match the desired semi-major axis by an asymptotic convergence, we only have freedom of the other control angle δ. This in term means that we have no control over first term in V_e' in Eq. (3.28); however, we can design δ such that V_e' is "as minimal as possible" (keeping in mind that the first term in Eq. (3.28) might make $V_e' > 0$). Note $-90^o \leq \beta \leq 90^o$, therefore $\cos\beta \geq 0 \;\forall\; \tau \geq 0$.

By choosing

$$\delta = \begin{cases} \cos^{-1}(+1) & \text{if} \quad S_e < 0 \\ \cos^{-1}(-1) & \quad\;\; \text{otherwise} \end{cases} \tag{3.29}$$

where the switching function

$$S_e = (\mathbf{u} \cdot \mathbf{u}')(\mathbf{R} \cdot \hat{\mathbf{P}}) \tag{3.30}$$

we ensure V_e' is as minimal as possible.

Because we have asymptotic convergence for the semi-major axis by the chosen β in Eq. (3.22) (see Proposition 3.2.1), once the semi-major axis of the spacecraft has been matched to be that of the target orbit (to within some specified tolerance), then $\sin\beta \approx 0$ and $\cos\beta \approx 1$. The time-derivative of the potential then becomes

$$\begin{aligned} V_e' &\approx \frac{2}{\mu}\frac{T}{m} r\alpha (\mathbf{u} \cdot \mathbf{u}')(\mathbf{R} \cdot \hat{\mathbf{P}}) \cos\delta \\ &= -\frac{2}{\mu}\frac{T}{m} r\alpha |S_e| \leq 0 \end{aligned} \tag{3.31}$$

which will indeed be made negative semi-definite by the chosen δ in Eq. (3.29). Note we have defined this δ to only match the desired eccentricity and does not take into account any inclination matching. However, by this design we ensure that the inclination of the spacecraft will not change, since the out-of-plane component of $\mathbf{F}$ remains at zero.

Proposition 3.3.1. ***Targeting Semi-Major Axis and Eccentricity:*** *Let a spacecraft with a constant available thrust T and initial mass m_0 be on a closed orbit. All solutions governed by the force model in Eq. (3.12) with thrust vector in Eq. (3.18) and mass varying according to Eq. (3.16), converge to an orbit with desired semi-major axis a^* and eccentricity e^*, when the control angles are chosen as β in Eq. (3.22) and δ in Eq. (3.29), with switching function S_e in Eq. (3.30).*

Proof. Control angle β ensures semi-major axis convergence, which occurs once $\alpha(\tau_i) \approx \alpha^*$. This has been proven in Proposition 3.2.1. Once $\alpha(\tau_i) \approx \alpha^*$, the eccentricity convergence can be guaranteed (note that it cannot be guaranteed before). At time τ_i, the quadratic potential in (3.26) is radially unbounded, decrescent and its time-derivative $V_e' \leq 0$ by the choice of control δ and switching scheme S_e in Eq. (3.30). Suppose $S_e(\tau) \neq 0 \; \forall \; \tau \geq \tau_i$. In this case, $V_e' < 0 \; \forall \; \tau \geq \tau_i$, which leads to $V_e \to 0$ as $\tau \to \infty$.

Let $\Pi_l = \{(\mathbf{u}, \mathbf{u}') \mid V_e \leq l^2\}$, where $l > 0$. By the invariance principle, all solutions converge to $\mathcal{M}$, the largest invariant subset in $\{(\mathbf{u}, \mathbf{u}') \in \Pi_l \mid \dot{V}_e = 0\}$, for which the only possible solution is $S_e = 0$. The proof follows by showing that $S_e = (\mathbf{u} \cdot \mathbf{u}')(\mathbf{R} \cdot \hat{\mathbf{P}}) = 0$ corresponds to the desired state $e = e^* = 0$. The value $(\mathbf{R} \cdot \hat{\mathbf{P}})$ can only become zero if $\mathbf{R} \perp \hat{\mathbf{P}}$, but recall that $\hat{\mathbf{P}}$ is perpendicular to the velocity direction $\mathbf{R}'$. Therefore $(\mathbf{R} \cdot \hat{\mathbf{P}}) = 0$ *iff* the position and velocity vectors become parallel, which can only happen if the orbit becomes unbounded. However, we are only dealing with closed orbits, therefore $(\mathbf{R} \cdot \hat{\mathbf{P}}) \neq 0 \; \forall \; \tau \geq \tau_i$. The term $(\mathbf{u} \cdot \mathbf{u}') = \frac{1}{2}\mathbf{r} \cdot \dot{\mathbf{r}} = 0$ only when $\mathbf{r} \perp \dot{\mathbf{r}}$. This will only happen at periapsis or apoapsis of the transfer orbit, *or* if the orbit is already circularized. If the spacecraft is at apoapsis or periapsis, it will only stay at zero for an infinitesimal amount of time before changing sign. On the other hand, if the orbit has already been circularized, then $e(\tau) = e^* = 0$, which is our desired condition. By LaSalle's invariance principle, any trajectory starting in Π_l remains in Π_l and asymptotically converges to the desired orbit. $\square$

When the semi-major axis is being matched, especially if using a high enough thrust, the eccentricity might become large enough to where the orbit is unbounded. This can be dealt with by adding a check point, where, during the semi-major axis matching section, the eccentricity is not allowed to get larger than a specified $e_{max} < 1$. It is possible to re-design β (which in general deals with the semi-major axis portion), such that if $\beta = 0$, $V'_\alpha = 0$, and $V'_e \leq 0$ in Eq. (3.31). This scheme can be used until the eccentricity falls below a certain threshold e_{min}, at which point the guidance scheme can be set back to the original.

During simulation, it sometimes happens that the switching function S_e in Eq. (3.30), which determines the value of the control δ, becomes small in magnitude. This can be observed in the schematic shown in Fig. 3.2. In fact, as the orbit becomes circularized, $S_e \to 0$ as time progresses. This happens because $\mathbf{u} \cdot \mathbf{u}' \to 0$ as the orbit is circularized. The switching function S_e has a sinusoidal behavior and, therefore, changes sign depending on the frequency of oscillation. Once the magnitude of S_e is within a small tolerance, $|S_e| \leq \epsilon$, any infinitesimal change in time results in a change of sign to S_e. This leads to chattering, which is undesirable due to the increase in integration time. Once this happens, a viable and effective solution is to implement δ by allowing the thrust T to be zero when the switching function changes sign. Once S_e reaches a maximum (if $S_e > 0$) or a minimum (if $S_e < 0$), the thrust can be turned on again by restarting the algorithm in Proposition 3.3.1. Note that theoretically this is not necessary, but for implementation purposes it increases the timing

performance of the integrator. This fix to avoid chattering is also potentially useful for real spacecraft guidance, and not just the integrator performance.

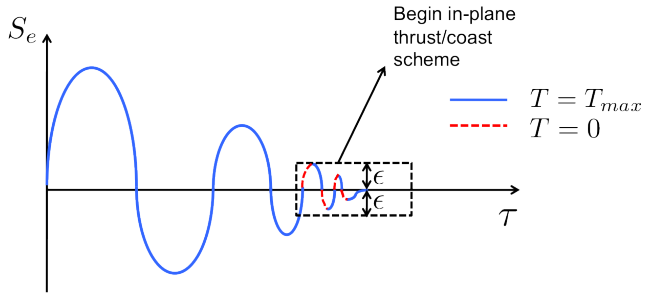

Figure 3.2: Schematic of the switching function S_e, defined in Eq. (3.30).

3.3.2 Targeting Eccentric Orbits ($0 \leq e^* < 1$)

The previous design has been derived to match $e^* = 0$, but in fact, any desired eccentricity $0 \leq e^* < 1$ can be matched by using the same control algorithm, with the following variation (an example is shown in Fig. 3.3(a)):

- If $e(\tau) > e^*$ (Achieve $V_e' \leq 0$)

$$\delta(\tau) = \begin{cases} \cos^{-1}(+1) & \text{if} \quad S_e < 0 \\ \cos^{-1}(-1) & \text{otherwise} \end{cases} \tag{3.32}$$

- If $e(\tau) < e^*$ (Achieve $V_e' \geq 0$)

$$\delta(\tau) = \begin{cases} \cos^{-1}(-1) & \text{if} \quad S_e < 0 \\ \cos^{-1}(+1) & \text{otherwise} \end{cases} \tag{3.33}$$

As an extended example, it is interesting to note that it is also possible to add thrust/coast mechanism to the algorithm. Using the same β in Eq. (3.22) and δ in Eq. (3.32), the algorithm would allow for thrusting *only*

when $V_e < 0$, and coast when $V_e \geq 0$ (even if the semi-major axis has not been previously matched), where V_e is defined in Eq. (3.26). An example of this algorithm is shown Fig. 3.3(b), which has been compared to the continuous thrust algorithm (shown in Fig. 3.3(a)). By Table 3.4 it is clear to see that the thrust/coast mechanism allows for better fuel performance solutions. In fact this result lies in the range of the heuristic Q-law algorithm [47], and comes close to the fuel-optimal final mass of 281 kg[1]. Even though effective, and more fuel-optimal is some cases, the main goal in the paper is to arrive at our desired convergence by continuous thrust and by making use of the fact that the semi-major axis convergence is asymptotic (and will never diverge).

Table 3.3: Initial and final orbital parameters for examples in Section 3.3

		a (km)	e range	i (^{o})	ω (^{o})	Ω (^{o})	T (N)	m_0 (kg)	I_{sp} (s)
Fig. 3.3	Initial Orbit	9222.7	0.2	0.00	0.00	0.00	9.3	300	3100
	Final Orbit	30000	0.7	0.00	free	free			
Fig. 3.4	Initial Orbit	30000	0.0	0.00	0.00	0.00	10	300	3100
	Final Orbit	30000	0.05,(0.1:0.1:0.9),0.99	0.00	free	free			

Table 3.4: Final mass and transfer time for example in Figure 3.3

	Continuous Thrust	Coast/Thrust Arcs
Transfer Time (days)	1.83	2.35
Final Mass (kg)	251.60	275.05

Even though the guidance scheme has been designed using the KS model, it is in fact possible to express the guidance scheme in the normal

[1]This result was taken from Reference [47], who used Mystic, and optimization software.

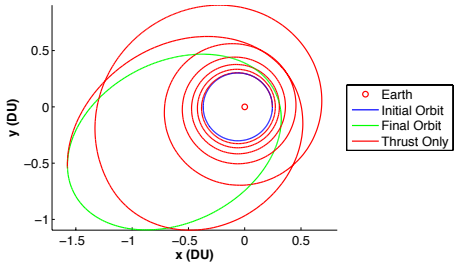

(a) x vs y transfer continuous thrust

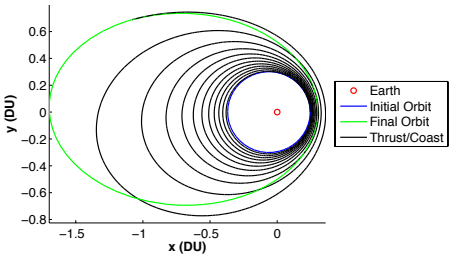

(b) x vs y transfer thrust/coast arcs

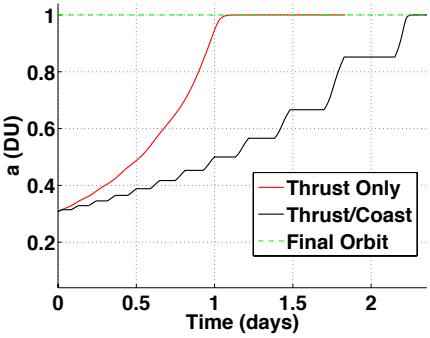

(c) Semi-major axis a vs time

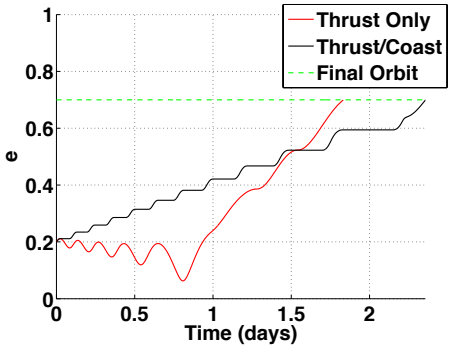

(d) Eccentricity e vs time

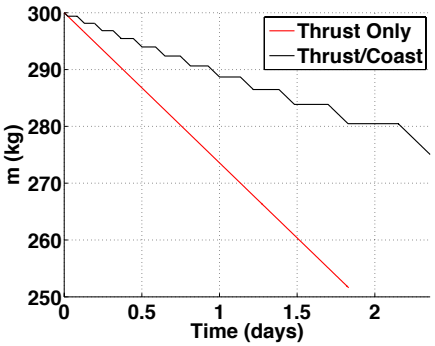

(e) Mass m vs time

Figure 3.3: Semi-major axis and eccentricity matching with parameters in Table 3.3.

(more common) two body model, where the state is position $\mathbf{r}$ and velocity $\dot{\mathbf{r}}$ (see Appendix C for the equivalent guidance scheme in the normal carte-

sian coordinates). As was mentioned in the introduction, the KS model is advantageous for propagating highly eccentric orbits. This is due to the time (Sundman) transformation, where an orbit segmented into equal time steps becomes segmented equally in position by using this model [6]. This transformation is useful to provide good resolution near periapsis, without having to take as many time steps as in the usual cartesian model. The efficiency in integration time between between each model can be seen in the example in Figure 3.4, where the desired final eccentricity was varied $0 \leq e^* < 1$ (the orbital parameters are in Table 3.3). Each solution is run 100 times, and the average machine computing time of each trajectory is plotted in Figure 3.4. From Figure 3.4 it is clear that the integration time varies linearly for both models, but the slope of the KS model is much less. In fact, when transferring to an orbit with $e^* = 0.99$ the computation time almost triples when using the cartesian coordinates vs. the KS variables.

3.4 Out-of-Plane Transfers by Holding Energy Constant

In this section we design δ to perform out-of-plane transfers. We consider three separate cases, all of which converge by holding energy constant, which occurs after the desired semi-major axis has been matched. In Section 3.4.1 we target a circular-equatorial orbit of prescribed radius. Section 3.4.2 discusses targeting the angular momentum vector, which in turn allows to transfer to any desired semi-major axis, eccentricity, inclination, and right ascension of the ascending node. The last problem we discuss is the full

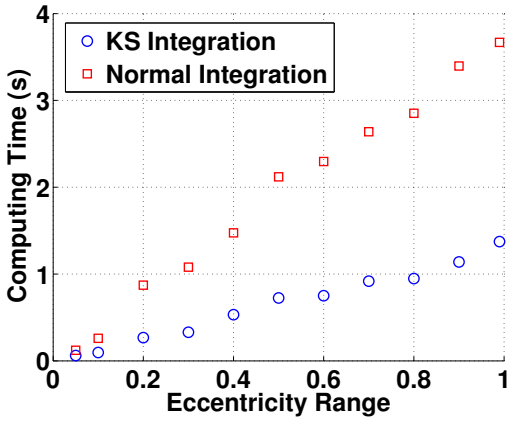

Figure 3.4: Comparison of integration time between using KS model and "normal" (cartesian) model, using parameters in Table 3.3.

orbit transfer in Section 3.4.3, which is performed by targeting the desired angular momentum vector and planar components of the eccentricity vector.

3.4.1 Transfer to a Circular Equatorial Orbit of Specified Radius

The inclination is

$$\cos i = \frac{h_3}{h} \tag{3.34}$$

where h_3 is the $\hat{\mathbf{k}}$ component of the angular momentum vector $\mathbf{h}$, and $h = \|\mathbf{h}\|$. The angular momentum magnitude is expressed as $h = \sqrt{\mu a(1-e^2)}$ and its

vector $\mathbf{h} = \mathbf{r} \times \dot{\mathbf{r}}$. The third component of $\mathbf{h}$ in KS variables is

$$\begin{aligned} h_3 &= r_1\dot{r}_2 - r_2\dot{r}_1 = \begin{bmatrix} r_1 & r_2 \end{bmatrix} \begin{bmatrix} 0 & 1 \\ -1 & 0 \end{bmatrix} \begin{bmatrix} \dot{r}_1 \\ \dot{r}_2 \end{bmatrix} = \mathbf{r}^T \begin{bmatrix} 0 & 1 & 0 \\ -1 & 0 & 0 \\ 0 & 0 & 0 \end{bmatrix} \dot{\mathbf{r}} \\ &= [\mathcal{L}(\mathbf{u})\mathbf{u}]^T \mathbf{Y}_C \left[\frac{2}{r}\mathcal{L}(\mathbf{u})\mathbf{u}'\right] \\ &= \frac{2}{r}\mathbf{u}^T \left(\mathcal{L}^T(\mathbf{u})\mathbf{Y}_C\mathcal{L}(\mathbf{u})\right)\mathbf{u}' \\ &= \frac{2}{r}\mathbf{u}^T\mathbf{C}\mathbf{u}' \end{aligned} \tag{3.35}$$

where $\mathbf{C} = \mathcal{L}^T(\mathbf{u})\mathbf{Y}_C\mathcal{L}(\mathbf{u})$ and

$$\mathbf{Y}_C = \left[\begin{array}{ccc|c} 0 & 1 & 0 & \\ -1 & 0 & 0 & \mathbf{0}^T \\ 0 & 0 & 0 & \\ \hline & \mathbf{0} & & 0 \end{array}\right] \tag{3.36}$$

The matrix $\mathbf{C}$ is skew-symmetric, $\mathbf{C} = -\mathbf{C}^T$ and a function of the position components of $\mathbf{u}$.

$$\mathbf{C} = \begin{bmatrix} 0 & a & -b & -c \\ -a & 0 & c & -b \\ b & -c & 0 & d \\ c & b & -d & 0 \end{bmatrix} \quad \text{where} \quad \begin{aligned} a &= u_1^2 + u_2^2 \\ b &= u_1u_4 - u_2u_3 \\ c &= u_1u_3 + u_2u_4 \\ d &= u_3^2 + u_4^2 \end{aligned} \tag{3.37}$$

The time-derivative of h_3 is

$$\begin{aligned} h_3' &= \frac{2}{r}\left(\mathbf{u}'^T\mathbf{C}\mathbf{u}' + \mathbf{u}^T\mathbf{C}'\mathbf{u}' + \mathbf{u}^T\mathbf{C}\mathbf{u}''\right) + \frac{2}{r^3}(\mathbf{r}\cdot\mathbf{r}')\mathbf{u}^T\mathbf{C}\mathbf{u}' \\ &= \frac{2}{r}\left[-\frac{\mu}{4}\alpha\mathbf{u}^T\mathbf{C}\mathbf{u} + \mathbf{u}'^T\mathbf{C}\mathbf{u}' + \mathbf{u}^T(\mathbf{C}' - 2(\mathbf{u}\cdot\mathbf{u}')C)\mathbf{u}' + \frac{r}{2}\mathbf{u}^T\mathbf{C}\mathcal{L}^T(\mathbf{u})\mathbf{F}\right] \end{aligned}$$

Note that because $\mathbf{C}$ is skew-symmetric, for any vector $\mathbf{x} \in \mathbb{R}^4$, $\mathbf{x}^T\mathbf{C}\mathbf{x} = \mathbf{0}$. Therefore, the first two terms in h_3' vanish. The third term in h_3', $\mathbf{u}^T(\mathbf{C}' -$

$2(\mathbf{u}\cdot\mathbf{u}')C)\mathbf{u}'$, also vanishes. Therefore, the time-derivative of h_3 is

$$h_3' = \mathbf{u}^T\mathbf{C}\mathcal{L}^T(\mathbf{u})\mathbf{F} = -\left(\mathcal{L}(\mathbf{u})\mathbf{C}\mathbf{u}\right)\cdot\mathbf{F} \tag{3.38}$$

The quadratic candidate function

$$V_i = \frac{1}{2}(h_3 - h_3^*)^2 \tag{3.39}$$

is minimized when $h_3 = h_3^*$. For a desired equatorial orbit, $h_3^* = h^*$ and the other two component of the angular momentum will be zero. In fact, by targeting h_3^*, we are in turn targeting $i = 0^*$, as well as also ensuring convergence on the magnitude of angular momentum, which in turn targets the eccentricity $e^* = 0$.

Defining the 4-dimensional vector

$$\mathbf{Q}_i = (h_3 - h_3^*)\mathcal{L}(\mathbf{u})\mathbf{C}\mathbf{u} \tag{3.40}$$

the time derivative of V_i' is

$$\begin{aligned} V_i' &= (h_3 - h_3^*)h_3' \\ &= -(h_3 - h_3^*)\left[(\mathcal{L}(\mathbf{u})\mathbf{C}\mathbf{u})\cdot\mathbf{F}\right] \\ &= -\frac{T}{m}\mathbf{Q}_i\cdot\left[\sin\beta\hat{\mathbf{R}}' + \cos\beta\cos\delta\hat{\mathbf{P}} + \cos\beta\sin\delta\hat{\mathbf{H}}\right] \end{aligned} \tag{3.41}$$

Note, that if the semi-major axis of the desired orbit has already been matched to a^* (to within a certain tolerance), the angle $\beta \approx 0$. The time derivative

$$V_i' = -\frac{T}{m}\mathbf{Q}_i\cdot\left[\cos\delta\hat{\mathbf{P}} + \sin\delta\hat{\mathbf{H}}\right] \tag{3.42}$$

We design δ to make $\left(\cos\delta\hat{\mathbf{P}} + \sin\delta\hat{\mathbf{H}}\right)$ in Eq. (3.42) lie in the same direction as $\mathbf{Q}_i$, which will result in $V_i' \leq 0$. Because the fourth component of $\hat{\mathbf{P}}$ and $\hat{\mathbf{H}}$ are null, we are only interested in aligning to the first three components of $\mathbf{Q}_i$. Defining

$$\mathbf{q}_i = \mathbf{Q}_{i_{1:3}} \tag{3.43}$$

The vector $\mathbf{q}_i$ can be written in two separate components: $\mathbf{q}_{\hat{\mathbf{p}}-\hat{\mathbf{h}}}$, which lies in the plane formed by $\hat{\mathbf{p}} - \hat{\mathbf{h}}$, and $\mathbf{q}_{\hat{\mathbf{r}'}}$, which is perpendicular to this plane (i.e., lies in the direction of $\hat{\mathbf{r}'}$), see Figure 3.5. The time-derivative of V_i in Eq. (3.42) becomes

$$\begin{aligned} V_i' &= -\frac{T}{m}\left[\mathbf{q}_i \cdot \left(\cos\delta\hat{\mathbf{p}} + \sin\delta\hat{\mathbf{h}}\right)\right] \\ &= -\frac{T}{m}\left[\left(\mathbf{q}_{\hat{\mathbf{p}}-\hat{\mathbf{h}}} + \mathbf{q}_{\hat{\mathbf{r}'}}\right) \cdot \left(\cos\delta\hat{\mathbf{p}} + \sin\delta\hat{\mathbf{h}}\right)\right] \\ &= -\frac{T}{m}\left[\left(q_{\hat{\mathbf{p}}-\hat{\mathbf{h}}}\hat{\mathbf{q}}_{\hat{\mathbf{p}}-\hat{\mathbf{h}}}\right) \cdot \left(\cos\delta\hat{\mathbf{p}} + \sin\delta\hat{\mathbf{h}}\right)\right] \end{aligned}$$

where $q_{\hat{\mathbf{p}}-\hat{\mathbf{h}}} = \|\mathbf{q}_{\hat{\mathbf{p}}-\hat{\mathbf{h}}}\|$. By designing δ as

$$\delta = \tan^{-1}\left(\frac{\hat{\mathbf{q}}_{\hat{\mathbf{p}}-\hat{\mathbf{h}}} \cdot \hat{\mathbf{h}}}{\hat{\mathbf{q}}_{\hat{\mathbf{p}}-\hat{\mathbf{h}}} \cdot \hat{\mathbf{p}}}\right) = \tan^{-1}\left(\frac{\mathbf{Q}_i \cdot \hat{\mathbf{H}}}{\mathbf{Q}_i \cdot \hat{\mathbf{P}}}\right) \tag{3.44}$$

results in

$$V_i' = -\frac{T}{m}\left[(\mathbf{Q}_i \cdot \hat{\mathbf{P}})^2 + (\mathbf{Q}_i \cdot \hat{\mathbf{H}})^2\right] \leq 0 \tag{3.45}$$

The proof of the full convergence is performed in two steps. First, a matching of the target semi-major axis a^*, by means of using β in Eq. (3.22). Recall, that the other spherical angle δ does not affect the semi-major axis

convergence. For this reason, we choose δ as in Eq. (3.44), which does not necessarily guarantee the negative semi-definiteness of V_i', *until* $a \approx a^*$. The second step, once the semi-major axis is converged to the desired one (to within a certain tolerance ϵ_a), involves converging the eccentricity and inclination to $e^* = 0$ and $i^* = 0$, by means of using the same δ.

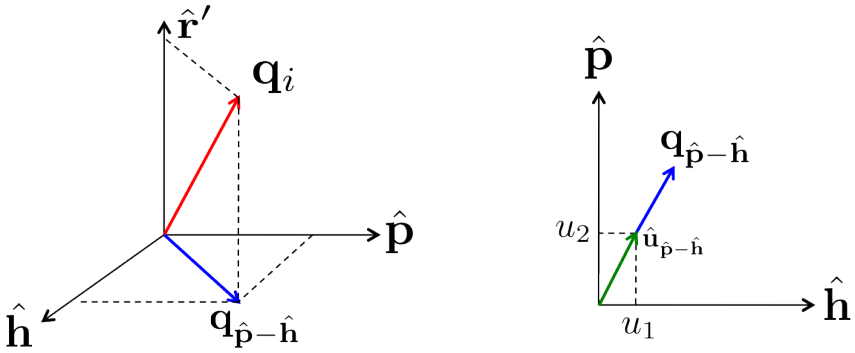

Figure 3.5: Representation of the vector $\mathbf{q}_i$ and its components.

Proposition 3.4.1. ***Targeting a Circular Equatorial Orbit:*** *Let a spacecraft with a constant available thrust T and initial mass m_0 be on any closed orbit. All solutions governed by the force model in Eq. (3.12) with thrust vector in Eq. (3.18) and mass varying according to Eq. (3.16), converge to a circular ($e^* = 0$), equatorial ($i^* = 0$), orbit with a prescribed semi-major axis a^*, when the control angles β and δ are chosen as in Eq. (3.22) and Eq. (3.44), respectively, and $\mathbf{Q}_i$ is defined in Eq. (3.40).*

Proof. Control angle β ensures semi-major axis convergence, which occurs once $\alpha(\tau_i) \approx \alpha^*$ (this has been shown in the proof of Proposition 3.2.1). At time τ_i, the quadratic potential V_i is radially unbounded, decrescent and its

time-derivative $V_i' \leq 0$ by the choice of control δ. Let $\Pi_l = \{(\mathbf{u}, \mathbf{u}') \mid V_i \leq l^2\}$, where $l > 0$. By the invariance principle, all solutions converge to $\mathcal{M}$, the largest invariant subset in $\{(\mathbf{u}, \mathbf{u}') \in \Pi_l \mid \dot{V}_i = 0\}$, for which solutions of $\mathcal{N} = \left[(\mathbf{Q}_i \cdot \hat{\mathbf{P}})^2 + (\mathbf{Q}_i \cdot \hat{\mathbf{H}})^2\right] = 0$ (from Eq. (3.45)) need to be examined. First, if $\mathbf{Q}_i \neq 0$, $\mathcal{N} = 0$ implies that $\mathbf{Q}_i$ does not have a projection in either the $\hat{\mathbf{P}}$ or $\hat{\mathbf{H}}$ frame, i.e. $\mathbf{Q}_i$ points solely in the velocity direction. In this case, regardless of the choice of δ, the time-derivative of the potential $V_i' = 0$. However, $\mathbf{Q}_i$ changes direction constantly since is a function of the sinusoidal vector $\mathbf{u}$, ensuring that $\mathcal{N}$ will not stay at zero indefinitely. On the other hand, if $\mathbf{Q}_i = 0$, the only possible solution is for $h_3 = h_3^*$, which is the desired orbit. By LaSalle's invariance principle, any trajectory starting in Π_l remains in Π_l and asymptotically converges to the desired orbit. □

An example simulation is shown in Figure 3.6 with initial and final parameters given in Table 3.6. The semi-major axis matching is asymptotic, and once it converges it does not diverge. The eccentricity and inclination are not matched until the semi-major axis has converged. The final results of flight time and propellant are shown in Table 3.5 and compared to two other closed-loop solutions, which are more optimal in both time and propellant than the algorithm presented here[1].

[1]Results of these two methods are taken from an example in Reference [23]. The Q-Law [47] is another closed-loop solution that uses Lyapunov stability theory based on Lagrange's planetary equation. The Q-Law, however, is singular at $i = 0$ and $e = 0$, and therefore, cannot fully target these values.

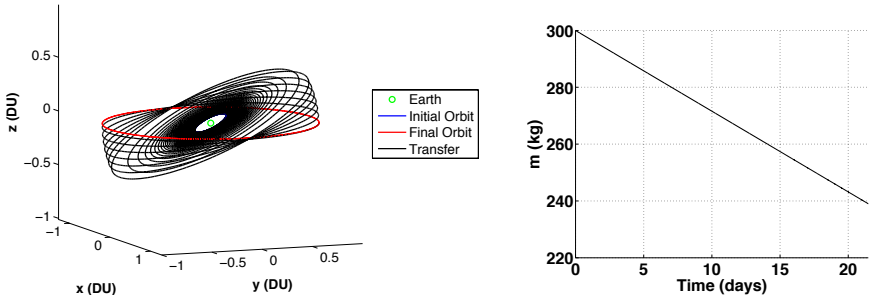

(a) Trajectory in 3D (b) Mass vs time

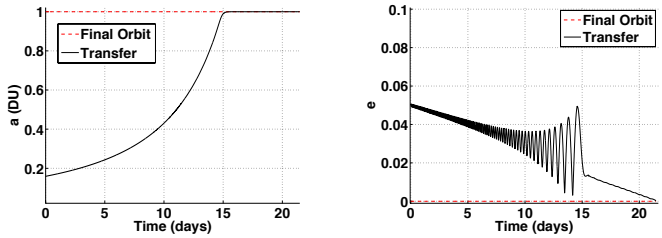

(c) Semi-major axis vs time (d) Eccentricity vs time

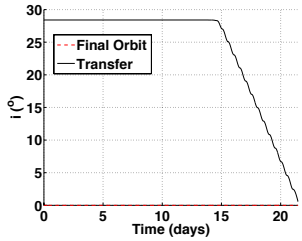

(e) Inclination vs time

Figure 3.6: Orbit transfer to a circular equatorial orbit with initial parameters in Table 3.6

For numerical implementation purposes, as h_3 approaches h_3^*, the vector $\mathbf{Q}_i \to 0$, making the variable step size integration slow down when defining δ in Eq. (3.44). To work around this issue, we have developed a switching scheme algorithm, that will begin a coast phase ($T = 0$) once $\|\mathbf{Q}_i\| \approx 0$. For implementation purposes, this occurs once $\|\mathbf{Q}_i\| \leq \epsilon_q$, where ϵ_q is some small

Table 3.5: Propellant used and flight time for the example in Figure 3.6

Control Law	Proposed	Optimal [16]	Q-law [47]
Propellant (kg)	60.10	49.69	56.62
Flight Time (days)	21.43	17.48	19.92

Table 3.6: Initial and final orbital parameters for the examples in Section 3.4

	Orbit	a (km)	e	i (^{o})	ω (^{o})	Ω (^{o})	T(N)	m_0 (kg)	I_{sp} (s)	Central Body
Fig. 3.6	Initial	6,700	0.05	28.40	0.00	0.00	1	300	3100	Earth
	Final	42,100	0.00	0.00	–	–				
Fig. 3.7	Initial	20,000	0.7	40.00	20.00	0.00	10	300	3100	Earth
	Final	40,000	0.0	0.00	–	–				
Fig. 3.8	Initial	6,700	0.2	40.00	0.00	0.00	0.25	1000	2000	Earth
	Final	41,000	0.0	0.00	–	–				
Fig. 3.9	Initial	1200	0.3	30.00	0.00	0.00	0.091	1000	3100	Ceres
	Final	500	0.6	50.00	free	50				
Fig. 3.10	Initial	20000	0.0	0.00	0.00	0.00	10	1000	3000	Earth
	Final	20000	0.8	60.00	-70	30				

enough number. An effective solution is to implement the switching function by allowing for coast arcs when $\|\mathbf{Q}_i\| \leq \epsilon_q$, which will cause $\|\mathbf{Q}_i\|$ to increase in value. The idea is to coast until $\|\mathbf{Q}_i\|$ reaches a maximum. At this point, the thrusting protocol can be re-started, which will lead $\|\mathbf{Q}_i\|$ to get closer to zero. A schematic of this behavior is shown in the next example, in Fig. 3.7 (f).

The full algorithm can be summarized in the following way

1. While $\|\mathbf{Q}_i\| > \epsilon_q$

$$\begin{aligned} T &= T_{max} \\ \beta &= \sin^{-1}(Ke_\alpha) \\ \delta &= \tan^{-1}\left(\frac{\mathbf{Q}_i \cdot \hat{\mathbf{H}}}{\mathbf{Q}_i \cdot \hat{\mathbf{P}}}\right) \end{aligned} \tag{3.46}$$

2. If $\|\mathbf{Q}_i\| \leq \epsilon_q$ and *until* $\|\mathbf{Q}_i\|$ reaches a maximum

$$T = 0 \tag{3.47}$$

where ϵ_q is an input parameter by the user.

An example simulation is shown in Fig. 3.7 with initial and final parameters given in Tab. 3.6. The transfer takes 2.35 days and the final mass is $m_f = 254.3$ kg. As can be observed, towards the end of the transfer, $\|\mathbf{Q}_i\|$ becomes small enough that it starts slowing down the integrator performance, which is why the algorithm in Eq. (3.47) is implemented, by allowing for two coast arcs.

The examples shown up to now are useful mostly for academic purposes, because the engine parameters used are still unavailable for realistic spacecraft applications. A GTO to GEO example with more realistic engine parameters is shown in Fig. 3.8 with initial and final parameters given in Tab. 3.6. The engine parameters used here are representative of a BPT-4000 Hall thruster. The final mass of the spacecraft is $m_f = 668$ kg. The results shown verify that the algorithm presented in this dissertation is also valid for realistic engine parameters and orbit transfers.

3.4.2 Targeting Angular Momentum Vector

Targeting the angular momentum vector $\mathbf{h}^* = [h_1^* \; h_2^* \; h_3^*]$ by holding energy constant (or holding a^* constant) is equivalent to matching three orbital elements: eccentricity e^*, inclination i^*, and right ascension of the ascending

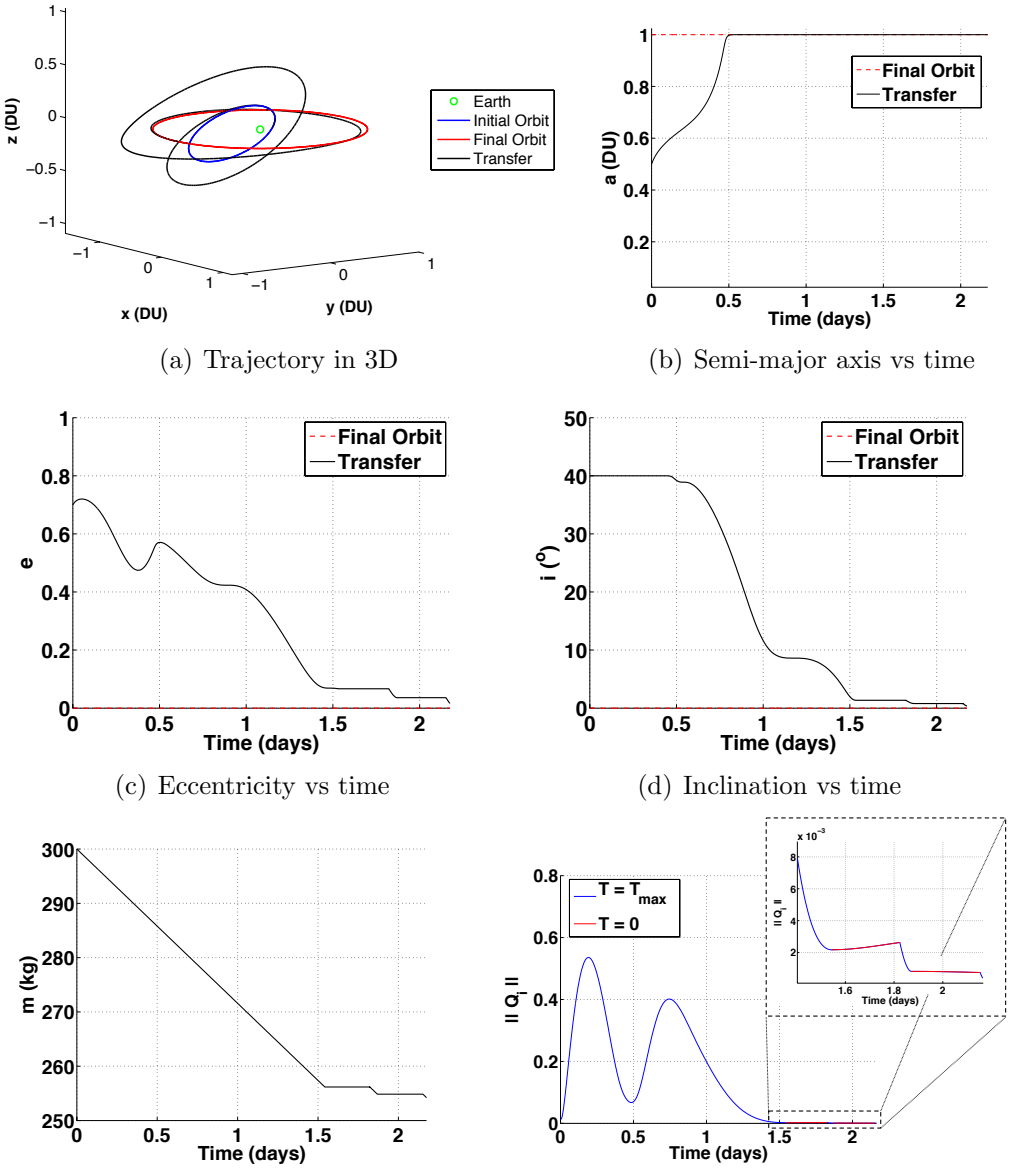

(a) Trajectory in 3D

(b) Semi-major axis vs time

(c) Eccentricity vs time

(d) Inclination vs time

(e) Mass vs time

(f) Norm of $\mathbf{Q}_i$ vs time

Figure 3.7: Orbit transfer to a circular equatorial orbit with initial parameters in Table 3.6.

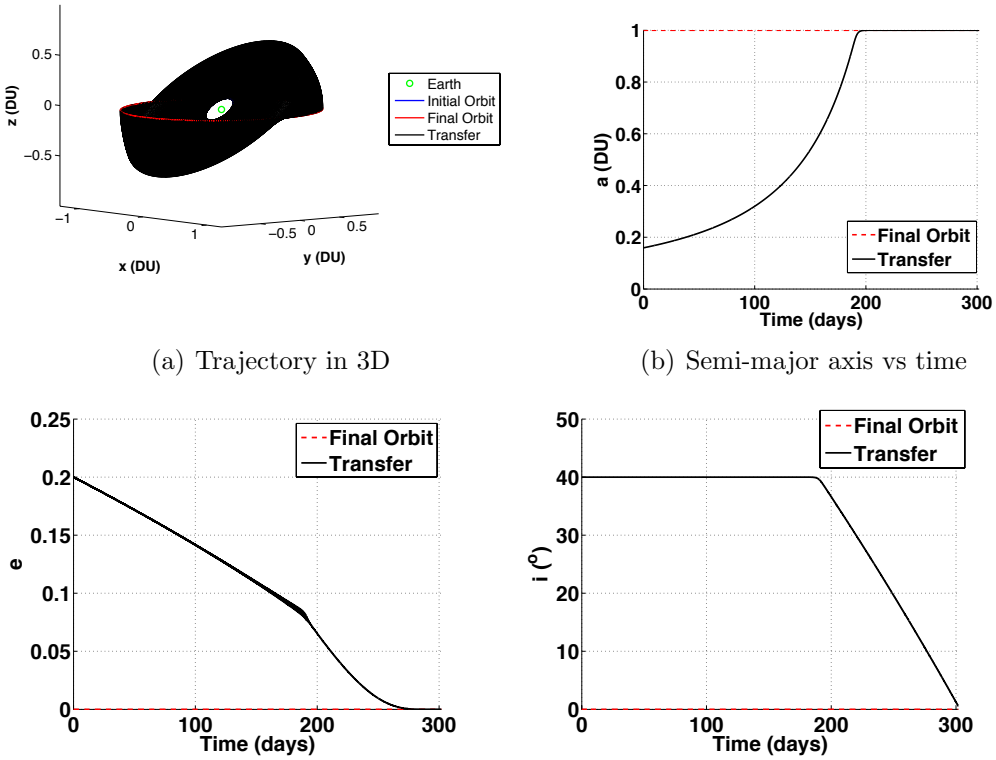

(a) Trajectory in 3D

(b) Semi-major axis vs time

(c) Eccentricity vs time

(d) Inclination vs time

Figure 3.8: Orbit transfer to a circular equatorial orbit with initial parameters in Table 3.6.

node Ω^*.[1]

The three-dimensional angular momentum vector $\mathbf{h} = \mathbf{r} \times \mathbf{v} = [h_1\ h_2\ h_3]$. The h_3 component in KS variables was derived in Eq. (3.35). Similarly, the

[1]Note that the algorithm derived here targets the components of $\mathbf{h}^*$. However, if the user knows the desired orbital elements e^*, i^*, and Ω^*, by any well-known algorithm to transform from orbital elements to cartesian coordinates, the vector $\mathbf{h}^*$ can be obtained.

components of the angular momentum are derived in KS variables to give

$$h_1 = r_2\dot{r}_3 - r_3\dot{r}_2 = \frac{2}{r}\mathbf{u}^T\mathbf{A}\mathbf{u}' \tag{3.48}$$

$$h_2 = r_3\dot{r}_1 - r_1\dot{r}_3 = \frac{2}{r}\mathbf{u}^T\mathbf{B}\mathbf{u}' \tag{3.49}$$

$$h_3 = r_1\dot{r}_2 - r_2\dot{r}_1 = \frac{2}{r}\mathbf{u}^T\mathbf{C}\mathbf{u}' \tag{3.50}$$

where

$$\begin{aligned} \mathbf{A} &= \mathcal{L}^T(\mathbf{u})\mathbf{Y}_A\mathcal{L}(\mathbf{u}) \\ \mathbf{B} &= \mathcal{L}^T(\mathbf{u})\mathbf{Y}_B\mathcal{L}(\mathbf{u}) \\ \mathbf{C} &= \mathcal{L}^T(\mathbf{u})\mathbf{Y}_C\mathcal{L}(\mathbf{u}) \end{aligned} \tag{3.51}$$

$$\mathbf{Y}_A = \left[\begin{array}{ccc|c} 0 & 0 & 0 & \\ 0 & 0 & 1 & \mathbf{0}^T \\ 0 & -1 & 0 & \\ \hline \multicolumn{3}{c|}{\mathbf{0}} & 0 \end{array}\right], \mathbf{Y}_B = \left[\begin{array}{ccc|c} 0 & 0 & -1 & \\ 0 & 0 & 0 & \mathbf{0}^T \\ 1 & 0 & 0 & \\ \hline \multicolumn{3}{c|}{\mathbf{0}} & 0 \end{array}\right], \mathbf{Y}_C = \left[\begin{array}{ccc|c} 0 & 1 & 0 & \\ -1 & 0 & 0 & \mathbf{0}^T \\ 0 & 0 & 0 & \\ \hline \multicolumn{3}{c|}{\mathbf{0}} & 0 \end{array}\right] \tag{3.52}$$

and $\mathbf{0} = [0\ 0\ 0]$. The matrices $\mathbf{A}$, $\mathbf{B}$, and $\mathbf{C}$ are all skew-symmetric.

The derivation of the time-derivative of the components of $\mathbf{h}$ follow similarly as h_3' in Eq. (3.38),

$$\begin{aligned} h_1' &= -\left(\mathcal{L}(\mathbf{u})\mathbf{A}\mathbf{u}\right)\cdot\mathbf{F} \\ h_2' &= -\left(\mathcal{L}(\mathbf{u})\mathbf{B}\mathbf{u}\right)\cdot\mathbf{F} \\ h_3' &= -\left(\mathcal{L}(\mathbf{u})\mathbf{C}\mathbf{u}\right)\cdot\mathbf{F} \end{aligned} \tag{3.53}$$

The quadratic candidate function

$$V_h = \frac{1}{2}(\mathbf{h} - \mathbf{h}^*)^T(\mathbf{h} - \mathbf{h}^*) \tag{3.54}$$

is minimized when the angular momentum vector $\mathbf{h}$ matches the desired $\mathbf{h}^* = [h_1^*\ h_2^*\ h_3^*]$. Defining the 4-dimensional vector

$$\mathbf{Q}_h = (h_1 - h_1^*)\left(\mathcal{L}(\mathbf{u})\mathbf{A}\mathbf{u}\right) + (h_2 - h_2^*)\left(\mathcal{L}(\mathbf{u})\mathbf{B}\mathbf{u}\right) + (h_3 - h_3^*)\left(\mathcal{L}(\mathbf{u})\mathbf{C}\mathbf{u}\right) \tag{3.55}$$

the time derivative of V_h' is

$$\begin{aligned} V_h' &= (\mathbf{h} - \mathbf{h}^*)^T\mathbf{h}' \\ &= (h_1 - h_1^*)h_1' + (h_2 - h_2^*)h_2' + (h_3 - h_3^*)h_3' \\ &= -\frac{T}{m}\mathbf{Q}_h \cdot \mathbf{F} \\ &= -\frac{T}{m}\mathbf{Q}_h \cdot \left[\sin\beta\hat{\mathbf{R}}' + \cos\beta\cos\delta\hat{\mathbf{P}} + \cos\beta\sin\delta\hat{\mathbf{H}}\right] \end{aligned} \tag{3.56}$$

If the semi-major axis of the desired orbit has already been matched to a^* (to within a certain tolerance), the angle $\beta \approx 0$. The time derivative

$$V_h' = -\frac{T}{m}\mathbf{Q}_h \cdot \left[\cos\delta\hat{\mathbf{P}} + \sin\delta\hat{\mathbf{H}}\right] \tag{3.57}$$

At this point the time-derivative of V_h' looks equivalent to V_i' in Eq. (3.42), with the exception of $\mathbf{Q}_h$ term versus $\mathbf{Q}_i$. Therefore, the exact same theoretical solution follows and δ is designed as

$$\delta = \tan^{-1}\left(\frac{\mathbf{Q}_h \cdot \hat{\mathbf{H}}}{\mathbf{Q}_h \cdot \hat{\mathbf{P}}}\right) \tag{3.58}$$

where $\mathbf{Q}_h$ is in Eq. (3.55). This ensures $V_h' \leq 0$.

Proposition 3.4.2. ***Targeting*** $\mathbf{a}^*$, $\mathbf{e}^*$, $\mathbf{i}^*$, $\mathbf{\Omega}^*$**:** *Let a spacecraft with a constant available thrust T and initial mass m_0 be on any closed orbit. All solutions governed by the force model in Eq. (3.12) with thrust vector in Eq. (3.18)*

and mass varying according to Eq. (3.16), converge to an orbit with prescribed semi-major axis a^*, eccentricity e^*, inclination i^*, and right ascension of the ascending node Ω^*, when the control angles β and δ are chosen as in Eq. (3.22) and Eq. (3.58), respectively, and $\mathbf{Q}_h$ is defined in Eq. (3.55).

Proof. The proof follows identically to the proof in Proposition 3.4.1. □

A simulation of a spacecraft around Ceres (which is assumed to be spherical) using low-thrust is shown in Figure 3.9, with initial and final parameters in Table 3.6. The algorithm targets first the desired semi-major axis (Figure 3.9(a)), and then the three components of angular momentum vector (Figure 3.9(b)). Equivalently, the three orbital elements e^*, i^*, and Ω^* are matched as shown in Figure 3.9(c-e). The transfer time is 60.70 days and the propellant used is 15.70 kg.

3.4.3 Targeting Angular Momentum and Eccentricity Vectors

We are now interested in doing a full orbit transfer, by matching five orbital elements: semi-major axis a^*, eccentricity e^*, inclination i^*, right ascension of the ascending node Ω^*, and the argument of periapsis ω^*. This is equivalent to matching the angular momentum vector $\mathbf{h}^*$ and the first two components of the eccentricity vector $\mathbf{e}^*$.

The eccentricity vector

$$\mathbf{e} = \frac{1}{\mu}\dot{\mathbf{r}} \times \mathbf{h} - \frac{1}{r}\mathbf{r} \tag{3.59}$$

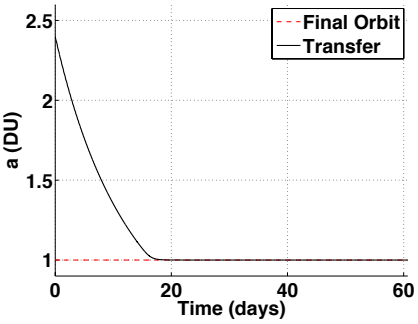

(a) Semi-major axis a vs time

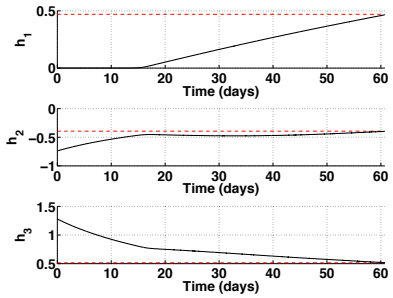

(b) Angular momentum $\mathbf{h}$ vs time

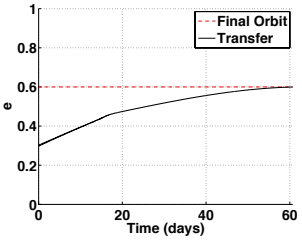

(c) Eccentricity e vs time

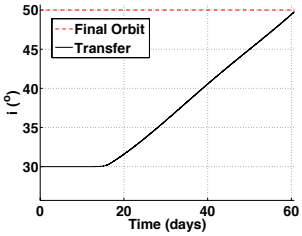

(d) Inclination i vs time

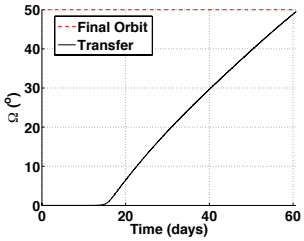

(e) Right ascension of ascending node Ω vs time

Figure 3.9: Semi-major axis and angular momentum matching around Ceres ($\mu = 63.1$ km^3/s^2), with parameters in Table 3.6.

can be written in components in KS variables as

$$e_1 = \frac{1}{r}\left(\frac{1}{\mu}\mathbf{R}'^T\mathbf{Y}_A\mathbf{H} - r_1\right) \tag{3.60}$$

$$e_2 = \frac{1}{r}\left(\frac{1}{\mu}\mathbf{R}'^T\mathbf{Y}_B\mathbf{H} - r_2\right) \tag{3.61}$$

$$e_3 = \frac{1}{r}\left(\frac{1}{\mu}\mathbf{R}'^T\mathbf{Y}_C\mathbf{H} - r_3\right) \tag{3.62}$$

where $\mathbf{R}'$ is in Eq. (2.7), the components r_1, r_2, and r_3 are defined in Eq. (3.5), and

$$\mathbf{H} = [h_1\ h_2\ h_3\ 0]^T \tag{3.63}$$

where h_1, h_2, and h_3 is defined in Eq. (3.48), (3.49), and (3.50) respectively.

Taking the time-derivative in τ of each component of the eccentricity vector

$$e_1' = \frac{1}{\mu}\left[r\mathbf{Y}_A\mathbf{H} - \frac{1}{r}\mathcal{L}(\mathbf{u})\left(r_2'\mathbf{C} - r_3'\mathbf{B}\right)\mathbf{u}\right]\cdot\mathbf{F} \tag{3.64}$$

$$e_2' = \frac{1}{\mu}\left[r\mathbf{Y}_B\mathbf{H} - \frac{1}{r}\mathcal{L}(\mathbf{u})\left(r_3'\mathbf{A} - r_1'\mathbf{C}\right)\mathbf{u}\right]\cdot\mathbf{F} \tag{3.65}$$

$$e_3' = \frac{1}{\mu}\left[r\mathbf{Y}_C\mathbf{H} - \frac{1}{r}\mathcal{L}(\mathbf{u})\left(r_1'\mathbf{B} - r_2'\mathbf{A}\right)\mathbf{u}\right]\cdot\mathbf{F} \tag{3.66}$$

where $\mathbf{A}$, $\mathbf{B}$, and $\mathbf{C}$ are defined in Eq. (3.51), and r_1', r_2', r_3' are the first three components of $\mathbf{R}'$.

The quadratic candidate function

$$V_o = \frac{1}{2}(\mathbf{h} - \mathbf{h}^*)^T(\mathbf{h} - \mathbf{h}^*) + \frac{1}{2}(e_1 - e_1^*)^2 + \frac{1}{2}(e_2 - e_2^*)^2 \tag{3.67}$$

is minimized when the angular momentum vector $\mathbf{h}$ matches the desired $\mathbf{h}^* = [h_1^*\ h_2^*\ h_3^*]$ and the two components of the eccentricity vector e_1^* and e_2^*. Defining

the 4-dimensional vector

$$\begin{aligned}\mathbf{Q}_o = \quad & \mathbf{Q}_h - (e_1 - e_1^*)\left[r\mathbf{Y}_A\mathbf{H} - \frac{1}{r}\mathcal{L}(\mathbf{u})\left(r_2'\mathbf{C} - r_3'\mathbf{B}\right)\mathbf{u}\right] \\ - \quad & (e_2 - e_2^*)\left[r\mathbf{Y}_B\mathbf{H} - \frac{1}{r}\mathcal{L}(\mathbf{u})\left(r_3'\mathbf{A} - r_1'\mathbf{C}\right)\mathbf{u}\right] \end{aligned} \tag{3.68}$$

If the semi-major axis of the desired orbit has already been matched to a^* (to within a certain tolerance), the angle $\beta \approx 0$. The time derivative

$$V_o' = -\frac{T}{m}\mathbf{Q}_o \cdot \left[\cos\delta\hat{\mathbf{P}} + \sin\delta\hat{\mathbf{H}}\right] \tag{3.69}$$

At this point the time-derivative of V_o' looks equivalent to V_i' in Eq. (3.42), with the exception of $\mathbf{Q}_o$ term versus $\mathbf{Q}_i$. Therefore, the exact same theoretical solution follows and δ is designed as

$$\delta = \tan^{-1}\left(\frac{\mathbf{Q}_o \cdot \hat{\mathbf{H}}}{\mathbf{Q}_o \cdot \hat{\mathbf{P}}}\right) \tag{3.70}$$

where $\mathbf{Q}_o$ is defined in Eq. (3.68). This ensures $V_o' \leq 0$.

Proposition 3.4.3. ***Targeting*** $\mathbf{a}^*$**,** $\mathbf{e}^*$**,** $\mathbf{i}^*$**,** $\boldsymbol{\omega}^*$**,** $\boldsymbol{\Omega}^*$**:** *Let a spacecraft with a constant available thrust T and initial mass m_0 be on any closed orbit. All solutions governed by the force model in Eq. (3.12) with thrust vector in Eq. (3.18) and mass varying according to Eq. (3.16), converge to an orbit with prescribed semi-major axis a^*, eccentricity e^*, inclination i^*, right ascension of the ascending node Ω^*, and argument of periapsis ω^* when the control angles β and δ are chosen as in Eq. (3.22) and Eq. (3.70), respectively, and $\mathbf{Q}_o$ is defined in Eq. (3.68).*

Proof. The proof follows equivalently to the proof in Proposition 3.4.1. □

Note that the algorithm derived here targets the components of $\mathbf{h}^*$, e_1^*, and e_2^*. However, if the desired orbital elements a^*, e^*, i^*, ω^*, and Ω^* are known, by any well-known algorithm to transform from orbital elements to cartesian coordinates, the vectors $\mathbf{h}^*$ and $\mathbf{e}^*$ can be obtained.

A low-thrust simulation of a spacecraft around Earth to perform a full orbit transfer is shown in Figure 3.10 with initial and final parameters in Table 3.6. The initial semi-major axis is already the desired a^*, therefore, the full transfer is performed by holding $a(\tau)$ constant throughout the transfer. All the orbital elements over time are shown in Figure 3.10(b-f). Equivalently, the three components of angular momentum are shown in Figure 3.11(a) and the two components of eccentricity in Figure 3.11(b). The transfer takes 9.46 days and the final mass is 724.1 kg.

3.5 Final Remarks

We take on a new approach to the problem of finite-thrust orbit transfers by working in a transformed model to design Lyapunov-based control laws. The model is the Kustaanheimo-Stiefel (KS) transformation of the two-body model, in which both time and position coordinates are transformed to a new model. This model is advantageous for propagating close encounter-type problems as well as highly eccentric orbits. It can greatly reduce the integration time when compared to using the original two-body equations of motion

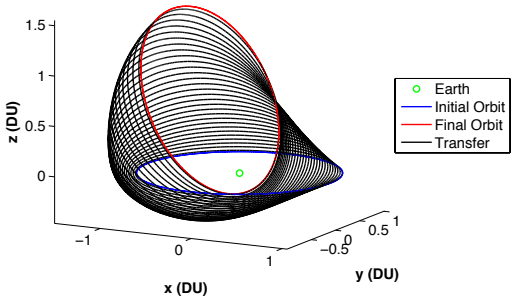

(a) Trajectory in 3D

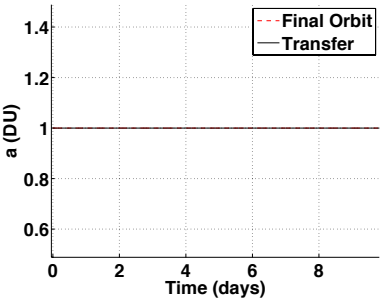

(b) Semi-major axis a vs time

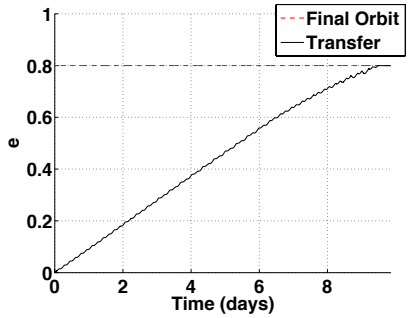

(c) Eccentricity e vs time

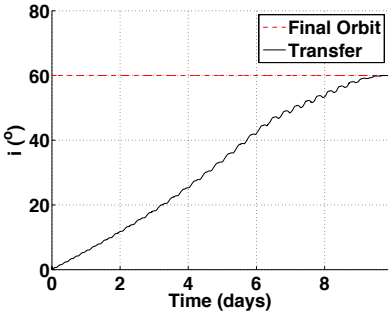

(d) Inclination i vs time

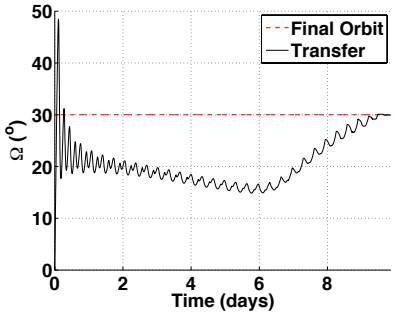

(e) Right ascension of ascending node Ω vs time

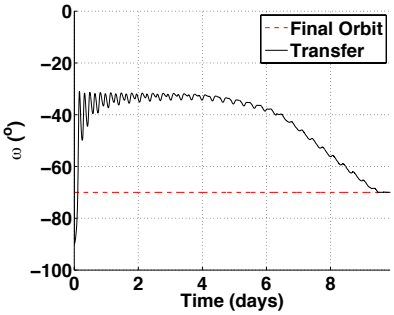

(f) Argument of Periapsis ω vs time

Figure 3.10: Full orbit transfer with initial parameters in Table 3.6.

(even though 9 variables are needed to be integrated in KS variables versus 6 in the two-body problem). We take advantage of the KS model to design the

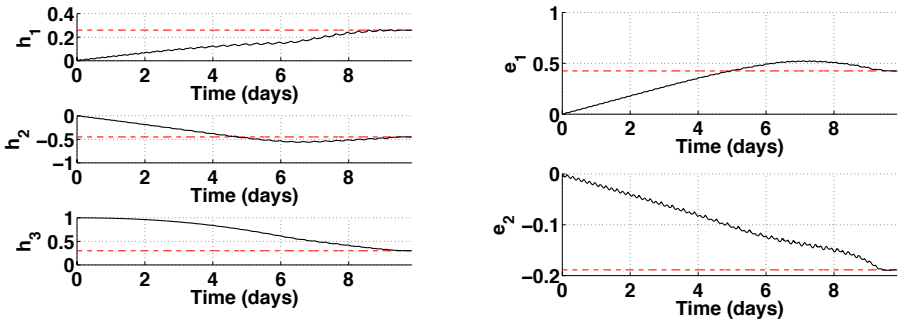

(a) Angular momentum vector $\mathbf{h}$ vs time (b) Eccentricity vector $\mathbf{e}$ vs time

Figure 3.11: Full orbit transfer with initial parameters in Table 3.6.

Lyapunov-based guidance schemes to perform different types of orbit transfers.

The solution procedure is implemented in one step, although the design procedure involves two steps. The first step involves converging the spacecraft orbit to the desired semi-major axis (or equivalently, the desired energy), by using a Lyapunov analysis that gives rise to an asymptotically stabilizing control law. Once the energy has been met, the second step involves converging the remaining subset desired orbital elements (by holding energy constant). We are able to guarantee that any orbital element can be targeted by holding energy constant, which is one of the major contributions to the chapter.

A summary of each algorithm discussed in the chapter is given in Table 3.7 for ease of implementation to the user. The spherical control angles β and δ determine the components of the thrust vector $\mathbf{F}$ in Eq. (3.18), which are used to integrate the equations of motion in Eq. (3.12). Algorithm 1 in Table 3.7 only targets a desired semi-major axis a^*. Algorithm 2 results in an

in-plane orbit transfer; whereas Algorithms $3-5$ are out-of-plane transfers, which include transfer to a circular-equatorial orbit, as well as any general orbit transfer.

Table 3.7: Summary of guidance schemes

	Target Orbital Elements						**Thrust Control Angles**	
	a	**e**	**i**	$\boldsymbol{\omega}$	$\boldsymbol{\Omega}$	$\boldsymbol{\beta}$	$\boldsymbol{\delta}$	**specification**
1	a^*	free	free	free	free	$\sin^{-1}(K_\alpha e_\alpha)$	–	$e_\alpha = \alpha - \alpha^*$
2	a^*	e^*	free	free	free	$\sin^{-1}(K_\alpha e_\alpha)$	$\cos^{-1}\{-\text{sign}\,[(e-e^*)S_e]\}$	S_e in Eq. (3.30)
3	a^*	0	0	n/a	n/a	$\sin^{-1}(K_\alpha e_\alpha)$	$\tan^{-1}\left(\frac{\mathbf{Q}_i\cdot\hat{\mathbf{H}}}{\mathbf{Q}_i\cdot\hat{\mathbf{P}}}\right)$	$\mathbf{Q}_i$ in Eq. (3.40)
4	a^*	e^*	i^*	free	Ω^*	$\sin^{-1}(K_\alpha e_\alpha)$	$\tan^{-1}\left(\frac{\mathbf{Q}_h\cdot\hat{\mathbf{H}}}{\mathbf{Q}_h\cdot\hat{\mathbf{P}}}\right)$	$\mathbf{Q}_h$ in Eq. (3.55)
5	a^*	e^*	i^*	ω^*	Ω^*	$\sin^{-1}(K_\alpha e_\alpha)$	$\tan^{-1}\left(\frac{\mathbf{Q}_o\cdot\hat{\mathbf{H}}}{\mathbf{Q}_o\cdot\hat{\mathbf{P}}}\right)$	$\mathbf{Q}_o$ in Eq. (3.68)

The KS model aids in the design of the guidance schemes, but the solutions can be explicitly characterized in the regular cartesian two-body model. They have been derived and written in cartesian coordinates in Appendix C. No constraint is imposed on the magnitude of the thrust; however, an emphasis is placed on the low-thrust solutions, since they compare well with the optimal ones. One of the main advantages of closed-loop guidance schemes is that they have a low computation time when compared to direct or indirect optimization methods, so they may be a good method to obtain an initial guess for mission design purposes. Also they permit for easy onboard implementation, since the control laws are based solely on the current state of the spacecraft.

For future work we plan on designing control algorithms that do not require the energy of the orbit to be pre-targeted in order to perform an orbit transfer. Another important aspect is to study how to add time-varying gains to explicitly control the rate of convergence of each orbital element. As was mentioned at the beginning of this chapter, solving the rendezvous problem in KS variables was not possible (see Appendix D.2). We plan on further investigating avenues to solve this problem.

Chapter 4

Perturbation Theory in Levi-Civita Coordinates with Constant Energy

In Chapter 2, a guidance scheme was designed to match any desired orbit in the plane by first matching the desired energy and then matching the remaining orbital elements, while keeping energy constant. The design was performed in the regularized Levi-Civita model, in which the equations of motion resemble a perturbed harmonic oscillator, where the period of oscillation is a function of the energy of the orbit. This system is only solvable via numerical integration methods. One of the motivating elements behind Chapter 4 is the desire to provide approximate analytical solutions (to some order of magnitude) to the transfer schemes designed in Chapter 2, by using *perturbation theory*. More specifically, in this chapter we model the second part of the guidance scheme, in which energy remains constant, using regularized coordinates. This perturbation work involves performing a Taylor series expansion about the acceleration magnitude, which is assumed to be constant and of small magnitude.

Perturbation theory belongs to a class of techniques known as *asymptotic methods*, in which analytical solutions are found to differential equations,

by making certain simplifications. Perturbation theory in orbital mechanics has been exploited quite a bit to achieve better integration performance by developing an analytical propagator (rather than having to use numerical integration algorithms). In the unperturbed two-body problem, an efficient propagation scheme is found using the so-called F and G series, which use a recursive formulation to find the propagation coefficients, by performing a Taylor series expansion about a small time step [4, 10, 53]. The F and G series formulation is extended to the perturbed two-body problem, in which the perturbation is inertially fixed in Reference [45].

Another example of asymptotic techniques used in orbital mechanics are averaging techniques, in which the orbital elements are averaged over each revolution, to give an approximate solution [11, 22]. For example, in [20], an analytical solution is found to the averaging problem for tangential thrust. In an impactful averaging paper, a low-thrust averaged trajectory is determined by a set of thrust acceleration coefficients, which are determined by a first-order averaging of the Gauss equations [27, 28, 33]. Representation of each component of the thrust acceleration is written as a Fourier series in eccentric anomaly [27].

In this chapter, we study an asymptotic method by performing a Taylor expansion about the acceleration magnitude. The assumptions here is that the acceleration magnitude is small and of constant magnitude. We do so by using the Levi-Civita model, and the continuous thrust is designed such as to maintain constant energy (equivalently, constant semi-major axis). A

mathematical introduction to perturbation theory using Taylor series expansion is given in Appendix E. Section 4.1 introduces the governing differential equation. This model is used to perform the Taylor series expansion about the acceleration magnitude in Section 4.2. In this section the time-varying coefficients of the expansion are solved for. A purely analytical solution only exists when the spacecraft is initially in a circular orbit, which is shown in Section 4.3.

4.1 Governing Differential Equation

The perturbed planar two-body equations of motion in regularized coordinates (derived in Chapter 2 in Eq. (2.13)) are,

$$\mathbf{u}'' = -\mathcal{W}^2\mathbf{u} + \mathbf{f}_u(\mathbf{u}, \mathbf{f}), \tag{4.1}$$

where $\mathbf{u}$ is a position representation of the spacecraft in regularized coordinates, $\mathcal{W}$ is a function of the energy of the orbit and $\mathbf{f}_u$ is the perturbing acceleration in the regularized frame,

$$\mathbf{f}_u = \frac{Ar^{3/2}}{2}\begin{bmatrix} \cos(\phi - \theta/2) \\ \sin(\phi - \theta/2) \end{bmatrix} \tag{4.2}$$

where the position magnitude $r = \mathbf{u} \cdot \mathbf{u}$, A is the acceleration magnitude of the thrust, θ is a polar angle representation of the position, and ϕ is the thrust control angle, which has been designed in Eq. (2.23) so as to ensure that the desired orbital energy is reached and maintained. The final equations

of motion are in Eq. (2.21). Recall that the independent variable in these equations is τ, which is related to "real" time t as

$$\frac{d}{dt} = \frac{1}{r}\frac{d}{d\tau} \tag{4.3}$$

Eq. (2.21) can be integrated in this regularized frame, and transformed back to normal position and velocity coordinates. These concepts are explained in detail in Section 2.1. Eq. (4.1) can be expressed as four first-order differential equations, where the state is defined as

$$\mathbf{X} = \begin{pmatrix} x_1 \\ x_2 \\ x_3 \\ x_4 \end{pmatrix} = \begin{pmatrix} u_1 \\ u_2 \\ u_1' \\ u_2' \end{pmatrix} \tag{4.4}$$

and the differential equation is given by

$$\mathbf{X}' = \begin{pmatrix} x_1' \\ x_2' \\ x_3' \\ x_4' \end{pmatrix} = \begin{pmatrix} x_3 \\ x_4 \\ -\mathcal{W}^2 x_1 + \frac{A}{2} r^{3/2} \cos(\phi - \theta/2) \\ -\mathcal{W}^2 x_2 + \frac{A}{2} r^{3/2} \sin(\phi - \theta/2) \end{pmatrix} \tag{4.5}$$

If the energy of the orbit is kept constant, the frequency of oscillation also becomes constant $\mathcal{W}(\tau) = \mathcal{W}$ and several simplifications can be made to

the control algorithm, such that

$$\cos(\phi - \theta/2) = \cos(-\lambda) = \cos(\lambda) = \frac{x_4}{(x_3^2 + x_4^2)^{1/2}} \tag{4.6}$$

$$\sin(\phi - \theta/2) = \sin(-\lambda) = -\sin(\lambda) = -\frac{x_3}{(x_3^2 + x_4^2)^{1/2}} \tag{4.7}$$

Assuming the acceleration magnitude A is constant and of small magnitude, $A = \varepsilon$, we re-write the equations of motion as

$$\begin{aligned} x_1' &= x_3 \\ x_2' &= x_4 \\ x_3' &= -\mathcal{W}^2 x_1 + \frac{\varepsilon}{2}\left[\frac{(x_1^2 + x_2^2)^3}{x_3^2 + x_4^2}\right]^{1/2} x_4 \\ x_4' &= -\mathcal{W}^2 x_2 - \frac{\varepsilon}{2}\left[\frac{(x_1^2 + x_2^2)^3}{x_3^2 + x_4^2}\right]^{1/2} x_3 \end{aligned} \tag{4.8}$$

Recall that the energy equation at all times in regularized coordinates is (derived in Eq. (2.12))

$$E = \frac{1}{r}\left(2\mathbf{u}' \cdot \mathbf{u}' - \mu\right) = -2\mathcal{W}^2 \tag{4.9}$$

which, using the state definition $\mathbf{X}$ in (4.4), can be written as

$$x_3^2 + x_4^2 = a - 4b(x_1^2 + x_2^2) \tag{4.10}$$

where

$$\begin{aligned} a &= \mu/2 \\ b &= \mathcal{W}^2 \end{aligned}$$

Eq. (4.10) gives an extra constraint which allows a simplification of the final differential equation,

$$\begin{aligned} x_1' &= x_3 \\ x_2' &= x_4 \\ x_3' &= -\mathcal{W}^2 x_1 + \frac{1}{2}\varepsilon f(x_1, x_2) x_4 \\ x_4' &= -\mathcal{W}^2 x_2 - \frac{1}{2}\varepsilon f(x_1, x_2) x_3 \end{aligned} \tag{4.11}$$

where

$$f(x_1, x_2) = \frac{x_1^2 + x_2^2}{\left[\frac{a}{x_1^2+x_2^2} - b\right]^{1/2}} \tag{4.12}$$

Eq. (4.11) is the differential equation used to perform the Taylor series expansion about the acceleration magnitude ε.

The above equations of motion represent thrusting in the plane, in a direction perpendicular to the velocity (to keep constant the energy of the orbit). There are two possible directions for thrusting perpendicular to the velocity, which we refer as

- Outwards: Thrusting 90^o clockwise from the velocity direction, which corresponds to $\epsilon > 0$.
- Inwards: Thrusting 90^o counter-clockwise from the velocity direction, which corresponds to $\epsilon < 0$.

Without loss of generality, for this chapter, we assume that thrusting is always in the outwards direction ($\epsilon > 0$).

4.2 Taylor Expansion About Acceleration Magnitude

We assume a solution to the differential equation (4.11) as a polynomial function in ε, where ε is assumed to be small,

$$x_i = x_{i_0} + x_{i_1}\varepsilon + x_{i_2}\varepsilon^2 + x_{i_3}\varepsilon^3 + ... + x_{i_n}\varepsilon^n + \varepsilon^{n+1}R_{x_{n+1}}, \quad i = 1, .., 4 \tag{4.13}$$

The solution is assumed to be an approximation of order n, and $R_{x_{n+1}}$ represents the remainder error from the exact solution. The goal is to find the time-varying coefficients x_{i_j} for each solution x_i up to order $j = n$. Explicitly, each solution x_i up to an order n, is

$$x_1 = x_{1_0} + x_{1_1}\varepsilon + x_{1_2}\varepsilon^2 + ... + x_{1_n}\varepsilon^n + O(\varepsilon^{n+1}) \tag{4.14}$$

$$x_2 = x_{2_0} + x_{2_1}\varepsilon + x_{2_2}\varepsilon^2 + ... + x_{2_n}\varepsilon^n + O(\varepsilon^{n+1}) \tag{4.15}$$

$$x_3 = x_{3_0} + x_{3_1}\varepsilon + x_{3_2}\varepsilon^2 + ... + x_{3_n}\varepsilon^n + O(\varepsilon^{n+1}) \tag{4.16}$$

$$x_4 = x_{4_0} + x_{4_1}\varepsilon + x_{4_2}\varepsilon^2 + ... + x_{4_n}\varepsilon^n + O(\varepsilon^{n+1}) \tag{4.17}$$

To begin, the differential equation (4.11) must be written in terms of the assumed x_i solution in Eq. (4.13). The function $f(x_1, x_2)$ in Eq. (4.12) requires a bit of algebraic work in order to express it in terms of x_i. Because the denominator has a square root, it requires another Taylor expansion about ε. Therefore, writing $f(x_1, x_2)$ will be performed in two steps, first the numerator and then the denominator. Rename Eq. (4.12) as

$$f(x_1, x_2) = h(x_1, x_2) \cdot g(x_1, x_2) \tag{4.18}$$

where $h(x_1, x_2) = x_1^2 + x_2^2$ and $g(x_1, x_2) = \left[\frac{a}{x_1^2+x_2^2} - b\right]^{-1/2}$. Expansion in $h(x_1, x_2)$ yields

$$\begin{aligned} h(x_1, x_2) &= \left(x_{1_0} + x_{1_1}\varepsilon + x_{1_2}\varepsilon^2 + ... + x_{1_n}\varepsilon^n\right)^2 + \left(x_{2_0} + x_{2_1}\varepsilon + x_{2_2}\varepsilon^2 + ... + x_{2_n}\varepsilon^n\right)^2 \\ &= h_0 + h_1\varepsilon + h_2\varepsilon^2 + ... + h_n\varepsilon^n \end{aligned} \tag{4.19}$$

where

$$\begin{cases} h_0 &= x_{1_0}^2 + x_{2_0}^2 \\ h_1 &= 2\left(x_{1_0}x_{1_1} + x_{2_0}x_{2_1}\right) \\ h_2 &= 2x_{1_0}x_{1_2} + x_{1_1}^2 + 2x_{2_0}x_{2_2} + x_{2_1}^2 \\ &\vdots \\ h_n &= f(x_{i_0}, x_{i_1}, ..., x_{i_n}), \quad i = 1, 2 \end{cases} \tag{4.20}$$

The function $g(x_1, x_2)$ can now be written as

$$g(x_1, x_2) = \frac{1}{\left[\frac{a}{h(x_1,x_2)} - b\right]^{1/2}} = \frac{1}{\left[\frac{a}{h_0+h_1\varepsilon+...+h_n\varepsilon^n} - b\right]^{1/2}} \tag{4.21}$$

Expanding about $\varepsilon = 0$ yields

$$\begin{aligned} g(\varepsilon) &= g(0) + \varepsilon g'(0) + \varepsilon^2 g''(0) + ... \\ &= g_0 + g_1\varepsilon + g_2\varepsilon^2 + ... + g_n\varepsilon^n \end{aligned} \tag{4.22}$$

where

$$\begin{cases} g_0 &= \frac{1}{(a/h_0-b)^{1/2}} \\ g_1 &= \frac{1}{2}\frac{ah_1}{h_0^2(a/h_0-b)^{3/2}} \\ g_2 &= \frac{a}{8}\frac{-ah_1^2+4ah_0h_2+4h_0h_1^2b-4h_0^2h_2b}{h_0(a/h_0-b)^{1/2}(-a+h_0b)^2} \\ & \vdots \\ g_n &= f(h_0,h_1,h_2,...,h_n), \quad i=1,2 \end{cases} \tag{4.23}$$

Therefore, the expansion of f in Eq. (4.18) in terms of ε and its coefficients is

$$\begin{aligned} f(\varepsilon) &= h(\varepsilon)\cdot g(\varepsilon) \\ &= \left[h_0+h_1\varepsilon+h_2\varepsilon^2+...+h_n\varepsilon^n\right]\left[g_0+g_1\varepsilon+g_2\varepsilon^2+...+g_n\varepsilon^n\right] \\ &= \underbrace{(h_0g_0)}_{f_0}+\underbrace{(h_0g_1+h_1g_0)}_{f_1}\varepsilon+\underbrace{(h_2g_0+h_1g_1+h_0g_2)}_{f_2}\varepsilon^2+...+f_n\varepsilon^n \end{aligned} \tag{4.24}$$

The differential equation in Eq. (4.11) can now be written in terms of the expansion coefficients. Expressing the second-order differential equation

$(x_1'' = x_3' \text{ and } x_2'' = x_4')$,

$$\begin{aligned} x_1'' &= -\mathcal{W}^2 x_1 + \frac{1}{2}\varepsilon f(\varepsilon) x_4(\varepsilon) \\ &= -w^2 x_1 + \frac{1}{2}\varepsilon \left[f_0 + f_1\varepsilon + ... + f_n\varepsilon^n\right]\left[x_{4_0} + x_{4_1}\varepsilon + ... + x_{4_n}\varepsilon^n\right] \\ &= -\mathcal{W}^2 x_1 + \frac{1}{2}\left[p_1\varepsilon + p_2\varepsilon^2 + ... + p_n\varepsilon^n\right] \qquad (4.25) \\ x_2'' &= -\mathcal{W}^2 x_2 - \frac{1}{2}\varepsilon f(\varepsilon) x_3(\varepsilon) \\ &= -\mathcal{W}^2 x_2 - \frac{1}{2}\varepsilon \left[f_0 + f_1\varepsilon + ... + f_n\varepsilon^n\right]\left[x_{3_0} + x_{3_1}\varepsilon + ... + x_{3_n}\varepsilon^n\right] \\ &= -w^2 x_2 - \frac{1}{2}\left[q_1\varepsilon + q_2\varepsilon^2 + ... + q_n\varepsilon^n\right] \qquad (4.26) \end{aligned}$$

where

$$\begin{cases} p_1 = f_0 x_{4_0} \\ p_2 = 2f_0 x_{4_1} + f_1 x_{4_0} \\ \quad \vdots \\ p_n = f(f_0, f_1, ..., f_{n-1}, x_{4_0}, x_{4_1}, ..., x_{4_{n-1}}) \end{cases} \qquad (4.27)$$

and

$$\begin{cases} q_1 = f_0 x_{3_0} \\ q_2 = 2f_0 x_{3_1} + f_1 x_{3_0} \\ \quad \vdots \\ q_n = f(f_0, f_1, ..., f_{n-1}, x_{3_0}, x_{3_1}, ..., x_{3_{n-1}}) \end{cases} \qquad (4.28)$$

4.2.1 Solving for the Expansion Coefficients

In this subsection, the time-varying coefficients x_{i_j} are found, by comparing equivalent orders of ε and solving each differential equation (4.25) and (4.26).

Taking the second time-derivative of Eq. (4.14) and Eq. (4.15) and comparing to Eq. (4.25) and Eq. (4.26), respectively

$$\begin{aligned} x''_{1_0} + x''_{1_1}\varepsilon + x''_{1_2}\varepsilon^2 + ... + x''_{1_n}\varepsilon^n &= -\mathcal{W}^2\left(x_{1_0} + x_{1_1}\varepsilon + x_{1_2}\varepsilon^2 + ... + x_{1_n}\varepsilon^n\right) \\ &\quad + \frac{1}{2}\left(p_1\varepsilon + p_2\varepsilon^2 + ... + p_n\varepsilon^n\right) \qquad (4.29) \\ x''_{2_0} + x''_{2_1}\varepsilon + x''_{2_2}\varepsilon^2 + ... + x''_{2_n}\varepsilon^n &= -\mathcal{W}^2\left(x_{2_0} + x_{2_1}\varepsilon + x_{2_2}\varepsilon^2 + ... + x_{2_n}\varepsilon^n\right) \\ &\quad - \frac{1}{2}\left(q_1\varepsilon + q_2\varepsilon^2 + ... + q_n\varepsilon^n\right) \qquad (4.30) \end{aligned}$$

To begin, we compare the ε^0 terms, which corresponds to the unperturbed differential equation (i.e., no thrusting),

$$\begin{aligned} x''_{1_0} &= -\mathcal{W}^2 x_{1_0}, \qquad \eta_{1_0} = x_1(0),\ \eta_{3_0} = x'_1(0) \qquad (4.31) \\ x''_{2_0} &= -\mathcal{W}^2 x_{2_0}, \qquad \eta_{2_0} = x_2(0),\ \eta_{4_0} = x'_2(0) \qquad (4.32) \end{aligned}$$

where η_{1_0}, η_{2_0}, η_{3_0}, and η_{4_0} are the initial conditions at time t_0. These equations represent a simple harmonic oscillator, and therefore, the solution is

$$\begin{aligned} x_{1_0}(\tau) &= \eta_{1_0}\cos(\mathcal{W}\tau) + \frac{1}{\mathcal{W}}\eta_{3_0}\sin(\mathcal{W}\tau) \qquad (4.33) \\ x_{2_0}(\tau) &= \eta_{2_0}\cos(\mathcal{W}\tau) + \frac{1}{\mathcal{W}}\eta_{4_0}\sin(\mathcal{W}\tau) \qquad (4.34) \\ x_{3_0}(\tau) &= -\mathcal{W}\eta_{1_0}\sin(\mathcal{W}\tau) + \eta_{3_0}\cos(\mathcal{W}\tau) \qquad (4.35) \\ x_{4_0}(\tau) &= -\mathcal{W}\eta_{2_0}\sin(\mathcal{W}\tau) + \eta_{4_0}\cos(\mathcal{W}\tau) \qquad (4.36) \end{aligned}$$

For higher orders of ε, the differential equation represents a perturbed harmonic oscillator. For order n,

$$x''_{1_n} = -\mathcal{W}^2 x_{1_n} + \frac{1}{2} p_n \varepsilon^n, \qquad \eta_{1_n} = 0,\ \eta_{3_n} = 0 \tag{4.37}$$

$$x''_{2_n} = -\mathcal{W}^2 x_{2_n} - \frac{1}{2} q_n \varepsilon^n, \qquad \eta_{2_n} = 0,\ \eta_{4_n} = 0 \tag{4.38}$$

Note that the initial conditions $\eta_{i_n} = 0$, where $i = 1, ..., 4$, are all zero for any $n \geq 1$, because they do not depend on ε. The solution is

$$\begin{aligned} x_{1_n}(\tau) &= \cancelto{0}{\eta_{1n}} \cos(\mathcal{W}\tau) + \frac{1}{\mathcal{W}} \cancelto{0}{\eta_{3n}} \sin(\mathcal{W}\tau) + \frac{1}{2\mathcal{W}} \int_0^\tau \frac{1}{2} p_n(s) \sin(\tau - s) ds \\ &= \frac{1}{2\mathcal{W}} \int_0^\tau \frac{1}{2} p_n(s) \sin(\tau - s) ds \end{aligned} \tag{4.39}$$

$$\begin{aligned} x_{2_n}(\tau) &= \cancelto{0}{\eta_{2n}} \cos(\mathcal{W}\tau) + \frac{1}{\mathcal{W}} \cancelto{0}{\eta_{4n}} \sin(\mathcal{W}\tau) - \frac{1}{2\mathcal{W}} \int_0^\tau \frac{1}{2} q_n(s) \sin(\tau - s) ds \\ &= -\frac{1}{2\mathcal{W}} \int_0^\tau \frac{1}{2} q_n(s) \sin(\tau - s) ds \end{aligned} \tag{4.40}$$

$$x_{3_n}(\tau) = \frac{d}{d\tau} x_{1_n}(\tau) \tag{4.41}$$

$$x_{4_n}(\tau) = \frac{d}{d\tau} x_{2_n}(\tau) \tag{4.42}$$

The coefficients of the assumed solution of x_i in Eq. (4.13) have been expressed as known analytical functions in Eqs. (4.33)–(4.36) and (4.39)–(4.42). The original nonlinear differential equation has now been simplified to a system of perturbed linear differential equations. In order to solve for the coefficients, an integration in time is necessary of Eqs. (4.39)–(4.40), which can obviously be performed using numerical techniques. In the next section we explore analytical solutions to these equations.

4.3 Analytical Solution for Initial Circular Orbits

Suppose a spacecraft begins on an orbit with specific position and velocity coordinates, which in regularized coordinates is equivalent to the following initial conditions

$$\begin{aligned} \text{Regularized Positon} \quad &\Rightarrow \quad \eta_{1_0} = x_1(0),\ \eta_{2_0} = x_2(0) \\ \text{Regularized Velocity} \quad &\Rightarrow \quad \eta_{3_0} = x_3(0),\ \eta_{4_0} = x_4(0) \end{aligned}$$

As it turns out, a pure analytical solution to Eqs. (4.39)–(4.42) only exists when the spacecraft is initially anywhere along a circular orbit. Any initial orbit with eccentricity $e \neq 0$ does not seem to allow for an analytical solution (based on the extensive search done), and a numerical integration needs to be performed. Without loss of generality, we choose the gravitational parameter $\mu = 1$ and the frequency of oscillation $\mathcal{W} = 1$. This scales the energy of the orbit $E = -2$, and therefore, the initial dimentionalized radius $r_0 = 1/4$, which is equal to the semi-major axis. The scaling was chosen in this way to make the frequency of oscillation unity, which allows for a cleaner analytical solution, but any other scaling can be chosen as well.

Recall from Chapter 2 that in the regularized coordinates the eccentricity is

$$e^2 = 1 - \left(\frac{4}{\mu} w\right)^2 (u_1 u_2' - u_2 u_1')$$

where u_1, u_2, u_1', and u_2' are the state coordinates. This equation when $e = 0$ and the energy constraint equation (2.12), gives the constraints necessary to

solve for the initial conditions of a circular orbit. We have the liberty of choosing one parameter for the initial condition, for example, η_{1_0}, which ranges from $0 \leq \eta_{1_0} \leq 1/2$ in the normalized units chosen ($w = 1$ and $\mu = 1$). The rest of the parameters η_{2_0}, η_{3_0}, and η_{4_0} are computed as follows

$$\begin{aligned} 0 \leq \eta_{1_0} \leq \frac{1}{2} \quad , \qquad & \eta_{2_0} = \pm\sqrt{\frac{1}{4} - \eta_{1_0}^2} \\ \eta_{3_0} = -\eta_{2_0} \quad , \qquad & \eta_{4_0} = \eta_{1_0} \end{aligned} \tag{4.43}$$

The range of initial conditions in Eq. (4.43) represents all the possible points on a circular orbit. Four example points are shown in Figure 4.1, where the regularized coordinates (η_{1_0}, η_{2_0}) are plotted in a cartesian frame in the x-y plane. The extreme points occur at $\eta_{1_0} = 1/2$, which corresponds to a spacecraft lying on the positive x-axis, and $\eta_{1_0} = 0$, which corresponds to a spacecraft lying on the negative x-axis. Note that the radius of the circle has been scaled to normalized units, but these conditions are valid for any circle radius.

4.3.1 Example: Spacecraft Initial Location on Positive x-Axis

The time-varying coefficients for a spacecraft with initial condition at time t_0 lying on the positive x-axis are derived here. These conditions correspond to the "red star" in Figure 4.1, and explicitly are

$$\begin{aligned} \eta_{1_0} = \frac{1}{2} \quad , \qquad & \eta_{2_0} = 0 \\ \eta_{3_0} = 0 \quad , \qquad & \eta_{4_0} = \frac{1}{2} \end{aligned}$$

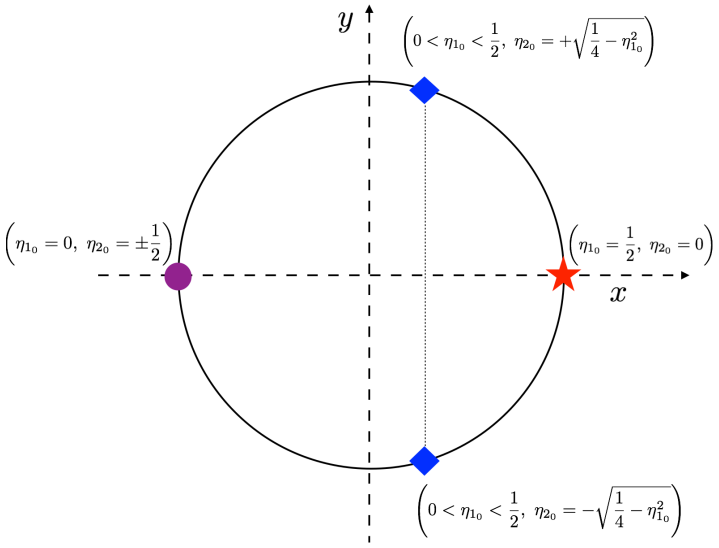

Figure 4.1: Initial conditions of a spacecraft on a circular orbit, with initial conditions in Eq. (4.43).

We solve for Eqs. (4.33)–(4.36) and (4.39)–(4.42) using these initial conditions up to an order $n = 5$. The solution of each component i (where $i = 1, 2, 3, 4$) is of the form

$$x_i(\tau) = x_{i_0}(\tau) + x_{i_1}(\tau)\varepsilon + x_{i_2}(\tau)\varepsilon^2 + x_{i_3}(\tau)\varepsilon^3 + x_{i_4}(\tau)\varepsilon^4 + x_{i_5}(\tau)\varepsilon^5 \quad (4.44)$$

where the time-varying coefficients for each order of magnitude are

- Zeroth Order Terms: ε^0

$$\begin{aligned} x_{1_0}(\tau) &= \frac{1}{2}\cos\tau \\ x_{2_0}(\tau) &= \frac{1}{2}\sin\tau \\ x_{3_0}(\tau) &= -\frac{1}{2}\sin\tau \\ x_{4_0}(\tau) &= \frac{1}{2}\cos\tau \end{aligned}$$

- First Order Terms: ε^1

$$\begin{aligned} x_{1_1}(\tau) &= \frac{1}{2^5}\left(\tau\sin\tau\right) \\ x_{2_1}(\tau) &= \frac{1}{2^5}\left(-(\tau\cos\tau)+\sin\tau\right) \\ x_{3_1}(\tau) &= \frac{1}{2^5}\left(\tau\cos\tau+\sin\tau\right) \\ x_{4_1}(\tau) &= \frac{1}{2^5}\left(\tau\sin\tau\right) \end{aligned}$$

- Second Order Terms: ε^2

$$\begin{aligned} x_{1_2}(\tau) &= -\frac{1}{2^{11}}\left(\left(2\tau^2+1\right)\cos\tau+6\tau\sin\tau+\cos(3\tau)\right) \\ x_{2_2}(\tau) &= \frac{1}{2^{10}}\left(\sin\tau\left(-\tau^2+\cos(2\tau)+4\right)-5\tau\cos\tau\right) \\ x_{3_2}(\tau) &= \frac{1}{2^{11}}\left(7\sin\tau-3\sin(3\tau)+2\tau(\tau\sin\tau+\cos\tau)\right) \\ x_{4_2}(\tau) &= -\frac{1}{2^{11}}\left(\left(2\tau^2+3\right)\cos\tau+6\tau\sin\tau+3\cos(3\tau)\right) \end{aligned}$$

It is obvious that for higher orders of magnitude, the expressions for the coefficients become more complex. To help better readability, the coefficients for ε^3, ε^4, and ε^5, have been written in Appendix F for sake of completeness.

Recall that the results have been found in regularized coordinates, which correspond to $x_1 = u_1$, $x_2 = u_2$, $x_3 = u_1'$, and $x_4 = u_2'$. In order to obtain the coordinates in a cartesian frame, refer back to Chapter 2, in which we derive the cartesian position coordinates (x, y) as

$$\begin{aligned} x &= u_1^2 - u_2^2 \\ y &= 2u_1u_2 \end{aligned}$$

The velocity cartesian coordinates can be found similarly.

Also recall that these equations are found τ, a fictitious time variable which is related to "real" time t as

$$\frac{d}{dt} = \frac{1}{r}\frac{d}{d\tau}$$

where $r = \mathbf{u} \cdot \mathbf{u} = x_1^2 + x_2^2$ and x_1 and x_2 are the results from Eq. (4.44). Therefore, the true time t is found by integrating

$$\begin{aligned} t &= \int_{t_0}^{t} \left(x_1(\tau)^2 + x_2(\tau)^2\right) d\tau \qquad (4.45) \\ &= \frac{\tau}{4} + \frac{(4058744094720\tau - 2029372047360\sin(2\tau))}{259759622062080}\varepsilon + \\ &\quad \frac{(507343011840\tau - 380507258880\sin(2\tau) + 253671505920\tau\cos(2\tau))}{259759622062080}\varepsilon^2 \\ &\quad +\ldots\ \varepsilon^3 + \ldots\ \varepsilon^4 + \ldots\ \varepsilon^5 \end{aligned}$$

The higher order terms are not written here because of their complexity, but they can be found analytically (they were found using symbolic computation software).

Several examples are shown for different values of acceleration magnitude ε. In Figure 4.2, $\varepsilon = 10\text{N} = 0.642\ \text{DU/TU}^2$, taking into account that the direction of the thrust could be inwards or outwards. The inwards firing trajectory results are in (a), (c), and (e). In (a), the initial orbit is plotted in green, the "true solution" corresponding to the numerically integrated solution is in red[1], and the approximate analytical solution of Eq. (4.44) is in blue.

[1]The smallest tolerance possible is used for numerical integration.

The semi-major axis and eccentricity are plotted in (c). It is interesting to note that the "true" eccentricity exhibits periodic motion, in which it reaches a maximum value, and then return to zero eccentricity, somewhere along the initial circle. Also, as is expected, the "true" semi-major axis does not vary. From the eccentricity plot in (c) it is clear to see that up to 3 revolutions of the spacecraft returning to the initial circular orbit, the "approximate analytical" solution is reasonably accurate when compared to the "true" solution. After that, the solution deviates more significantly from the truth. In (e) the position and velocity error norms between the true and the approximate solutions are plotted. The outwards firing results are in (b), (d), and (f).

Two more example simulations are shown in Figure 4.3 and 4.4. Using a lower thrust magnitude (ε = 3N = 0.193 DU/TU^2) in Figure 4.3, it is clear that the analytical solution is a very good approximation of the truth for many revolutions. In fact, this is to be expected since the results of the Taylor expansion in this chapter are valid for small values of acceleration ε. A higher acceleration magnitude (ε = 20N = 1.285 DU/TU^2) is shown in Figure 4.4. It is clear to see that the analytical solution breaks down after one revolution. The solutions in these examples are found up to an order of magnitude of ε^5. Higher orders of the analytical solution in (4.44) can be found to make the solution even more accurate for higher acceleration magnitudes.

For any general initial condition on the circle from Eq. (4.43), and as shown by the blue diamonds in Figure 4.1, the analytical approximate solution has also been found. The results are in Appendix F.

4.4 Final Remarks

In this chapter we are able to solve for an analytical approximation (up to order 5) of a two-body perturbed model, in which the perturbation comes from a constant acceleration thrust, which is always in the direction perpendicular to the velocity. The model used is the regularized Levi-Civita equations of motion. The analytical expression is solved for spacecraft which are initially in a circular orbit. The approximation is found by performing a Taylor series expansion about the acceleration magnitude, which is assumed to be constant and small, and the time-varying coefficients of the solution are solved by performing the necessary analytical integration. From simulation examples it is clear that the solution is accurate for small acceleration magnitudes, but breaks down for higher magnitudes after several revolutions.

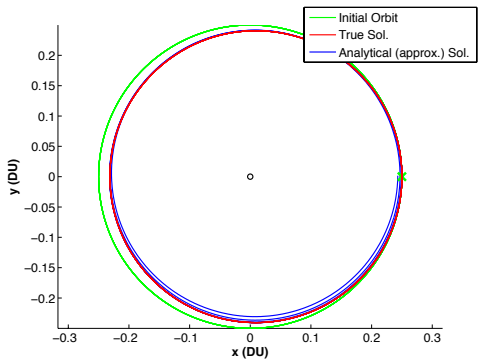

(a) x-y Trajectory Firing Inwards

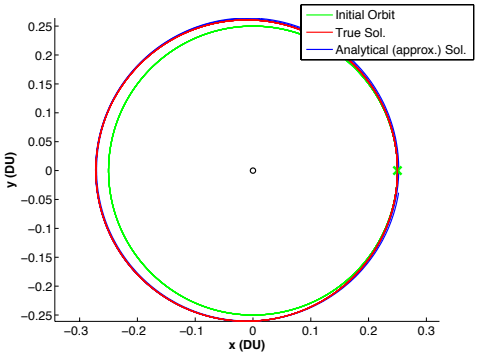

(b) x-y Trajectory Firing Outwards

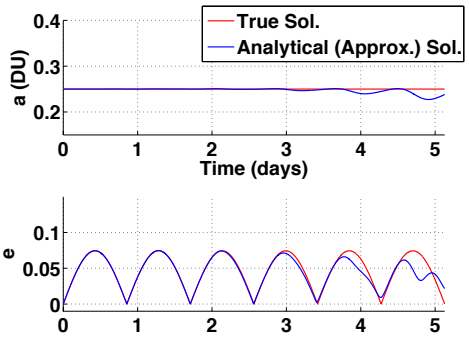

(c) Sma and Ecc Firing Inwards

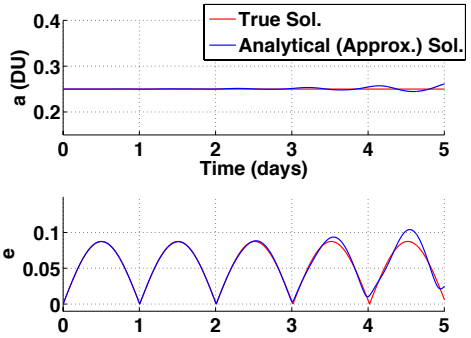

(d) Sma and Ecc Firing Outwards

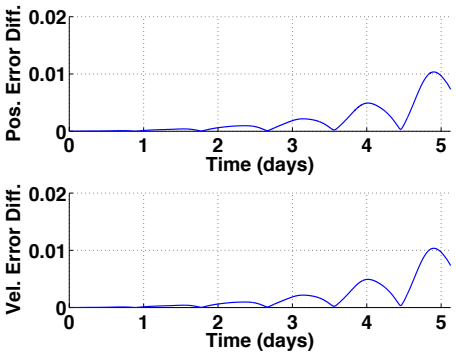

(e) Pos and Vel Errors Firing Inwards

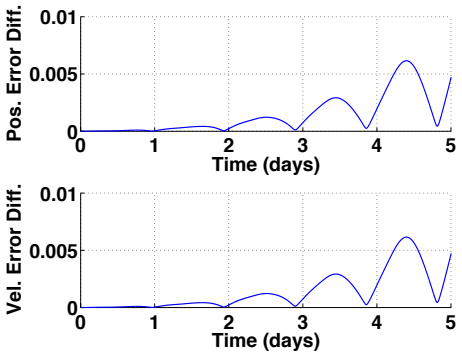

(f) Pos and Vel Errors Firing Outwards

Figure 4.2: Comparison of "True" solution and "Analytical" solution with an acceleration magnitude $\varepsilon = 0.642$, when firing inwards ((a),(c),(e)) and firing outwards ((b),(d),(f)).

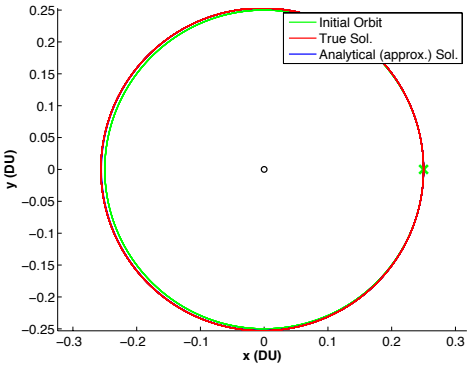

(a) x-y Trajectory

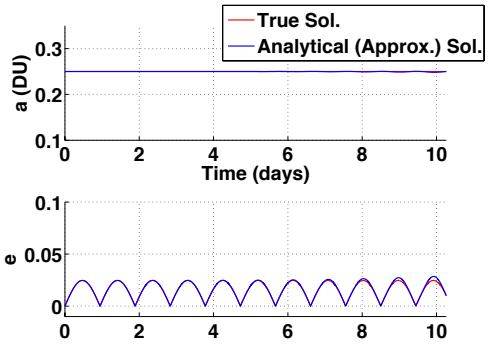

(b) Semi-major axis and Eccentricity

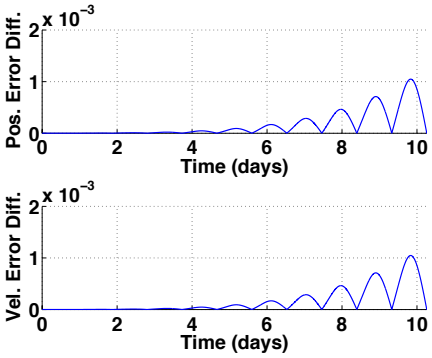

(c) Position and Velocity Errors

Figure 4.3: Comparison of "True" solution and "Analytical" solution with an acceleration magnitude $\varepsilon = 0.193$.

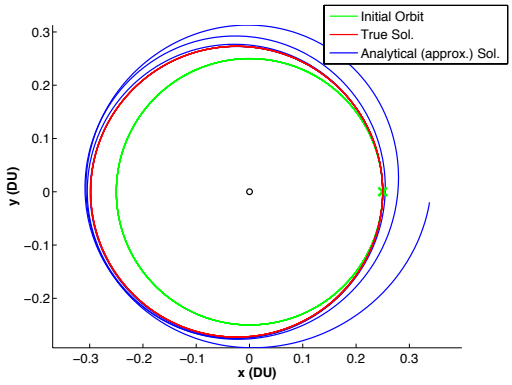

(a) x-y Trajectory

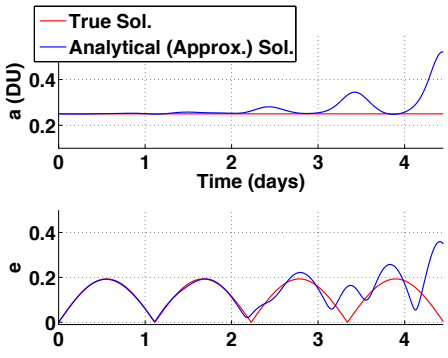

(b) Semi-major axis and Eccentricity

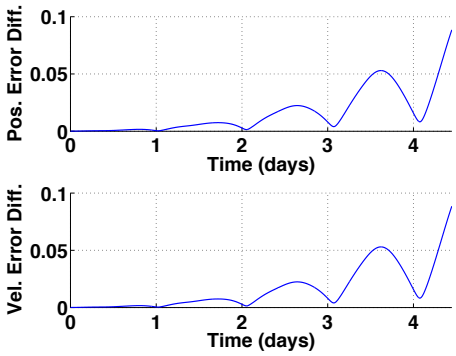

(c) Position and Velocity Errors

Figure 4.4: Comparison of "True" solution and "Analytical" solution with an acceleration magnitude $\varepsilon = 1.285$.

Chapter 5

Energy Conserved Planar Spacecraft Motion with Constant Thrust Acceleration

5.1 Introduction

[1]In Chapter 4 we worked with a regularized two-body model, in which the thrust was always of constant magnitude, and normal to the velocity, so as to conserve the energy of the orbit. In that chapter we found that an approximate solution can be found when a spacecraft is initially in a circular orbit, for small values of acceleration. From some of the simulations, we noted that in fact, there seemed to be some periodic motion, since the spacecraft always returns to the initial circular orbit after some period of time. This led us to study the problem of constant thrust acceleration spacecraft motion, with conserved energy, from a slightly different perspective, which is the topic of this chapter.

The problem of continuous thrusting in the two-body problem has been studied in many different ways for a vast number of spacecraft applications. Only in a few specific situations does this problem have an analytical solution. For example, some of the earliest work was done by Tsien studying

[1]The work presented in this chapter is in Ref. [24].

circumferential thrust to solve the problem of escaping from an initial circular orbit [65]. The classical problem of spacecraft motion subject to a constant radial thrust has been extensively investigated and allows for analytical solutions [2, 3, 5, 8, 49]. The problem of tangential thrust acceleration also allows for some partial analytical solutions [9, 48], as well as an exponential sinusoid solution for many revolution transfers and interplanetary trajectories [47]. Therefore, the problem of thrusting radially (in the position direction), circumferentially (perpendicular to the position), and tangentially (in the velocity direction) have been studied fairly extensively. The problem that has not yet been explored is thrusting in the direction perpendicular to the velocity, which is the focus of this chapter.

We assume a spacecraft that is allowed to thrust in a planar two-body model, where the thrust is continuous, in the direction perpendicular to the velocity, and with a constant magnitude. For ease of notation, this thrusting protocol will be referred to as "vel-normal" thrust. There is one integral of motion in this system, since the energy of the system is conserved. This is a consequence of thrusting perpendicular to the velocity, because the energy is only changed by a perturbation along the velocity direction. This is reminiscent of the constant radial thrust problem, in which the angular momentum of the system is conserved rather than the energy. In the radial problem there is one more integral of motion, and therefore, the problem is solved analytically [2]. However, a full analytical solution is not possible in the vel-normal thrusting problem.

Even though the problem cannot be analytically solved, some analytical insights have been found. By expressing the equations of motion along the velocity direction and normal to the velocity, and using the radius of curvature and arc length as parameters for the problem, we are able to solve for the flight direction angle in terms of *only* the position magnitude. This angle represents the angle between the position and velocity direction. The solution to the flight direction angle lends to an analytical bound on the possible acceleration magnitudes for the spacecraft to remain bounded. We are also able to show that, regardless of the acceleration magnitude, the position norm will never surpass twice its initial value.

A spacecraft starting in an initial circular orbit of radius r_0 will obtain a minimum (perigee) radius r_p along an *inbound* trajectory. If the thrust is maintained, the spacecraft returns to the initial circular orbit, but on a different location on the circle. The spacecraft encompasses a ring of inner radius r_p and outer radius r_0. A similar behavior occurs during an *outbound* trajectory: a maximum (apogee) radius r_a is obtained when starting in a circular orbit, after which the vehicle will return again to the initial circular orbit if thrusting is maintained. The behavior of this dynamical system implies periodicity for the position magnitude, which we prove in this chapter. It takes the same amount of time to reach the minimum (during inbound) or maximum (during outbound) distance, as to return from this point back to the initial circular orbit. The eccentricity also exhibits periodic motion, ranging from $0 \leq e \leq 1 - \delta$, where $\delta > 0$ is a unique value corresponding to a specific

acceleration. The minimum radius $r_p = 1 - \delta$ for an inbound trajectory and the maximum radius $r_a = 1 + \delta$ for an outbound trajectory.

Periodic orbits are also found in this system for different values of acceleration, such that the spacecraft returns to the initial starting location on the circular orbit after n number of revolutions, where each revolution represents each time the spacecraft returns to the circular orbit, but with a phase difference from the initial position. The periodic orbits are classified according to the type of motion, and their stability is addressed.

This chapter is organized as follows. In Section 5.2 the equations of motion are derived in both cartesian coordinates and polar coordinates. The solution to the flight direction angle is also derived in this section. Several examples are shown in Section 5.3. A differential correction procedure is derived in Section 5.5 to find all the possible periodic orbit of this system. We conclude the chapter with some final remarks in Section 5.6.

5.2 Equations of Motion

Let a spacecraft be governed by a perturbed planar two-body motion with position vector $\mathbf{r} = [r_1 \; r_2]^T$ and velocity vector $\mathbf{v} = [v_1 \; v_2]^T$, referenced from an inertial frame $\mathcal{I} = \{\hat{\mathbf{i}}, \hat{\mathbf{j}}\}$. This reference frame is centered at the origin of the central body, whose gravitational parameter is given by μ. A frame $\mathcal{R} = \{\hat{\mathbf{i}}_t, \hat{\mathbf{i}}_n\}$, is attached to the spacecraft that forms an orthogonal basis in $\mathbb{R}^2$, where $\hat{\mathbf{i}}_t$ is a unit vector in the velocity direction, and $\hat{\mathbf{i}}_n$ is normal to $\hat{\mathbf{i}}_t$. The spacecraft is assumed to continuously thrust with a constant acceleration

magnitude a_T, always perpendicular to the velocity direction (i.e., in the $\pm\hat{\mathbf{i}}_n$ direction).

5.2.1 Equations of Motion in Cartesian Coordinates

In cartesian coordinates, the equations of motion of a spacecraft with a perturbation are given by

$$\ddot{\mathbf{r}} = -\frac{\mu}{r^3}\mathbf{r} + \mathbf{f} \tag{5.1}$$

where $r = \|\mathbf{r}\|$ and $\mathbf{f}$ is the perturbing acceleration due to the thrusting protocol, given by

$$\mathbf{f} = \sigma a_T \hat{\mathbf{i}}_n = \sigma a_T \begin{pmatrix} \cos\alpha \\ \\ \sin\alpha \end{pmatrix} \tag{5.2}$$

Here, a_T is the constant acceleration magnitude, and $\sigma = \pm 1$. The sign of σ depends on the direction of thrusting motion. In the notation adopted in this chapter, $\sigma = +1$ if the thrusting is in the inward direction ($+\hat{\mathbf{i}}_n$ direction), and $\sigma = -1$ if the thrusting is in the outward direction ($-\hat{\mathbf{i}}_n$ direction). The angle α represents the thrust angle measured from the positive inertial $\hat{\mathbf{i}}$ axis. Refer to Figure 5.1.

The energy of an orbit is given by

$$E = \frac{v^2}{2} - \frac{\mu}{r} = -\frac{\mu}{2a} \tag{5.3}$$

where $r = \|\mathbf{r}\|$ and $v = \|\mathbf{v}\|$. Its time-derivative is

$$\dot{E} = \mathbf{v}^T\mathbf{f} = 0 \tag{5.4}$$

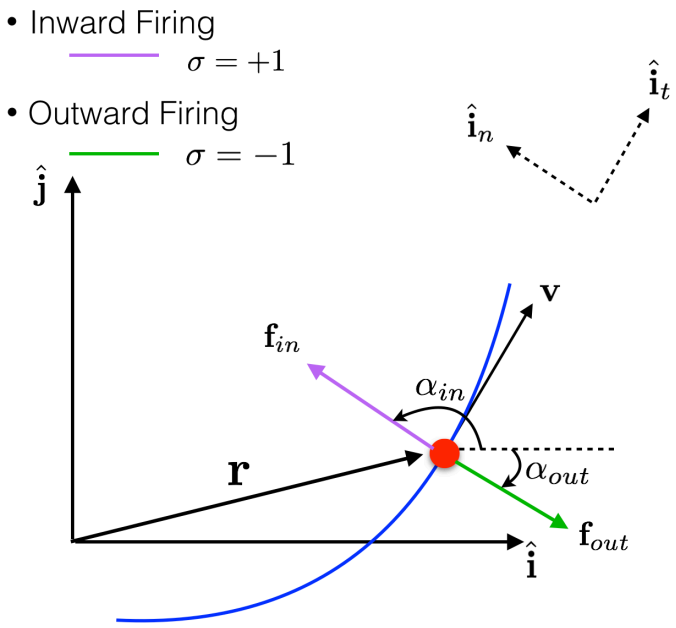

Figure 5.1: Spacecraft motion with vel-normal thrust.

since $\mathbf{f} = \sigma a_T \hat{\mathbf{i}}_n$, which is always perpendicular to the velocity vector $\mathbf{v}$. In cartesian coordinates this condition is met if

$$a_T \left(v_1 \cos\alpha + v_2 \sin\alpha \right) = 0 \quad \Rightarrow \quad \tan\alpha = -\frac{v_2}{v_1} \tag{5.5}$$

Equivalently,

$$\cos\alpha = -\frac{v_2}{v} \quad \text{and} \quad \sin\alpha = \frac{v_1}{v} \tag{5.6}$$

Therefore the equations of motion in cartesian coordinates are

$$\begin{pmatrix} \ddot{r}_1 \\ \\ \ddot{r}_2 \end{pmatrix} = -\frac{\mu}{r^3} \begin{pmatrix} r_1 \\ \\ r_2 \end{pmatrix} + \sigma \frac{a_T}{v} \begin{pmatrix} -v_2 \\ \\ v_1 \end{pmatrix} \tag{5.7}$$

Recall that by convention

$$\sigma = \begin{cases} +1 & \text{if} \quad \text{firing inwards} \quad (+\hat{\mathbf{i}}_n) \\ -1 & \text{if} \quad \text{firing outwards} \quad (-\hat{\mathbf{i}}_n) \end{cases} \tag{5.8}$$

5.2.2 Equations of Motion in a Body-Fixed Frame

In polar coordinates, its position is expressed by its position magnitude r and a polar angle θ, measured counter-clockwise from the inertial $\hat{\mathbf{i}}$ axis (see Figure 5.2). Let ρ represent the radius of curvature of the path, $\rho = ds/d\phi$, where s is the arc length of the path at any point in time t.

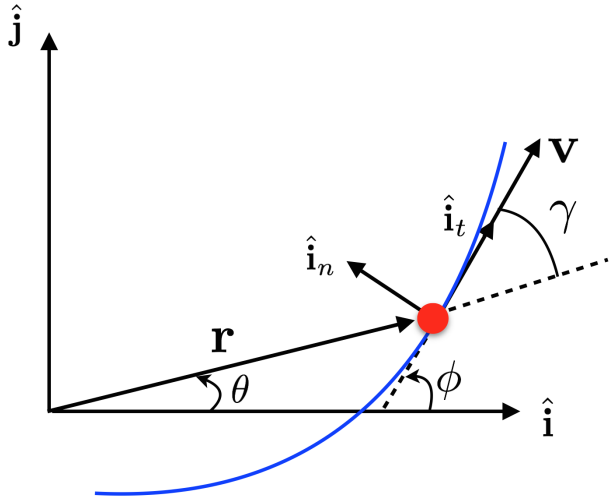

Figure 5.2: Spacecraft motion in inertial and body-fixed frame.

From pure kinematics

$$\mathbf{v} = v\hat{\mathbf{i}}_t = \frac{ds}{dt}\hat{\mathbf{i}}_t \tag{5.9}$$

$$\mathbf{a} = v\frac{dv}{ds}\hat{\mathbf{i}}_t + \frac{v^2}{\rho}\hat{\mathbf{i}}_n = \frac{dv}{dt}\hat{\mathbf{i}}_t + \frac{v^2}{\rho}\hat{\mathbf{i}}_n \tag{5.10}$$

Note,

$$v\frac{dv}{ds} = \frac{ds}{dt}\frac{dv}{ds} = \frac{dv}{dt} \tag{5.11}$$

The equations of motion of the spacecraft, when a constant perturbation a_T is in the $\pm\hat{\mathbf{i}}_n$ direction, i.e. perpendicular to the velocity, are given by

$$\mathbf{a} = -\frac{\mu}{r^2}\hat{\mathbf{i}}_r + \sigma a_T \hat{\mathbf{i}}_n \tag{5.12}$$

where $\hat{\mathbf{i}}_r$ is a unit vector along the position $\mathbf{r}$ direction, which can be resolved in components as

$$\hat{\mathbf{i}}_r = \cos\gamma\hat{\mathbf{i}}_t - \sin\gamma\hat{\mathbf{i}}_n \tag{5.13}$$

where γ is the angle between the position $\mathbf{r}$ and velocity $\mathbf{v}$, known as the flight-direction angle.

Comparing components of acceleration between Eq. (5.10) and Eq. (5.12) (along the $\hat{\mathbf{i}}_t$ and $\hat{\mathbf{i}}_n$) directions,

$$\frac{dv}{dt} = -\frac{\mu}{r^2}\cos\gamma \tag{5.14}$$

$$\frac{v^2}{\rho} = \sigma a_T + \frac{\mu}{r^2}\sin\gamma \tag{5.15}$$

Since $ds^2 = (dr)^2 + (rd\theta)^2$, then

$$\begin{aligned} \sin\gamma &= r\frac{d\theta}{ds} \\ \cos\gamma &= \frac{dr}{ds} \end{aligned} \tag{5.16}$$

Rearranging Eq. (5.14) and (5.15) by using the relation in Eq. (5.16),

$$\frac{d}{ds} \quad \left(\frac{v^2}{2} - \frac{\mu}{r}\right) = 0 \tag{5.17}$$

$$\frac{d\theta}{ds} \quad = \frac{r}{\mu}\left(\sigma a_T - \frac{v^2}{\rho}\right) \tag{5.18}$$

From Eq. (5.17), it is clear to see that the energy E of the spacecraft is conserved, regardless of the magnitude of the thrust. This in fact verifies the known fact that the change of energy is determined by the perturbation component *only* in the velocity direction. Therefore, by thrusting *perpendicular* to the velocity, the energy remains constant.

Assuming we start on an orbit with initial circular radius r_0 and velocity v_0, the velocity at any point on the path can be written as

$$v^2 = \mu\left(\frac{2}{r} - \frac{1}{r_0}\right) \tag{5.19}$$

Since we know the velocity norm must be greater than zero,

$$r \leq 2r_0 \ \forall \ s \tag{5.20}$$

Therefore the position magnitude is bounded between $0 \leq r(s) \leq 2r_0$.

From Eq. (5.15), and using the following definition for the inverse of ρ,

$$\frac{1}{\rho} = \frac{1}{r}\left[1 - \left(\frac{dr}{ds}\right)^2 - r\frac{d^2r}{ds^2}\right]\left[1 - \left(\frac{dr}{ds}\right)^2\right]^{-1/2} \tag{5.21}$$

the following equations can be written

$$\frac{\frac{v^2}{r}\left[1 - \left(\frac{dr}{ds}\right)^2 - r\frac{d^2r}{ds^2}\right]}{\sqrt{1 - \left(\frac{dr}{ds}\right)^2}} = \sigma a_T + \frac{\mu}{r^2}\sqrt{1 - \left(\frac{dr}{ds}\right)^2} \tag{5.22}$$

which can be written as a second order nonlinear differential equation in $r(s)$

$$v^2 r\frac{d^2r}{ds^2} - \left(v^2 - \frac{\mu}{r}\right)\left[1 - \left(\frac{dr}{ds}\right)^2\right] = -\sigma a_T r\left[1 - \left(\frac{dr}{ds}\right)^2\right]^{1/2} \quad (5.23)$$

From calculus,

$$\frac{d^2r}{ds^2} = \frac{1}{2}\frac{d}{dr}\left(\frac{dr}{ds}\right)^2, \quad (5.24)$$

and defining

$$w^2(r) \equiv \sin\gamma = 1 - \cos^2\gamma = 1 - \left(\frac{dr}{ds}\right)^2, \quad (5.25)$$

simplifies the differential equation (5.23) to

$$\frac{v^2 r}{2}\frac{d}{dr}\left(1 - w^2\right) - \left(v^2 - \frac{\mu}{r}\right)w^2 + \sigma a_T r w = 0 \quad (5.26)$$

Substituting for v^2 (Eq. (5.19)) and performing some algebra on Eq. (5.26), results in a linear differential equation with a perturbating term,

$$\frac{dw}{dr} = -\frac{1}{r}\frac{r_0 - r}{2r_0 - r}w + \sigma a_T \frac{r_0}{\mu}\frac{r}{2r_0 - r} \quad (5.27)$$

The solution to Eq. (5.27) is

$$w(r) = \frac{r_0}{\sqrt{r(2r_0 - r)}}\left[1 + \sigma\frac{a_T r_0^2}{\mu}\left\{3\sin^{-1}\left(\sqrt{\frac{r}{2r_0}}\right) - \left(\frac{3\pi}{4} - 2\right)\right\}\right] - \sigma\frac{a_T r_0}{2\mu}\left(r + 3r_0\right) \quad (5.28)$$

which represents an analytical solution for $\sin\gamma(r)$, where $0 \leq \gamma \leq 180^o$. There is no sign ambiguity in $w(r)$, since $0 \leq \sin\gamma \leq 1 \ \forall \ \gamma$. However, for computing $\cos\gamma = \pm\sqrt{1 - w^2}$, the magnitude is known, but the sign needs to

be carefully determined, since $-1 \leq \cos\gamma \leq 1$. When going from perigee to apogee (i.e., $0 \leq \nu \leq 180^o$, where ν is the true anomaly), the flight direction angle $0 \leq \gamma \leq 90^o$, and therefore $\cos\gamma = +\sqrt{1-w^2}$. On the other hand, when going from apogee to perigee (i.e., $180 \leq \nu \leq 360^o$), the flight direction angle $90^o \leq \gamma \leq 180^o$, so $\cos\gamma = -\sqrt{1-w^2}$.

The motion the spacecraft can be characterized by two variables, the position magnitude r and the polar angle θ. Their time-derivatives are

$$\begin{pmatrix} dr/dt \\ d\theta/dt \end{pmatrix} = \sqrt{\frac{2-r}{r}} \begin{pmatrix} K\sqrt{1-w^2(r)} \\ w(r)/r \end{pmatrix} \tag{5.29}$$

where $w(r)$ is given in Eq. (5.28) and

$$K = \begin{cases} 1 & \text{if} \quad 0^o \leq \gamma \leq 90^o \text{ (perigee to apogee)} \\ -1 & \text{if} \quad 90^o \leq \gamma \leq 180^o \text{ (apogee to perigee)} \end{cases} \tag{5.30}$$

5.3 Trajectory Solution Starting From a Circular Orbit

The trajectory solution, which begins on a circular orbit, reaches a perigee value (when firing in) or an apogee value (when firing out). Two example trajectories are shown in Section 5.3.1 to give the reader a feeling for the behavior of the dynamical system. Using the solution to the flight direction angle found in the previous section, several results are obtained in Section 5.3.2, such as placing a bound on the valid acceleration magnitude, as well as proving periodicity on the position magnitude r. The orbital elements

are derived in Section 5.3.3 in terms of only r. Without loss of generality, for the remainder of the chapter the units are normalized such that $\mu = 1$ and $r_0 = 1$.

5.3.1 Example Trajectories

To begin studying the behavior of the vel-normal thrust system, given by the differential equation in Eq. (5.29), two examples are shown. Both examples begin on an initial circular orbit at $r_0 = 1$ and $\theta_0 = 0^o$.

The example in Fig. 5.3, shows a trajectory integrated by *firing in* ($\sigma = +1$) by using $a_T = 1.5878$, which is chosen because the spacecraft reaches a perigee of $r_p = 0.1$. The trajectory solution is shown in Fig. 5.3(a). The orbit reaches its minimum radius r_p, after which it returns to the initial circular orbit at some time T_p, where $r(T_p) = 1$, but on a different location on the circle, $\theta(T_p) \neq \theta_0$. The trajectory has been propagated for four revolutions. Fig. 5.3(b) shows the orbital elements as a function of time. As is to be expected, the semi-major axis (sma) does not vary, and the eccentricity (ecc) varies and is a periodic function in time. The position magnitude r over time is shown in Fig. 5.3(c), which is also periodic in time, varying from $0.1 \leq r \leq 1 \; \forall \, t$. The function $w(r)$ as a function of time is shown in Fig. 5.3(d), which reaches unity value at two points on the orbit: at $r = 1$ and at $r = r_p$.

The example in Fig. 5.4 shows a trajectory integrated by *firing out* ($\sigma = -1$) using an acceleration magnitude $a_T = 0.2160$, to achieve an apogee radius $r_a = 1.9$. The trajectory solution is shown in Fig. 5.4(a). The orbit

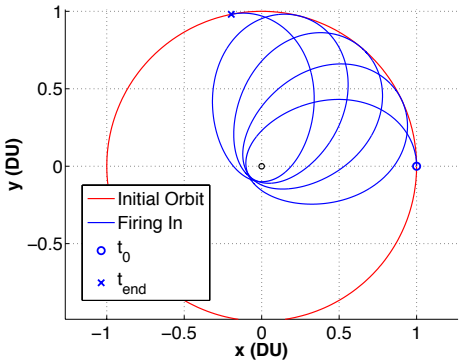

(a) Trajectory in Cartesian Coordaintes

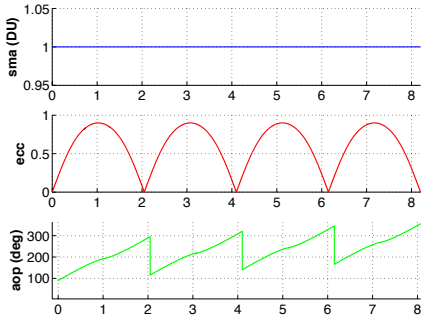

(b) Orbital Elements vs. time

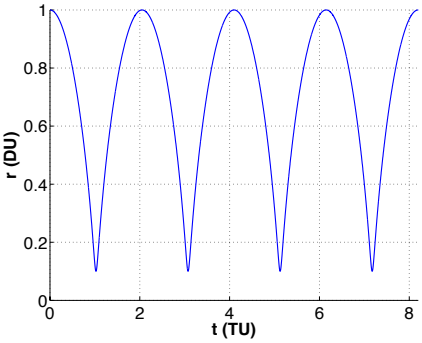

(c) Position r vs. time

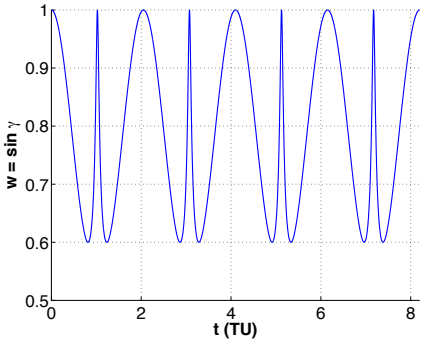

(d) Function w vs. time

Figure 5.3: Trajectory solution integrated firing in, to a perigee distance $r_p = 0.1$ for four revolutions, using $a_T = 1.5878$.

reaches its maximum radius r_a, after which it returns to the initial circular orbit, where $r(T_p) = 1$, but on a different location on the circle, $\theta(T_p) \neq \theta_0$. Note, that in the example in Fig. 5.3, the angular displacement when returning to the initial circular orbit is positive; whereas the angular displacement $\theta(t_i)$ in when firing out is negative. The trajectory has been propagated for four revolutions. Fig. 5.4(b) shows the orbital elements as a function of time.

Again, the semi-major axis (sma) does not vary, and the eccentricity (ecc) varies and is a periodic function in time. The position magnitude r over time is shown in Fig. 5.4(c), which is also periodic in time, varying from $1 \leq r \leq 1.9 \,\forall\, t$. The function $w(r)$ as a function of time is shown in Fig. 5.4(d), which reaches unity value at two points on the orbit: at $r = 1$ and at $r = r_a$.

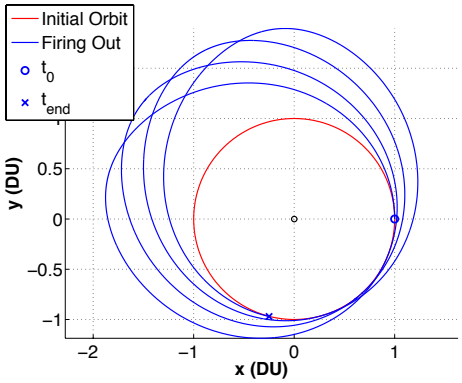

(a) Trajectory in Cartesian Coordinates

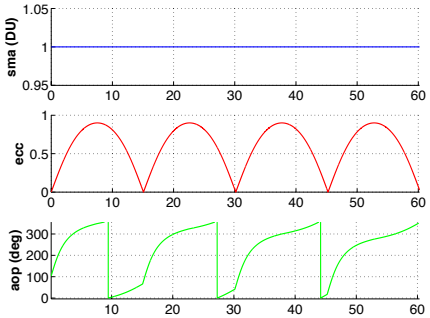

(b) Orbital Elements vs. time

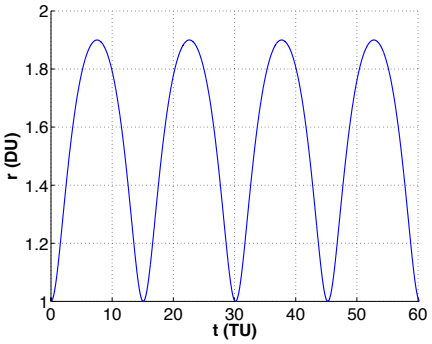

(c) Position r vs. time

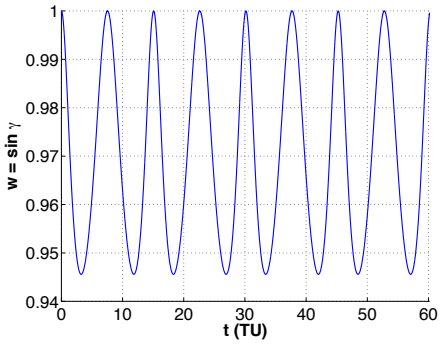

(d) Function w vs. time

Figure 5.4: Trajectory solution integrated firing out, to an apogee distance $r_a = 1.9$ for four revolutions, using $a_T = 0.2160$.

5.3.2 Semi-Analytical Solution to the Dynamical System

The function $w(r)$ in Eq. (5.28) represents the sine of the flight direction angle, which is the angle between the position and velocity vectors. The range of $w(r) = \sin\gamma$ is $\mathcal{R} \in [0\ 1]$. If the spacecraft is initially in a circular orbit of radius $r_0 = r(t_0) = 1$, the function $w(r_0) = 1$, since the position and velocity vector are perpendicular to each other in a circular orbit. As the thrusting begins at t_0, $w(r)$ changes until the orbit reaches perigee r_p (or apogee r_a), at which point $w(r_p) = 1$ again, since position and velocity are perpendicular to each other.

It is readily verified that for $r = 1$, the function $w(1) = 1$ regardless of the value of acceleration magnitude a_T. This always corresponds to an instantaneous circular obit, where the eccentricity $e = 0$. The function will reach unity value again when the position and velocity become perpendicular to each other, which will occur at perigee r_p when firing in (or apogee r_a when firing out). It is not possible to analytically solve Eq. (5.28) for the values of r_p (reps. r_a) that will make $w(r) = 1$. However, it is possible to solve for the acceleration magnitude a_T required to reach a specific r_p (reps. r_a). When $w(r) = 1$ in Eq. (5.28),

$$a_T = \sigma \frac{\sqrt{r_m(2 - r_m)} - 1}{3\sin^{-1}\left(\sqrt{\frac{r_m}{2}}\right) - \frac{3\pi}{4} + 2 - \frac{1}{2}(r_m + 3)\sqrt{r_m(2 - r_m)}} \tag{5.31}$$

where r_m represents the minimum radius reached when firing in (corresponding to the perigee $r_m = r_p$), or the maximum radius reached when firing out (corresponding to the apogee $r_m = r_a$). The extreme values that a_T can

achieve without becoming retrograde at $r_p = r_{min} = 0$ and $r_p = r_{max} = 2$ are, respectively

$$a_T|_{r_{min}} = \frac{4}{3\pi - 8} \qquad \text{and} \qquad a_T|_{r_{max}} = \frac{4}{3\pi + 8} \tag{5.32}$$

Fig. 5.5 shows the different values of thrust magnitude a_T to reach a specific minimum radius r_p when firing in (blue squares), or maximum radius r_a when firing out (red dots).

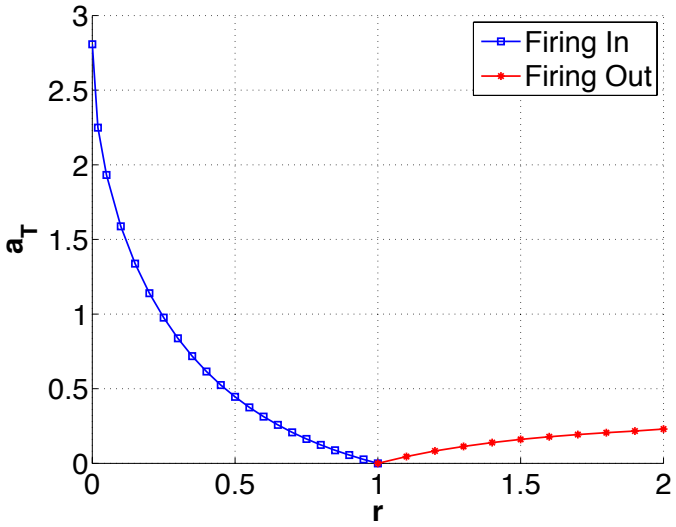

Figure 5.5: Perigee/Apogee radius reached versus acceleration magnitude a_T when starting in an initial circular orbit of radius $r = 1$.

From Eq. (5.29), the time it takes to go from initial $r_0 = 1$ to perigee r_p (or apogee r_a) is given by the following integral

$$\begin{aligned} \Delta T_{r_0 \to r_p} &= \int_{r_0}^{r_p} \sqrt{\frac{r}{2-r}} \frac{K}{\sqrt{1 - w^2(r)}} dr \\ &= -\int_{r_0}^{r_p} \sqrt{\frac{r}{2-r}} \frac{1}{\sqrt{1 - w^2(r)}} dr \end{aligned} \tag{5.33}$$

which is indeed only a function of r. However, the integral does not have an analytical solution, so a numerical method of integration needs to be used. The definite integral has the same form when returning from perigee back to the circular orbit,

$$\begin{aligned}
\Delta T_{r_p \to r_0} &= \int_{r_p}^{r_0} \sqrt{\frac{r}{2-r}} \frac{K}{\sqrt{1-w^2(r)}} dr \\
&= +\int_{r_p}^{r_0} \sqrt{\frac{r}{2-r}} \frac{1}{\sqrt{1-w^2(r)}} dr \\
&= -\int_{r_0}^{r_p} \sqrt{\frac{r}{2-r}} \frac{1}{\sqrt{1-w^2(r)}} dr \\
&= \Delta T_{r_0 \to r_p}
\end{aligned} \tag{5.34}$$

Therefore, the time to complete one full revolution, i.e. to come back to the initial radius, is

$$T_p = \Delta T_{r_0 \to r_p} + \Delta T_{r_p \to r_0} = 2\Delta T_{r_0 \to r_p} \tag{5.35}$$

where $\Delta T_{r_0 \to r_p}$ is in Eq. (5.33).

The time T_p for each possible value of r_p and r_a is shown in Fig. 5.6(a). Each radius value corresponds to a unique a_T, as given in Eq. (5.31). When $a_T = 0$, the period $T_p = 2\pi$. When firing in, the time from initial circular radius $r_0 = 1$ to reach perigee r_p is the same as going from perigee back to the initial circular orbit, as per Eq. (5.35). Similar behavior occurs when firing outwards. Also, once the spacecraft reaches the initial circular orbit after one revolution, the state conditions are the same as the initial ones, with an angular displacement offset. The spacecraft conditions at T_p can be expressed

as equivalent to the initial conditions at t_0, relative to the offset angle. This verifies that the position magnitude r is a periodic function of time (as can be observed in the examples in Fig. 5.3(c) and Fig. 5.4(c)).

Proposition 5.3.1. *The position magnitude r is a periodic function of time, varying from $r_p \leq r \leq 1$ when firing in, and $1 \leq r \leq r_a$ when firing out. The period of oscillation T_p is given by Eq. (5.35).*

The angular displacement θ after one revolution of returning to the initial circular orbit appears to be symmetric for inbound/outbound segments. That is, suppose $\delta > 0$ is the off-set from unity such that $r_p = 1 - \delta$ is the perigee for firing inwards, and $r_a = 1 + \delta$ is the apogee for firing out. The angular displacement θ is, in this case, equal in magnitude, but opposite sign (see Fig. 5.6(b)). This is true even though the acceleration magnitude a_T is very different for each case, as can be observed in Fig. 5.5.

Conjecture 1. *The angular displacement after one revolution of returning to the initial circular orbit is symmetric in perigee/apogee radius. That is, for any $0 \leq \delta \leq 1$, $\theta_{r_p} = -\theta_{r_a}$ when $r_p = 1 - \delta$ and $r_a = 1 + \delta$.*

5.3.3 Orbital Elements as a Function of Position Magnitude

In this section, an overview study of the three orbital elements required to describe a 2D trajectory are presented: semi-major axis a, eccentricity e, and argument of periapsis *aop*. The elements can be described by the state r and θ, whose differential equation is given in Eq. (5.29). Again, without loss

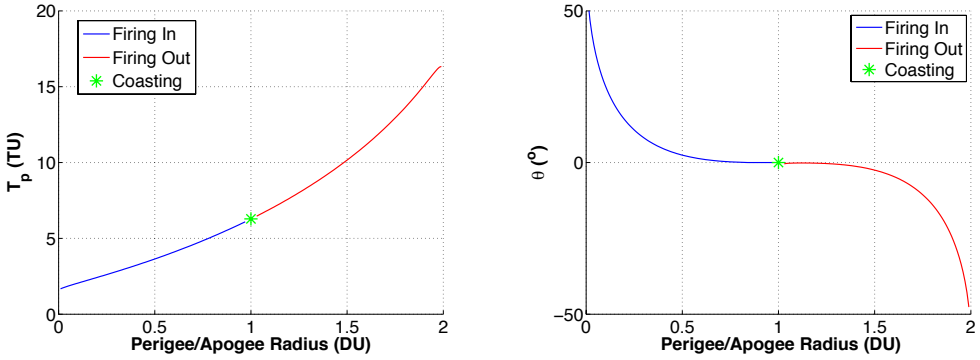

(a) Period to complete one revolution

(b) Angular displacement θ

Figure 5.6: Symmetry properties of angular displacement and period of an orbit after one revolution.

of generality, choosing $\mu = 1$, and $r_0 = 1$, and since the semi-major axis does not vary by Eq. (5.4), then $a = 1 \; \forall \; t$.

The eccentricity e can be expressed *only* as a function of r, in the following way:

$$p = a(1 - e^2) = \frac{h^2}{\mu} \quad \Rightarrow \quad e^2 = 1 - \frac{h^2}{a\mu} = 1 - h^2 \tag{5.36}$$

where p is the semi-latus rectum, h is the angular momentum, $h = rv \sin\gamma$. Using the definition for $w(r) = \sin\gamma$ in Eq. (5.28) and v in Eq. (5.19), the eccentricity is

$$e(r) = \sqrt{1 - r^2 v^2 \sin^2\gamma} = \sqrt{1 - r(2 - r)w^2} \tag{5.37}$$

To show that the the maximum eccentricity is achieved at the minimum radius r_p when firing in (equivalently the maximum radius r_a when firing out), the

time derivative of eccentricity is studied.

$$\frac{de}{dt} = \frac{de}{dr}\frac{dr}{dt} = 0, \tag{5.38}$$

where $\frac{dr}{dt}$ is in Eq. (5.29) and $\frac{de}{dr}$ is

$$\begin{aligned} \frac{de}{dr} &= \frac{w}{\sqrt{1-r(2-r)w^2}}\left[w(r-1)+r(r-2)\frac{dw}{dr}\right] \\ &= -\frac{a_T r^2 w}{e}. \end{aligned} \tag{5.39}$$

Here, $\frac{dw}{dr}$ has been substituted from Eq. (5.27). The extrema of the eccentricity are found by

$$\frac{de}{dt} = -K\frac{a_T r^2 w}{e}\sqrt{\frac{2-r}{r}}\sqrt{1-w^2} = 0 \tag{5.40}$$

Indeed, as long as the trajectory does not reach its limiting values, $r_{min} = 0$ or $r_{max} = 2$, the eccentricity has an extrema at

$$\sqrt{1-w^2} = 0 \quad \Rightarrow \quad w = 1 \tag{5.41}$$

The solution $w = -1$ is discarded, since w only admits positive values. As was discussed in Section 5.3.2, $w = 1$ admits two solutions of position magnitude, at $r = 1$ and $r = r_p$ (or respectively $r = r_a$). By looking at the second time derivative of eccentricity,

$$\begin{aligned} \frac{d^2e}{dt^2} &= \frac{d}{dt}\left(\frac{de}{dt}\right) = \frac{d}{dt}\left(\frac{de}{dr}\cdot\frac{dr}{dt}\right) \\ &= \frac{d}{dt}\left(\frac{de}{dr}\right)\cdot\frac{dr}{dt} + \frac{de}{dr}\cdot\frac{d^2r}{dt^2} \end{aligned} \tag{5.42}$$

where

$$\begin{aligned}\frac{d}{dt}\left(\frac{de}{dr}\right) &= -a_T\frac{r}{e}\left(2w\frac{dr}{dt}+r\frac{dw}{dt}-\frac{rw}{e}\frac{de}{dt}\right)\\ \frac{d^2r}{dt^2} &= -K\left[\sqrt{1-w^2}\sqrt{\frac{1}{r^3(2-r)}}\frac{dr}{dt}+\sqrt{\frac{2-r}{r}}\frac{w}{\sqrt{1-w^2}}\frac{dw}{dt}\right]\end{aligned}$$

and $\frac{dw}{dt} = \frac{dw}{dr}\frac{dr}{dt}$, where $\frac{dr}{dt}$, $\frac{dw}{dr}$, and $\frac{de}{dt}$ are in Eq. (5.29), (5.27), and (5.40), respectively.

The maximum and minimum eccentricity values are

$$\begin{aligned}&\frac{de}{dt}=0 \text{ and } \frac{d^2e}{dt^2}=0 \quad \Rightarrow \quad e_{min}=0 \text{ at } r=1\\ &\frac{de}{dt}=0 \text{ and } \frac{d^2e}{dt^2}<0 \quad \Rightarrow \quad e_{max}=\delta \text{ at } r_p=1-\delta \text{ (or } r_a=1+\delta)\end{aligned}$$

The eccentricity e, its time-derivative de/dt, and its second time-derivative d^2e/dt^2 are plotted in Fig. 5.7(a) for the same conditions as the firing in trajectory example shown in Fig. 5.3. The acceleration magnitude a_T is chosen so as to achieve an $r_p = 0.1$, which corresponds to a maximum eccentricity $e_{max} = 1 - r_p = 0.9$. A second example firing out is shown in Fig. 5.7(b), which corresponds to the same conditions as in the example shown in Fig. 5.4. Here, a_T is chosen to achieve an $r_a = 1.9$, which corresponds to a maximum eccentricity $e_{max} = r_a - 1 = 0.9$.

The argument of periapsis aop can be written also as a function of r as

$$\tan(aop) = \frac{e_y}{e_x} \tag{5.43}$$

where the components of eccentricity vector $\mathbf{e} = [e_x \; e_y]^T$ are

$$\mathbf{e} = \frac{1}{\mu}\left[\left(v^2-\frac{\mu}{r}\right)\mathbf{r}-(\mathbf{r}\cdot\mathbf{v})\,\mathbf{v}\right] \tag{5.44}$$

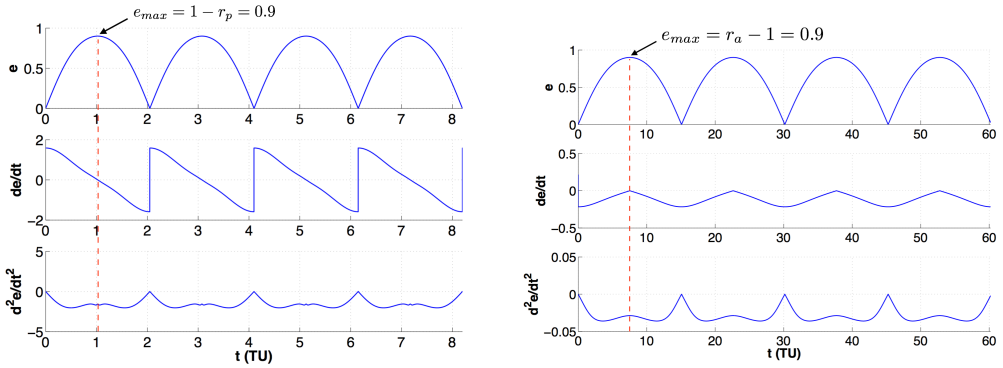

(a) Firing in to $r_p = 0.1$ (b) Firing out to $r_a = 1.9$

Figure 5.7: Eccentricity, its time-derivative and second time-derivative for two different examples.

In polar coordinates,

$$\mathbf{r} = \begin{pmatrix} r\cos\theta \\ \\ r\sin\theta \end{pmatrix} \quad \text{and} \quad \mathbf{v} = \begin{pmatrix} v\cos(\gamma+\theta) \\ \\ v\sin(\gamma+\theta) \end{pmatrix} \tag{5.45}$$

and $\mathbf{r}\cdot\mathbf{v} = rv\cos\gamma$. The eccentricity vector is re-written as

$$\begin{pmatrix} e_x \\ \\ e_y \end{pmatrix} = \begin{pmatrix} a\cos\theta + b\cos\theta \\ \\ a\sin\theta - b\cos\theta \end{pmatrix} \tag{5.46}$$

where

$$\begin{aligned} a &= \frac{1}{2}(v^2-1)r - rv^2\cos^2\gamma = -1 + (2-r)w^2 \\ b &= rv^2\cos\gamma\sin\gamma = (2-r)w\sqrt{1-w^2} \end{aligned}$$

The velocity $v(r)$ has been substituted in Eq. (5.19), $\cos\gamma = \sqrt{1-w^2}$, and

$\sin\gamma = w$. The argument of periapsis is

$$aop = \tan^{-1}\left(\frac{e_y}{e_x}\right) = \tan^{-1}\left(\frac{a\tan\theta + b}{a - b\tan\theta}\right) \tag{5.47}$$

At perigee r_p when firing in (or apogee r_a when firing out), $\sin\gamma = 1$, and therefore, it is readily seen that $(aop)_{r_p} = \theta_{r_p}$, which is the only location where the argument of periapsis and the angular displacement are equal.

5.4 Comparison with the Radial Thrust Problem

The radial thrust problem, in which two-body motion is assumed with a continuous perturbation from a constant acceleration magnitude in the position vector admits an analytical solution [2, 49]. The radial thrust problem is reminiscent of the vel-normal thrust problem in that, when starting from an initial circular orbit, the spacecraft will reach a minimum radius (perigee) when firing inwards, after which it will return to the initial circular orbit, but on a different location on the orbit. Similar behavior occurs when firing outwards, in which the spacecraft reaches a maximum radius (apogee), before returning to the initial circular orbit. In this section, we compare the behavior of a spacecraft under constant radial thrust with the behavior of a spacecraft under constant vel-normal thrust. The radial thrust problem admits an analytical solution in terms of elliptic integrals to the time T_p to complete one revolution, as well as the angular displacement in terms of a_T [2].

The radial thrust problem has an analytical expression for the no-escape condition [2, 5]. In fact, it is proven that for radial inwards firing, a spacecraft

will never escape or collide with the central body, which is not the case for the vel-normal inwards thrusting (recall Eq. (5.32)). For radial outwards thrusting, the acceleration $a_T \leq 1/8$ for bounded motion (for initial conditions $\mu = 1$ and $r_0 = 1$) [2], which is smaller than the maximum allowed acceleration thrust for bounded vel-normal outwards thrusting.

Figure 5.8 shows a comparison between radial and vel-normal thrust when firing inwards. For the radial problem this corresponds to thrusting in the negative direction of the position magnitude. Again, there is no maximum acceleration bound for inwards radial thrusting, whereas for inwards vel-normal thrust, the maximum allowed thrust is $a_T = 4/(3\pi - 8)$. Figure 5.8(a) shows the time T_p to complete one revolution for different a_T values. The time T_p for both radial and vel-normal thrust are very similar. In fact, they become equal to each other for $a_T = 1.93$. The angular displacement after one revolution is in Figure 5.8(b). For the radial thrust problem, the angular displacement is negative, meaning that the spacecraft completes less than one 360^o revolution. In terms of magnitude, the angular displacement is greater for the radial thrust problem. For the same acceleration a_T, lower perigee radii r_p are obtained with the vel-normal thrusting protocol than with the radial thrusting protocol, as can be observed in Figure 5.8(c).

Figure 5.9 shows a comparison between radial and vel-normal thrust when firing outwards. For the radial problem this corresponds to thrusting in the same direction as the position magnitude. For an outwards vel-normal thrust, the maximum allowed thrust is $a_T = 4/(3\pi + 8)$, whereas for the out-

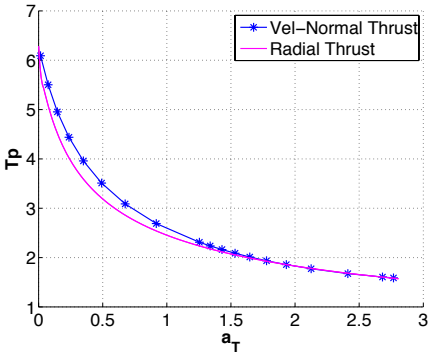

(a) Period T_p vs. a_T

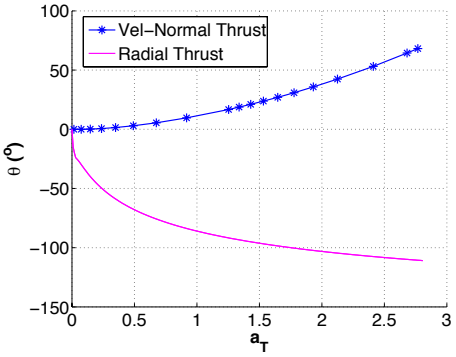

(b) Angular displacement θ vs. a_T

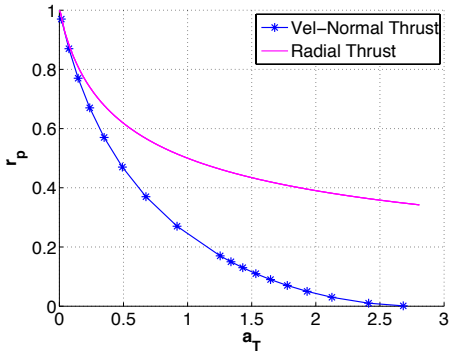

(c) Apogee radius vs. a_T

Figure 5.8: Comparison between vel-normal thrust and radial thrust when firing inwards.

wards radial thrust the maximum thrust is $a_T = 1/8$, which is a bit over half of the maximum vel-normal thrust. Figure 5.9(a) shows the time T_p to complete one revolution for different a_T values. The time T_p is much higher (and gets asymptotically higher) for the radial thrust dynamics. The angular displacement after one revolution is in Figure 5.9(b). For the radial thrust problem, the angular displacement is positive, whereas for the vel-normal thrust it is

negative. The angular displacement magnitude is greater for the radial thrust problem. For the same acceleration a_T, higher apogee radii r_a are obtained with the radial thrust problem, as can be observed in Figure 5.9(c).

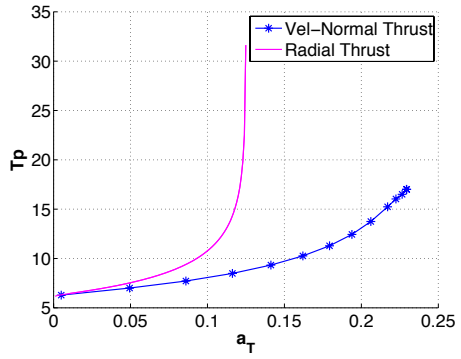

(a) Period T_p vs. a_T

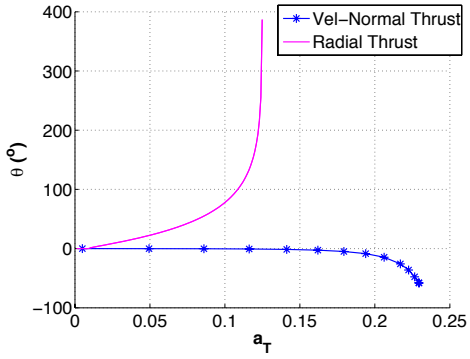

(b) Angular displacement θ vs. a_T

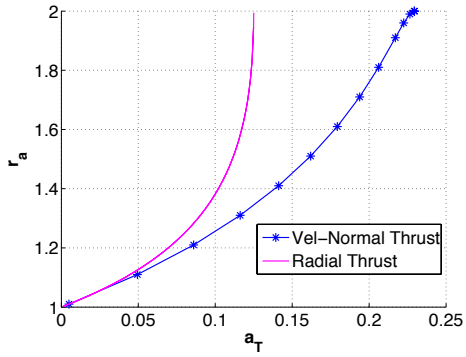

(c) Apogee radius vs. a_T

Figure 5.9: Comparison between vel-normal thrust and radial thrust when firing outwards.

5.5 Periodic Motion

Next, we seek to determine periodic motion with some period T using the equations of motion in Eq. (5.7), which is the cartesian coordinate equivalent of the equations in (5.29). By periodic motion we understand that the trajectory returns to its initial conditions after a period T_p has elapsed. In order to obtain the necessary conditions to achieve this, a differential correction procedure is developed to adjust the values of the acceleration magnitude a_T and period T_p.

There exist many periodic orbits in this system. What differentiates each orbit is the number of revolutions n that the trajectory performs before returning to its initial condition. By n here we refer to the times the trajectory returns to the initial circular orbit radius. In fact, the number of revolutions n is bounded above by a finite integer $n_{min} = 6$, because no matter if the spacecraft is firing outbound or inbound, the maximum phase difference obtained per revolution is approximately 60^o, by Fig. 5.6(b). The problem is posed as: for any integer $n \geq n_{min}$, determine the corresponding acceleration a_T and period T_p, such that the trajectory returns exactly to the starting location on the initial circular orbit exactly n revolutions later. Note that when n is even, the same question could be posed to find a_T and the half period $T_p/2$, such that the negative x-axis is crossed at a value exactly equal to the initial circular radius after $n/2$ revolutions.

Writing Eq. (5.7) as a set of first order differential equations

$$\mathbf{X} = \begin{pmatrix} x_1 \\ x_2 \\ x_3 \\ x_4 \end{pmatrix}, \quad \dot{\mathbf{X}} = \begin{pmatrix} x_3 \\ x_4 \\ -\frac{\mu}{r^3}x_1 - \sigma a_T \frac{x_4}{v} \\ -\frac{\mu}{r^3}x_2 - \sigma a_T \frac{x_3}{v} \end{pmatrix} \tag{5.48}$$

where $r = \sqrt{x_1^2 + x_2^2}$ and $v = \sqrt{x_3^2 + x_4^2}$. The initial conditions of the periodic orbit are fixed, since it is starting in a circular orbit assumed to be on the x-axis at an initial time t_0.

$$\left.\begin{array}{l} r_0 = 1 \\ \theta_0 = 0 \end{array}\right\} \quad \Rightarrow \quad \mathbf{X}_0 = [1\ 0\ 0\ 1]^T \tag{5.49}$$

We target the final conditions $\tau = T_p$

$$\begin{aligned} y(\tau) &= 0 \\ \dot{x}(\tau) &= 0 \end{aligned}$$

The total differential is written as

$$d\mathbf{X}_f = \mathbf{\Phi}(\tau, t_0)\delta\mathbf{X}_0 + \boldsymbol{\phi}_a(\tau, t_0)da_T + \dot{\mathbf{X}}_f d\tau, \tag{5.50}$$

where $d\mathbf{X}_f = [0,\ 0 - y_f,\ 0 - \dot{x}_f,\ 0]^T$. Since the initial conditions are fixed, and only the final time and acceleration magnitude are variable, then $\delta\mathbf{X}_0 = \mathbf{0}$. Here, $\boldsymbol{\phi}_a(\tau, t_0)$ is the state transition vector associated with the variation in

acceleration magnitude,

$$\boldsymbol{\phi}_{a_T}(t_f, t_0) = \left(\frac{\partial \mathbf{X}_f}{\partial a_T}\right)_{4\times 1} \tag{5.51}$$

whose differential equation is

$$\dot{\boldsymbol{\phi}}_{a_T} = \mathbf{F}\boldsymbol{\phi}_{a_T} + \mathbf{F}_{a_T}, \qquad \boldsymbol{\phi}_{a_T}(t_0) = \mathbf{0}_{4\times 1} \tag{5.52}$$

and the state transition matrix $\boldsymbol{\Phi}(\tau, t_0)$ is

$$\boldsymbol{\Phi}(t_f, t_0) = \left(\frac{\partial \mathbf{X}_f}{\partial \mathbf{X}_0}\right)_{4\times 4} \tag{5.53}$$

whose differential equation is governed by

$$\dot{\boldsymbol{\Phi}} = \mathbf{F}\boldsymbol{\Phi}, \qquad \boldsymbol{\Phi}(t_0) = \mathbf{I}_{4\times 4} \tag{5.54}$$

The matrix $\mathbf{F}$ is

$$\mathbf{F} = \frac{\partial \dot{\mathbf{X}}}{\partial \mathbf{X}} = \begin{bmatrix} \mathbf{0} & \mathbf{I} \\ \mathbf{G} & \mathbf{H} \end{bmatrix} \tag{5.55}$$

where $\mathbf{0}$ is a 2×2 matrix of zeros, $\mathbf{I}$ is a 2×2 identity matrix, and

$$\mathbf{G} = \begin{bmatrix} g_{11} & g_{12} \\ g_{21} & g_{22} \end{bmatrix} \quad \text{and} \quad \mathbf{H} = \begin{bmatrix} h_{11} & h_{12} \\ h_{21} & h_{22} \end{bmatrix}$$

$$g_{11} = \frac{\mu}{r^3}\left(\frac{3}{r^2}x_1^2 - 1\right) \qquad \text{and} \qquad h_{11} = a_T\frac{x_3 x_4}{v^3} = -h_{22}$$

$$g_{12} = 3\frac{\mu}{r^5}x_1 x_2 = g_{21} \qquad \text{and} \qquad h_{12} = \frac{a_T}{v}\left(\frac{x_4^2}{v^2} - 1\right)$$

$$g_{22} = \frac{\mu}{r^3}\left(\frac{3}{r^2}x_2^2 - 1\right) \qquad \text{and} \qquad h_{21} = -\frac{a_T}{v}\left(\frac{x_3^2}{v^2} - 1\right)$$

The first and last rows of (5.50) can be discarded, such that

$$\begin{pmatrix} -y_f \\ -\dot{x}_f \end{pmatrix} = \boldsymbol{\phi}_a(\tau, t_0) da_T + \begin{pmatrix} \dot{y}_f \\ \ddot{x}_f \end{pmatrix} d\tau \tag{5.56}$$

Solving for the unknowns δa_T and $d\tau$,

$$\begin{pmatrix} da_T \\ d\tau \end{pmatrix} = \begin{pmatrix} \phi_{a_2} & \dot{y}_f \\ \phi_{a_3} & \ddot{x}_f \end{pmatrix}^{-1} \begin{pmatrix} -y_f \\ -\dot{x}_f \end{pmatrix} \tag{5.57}$$

With the above differential corrector procedure, several types of periodic orbits are found. When firing in, the minimum number of revolutions a trajectory can have before becoming retrograde is $n_{min} = 6$. The initial conditions, a_T and T for $n_{min} \leq n \leq 24$ when firing in are in Table 5.1. Periodic solutions with higher number of revolutions can also be found. The same is possible for periodic orbits when firing out. Several trajectory examples are shown in Fig. 5.10, with corresponding initial conditions in Table 5.2. In Fig. 5.10(a)-(b) two bounded trajectories are shown when firing in, with $n = 6$ and $n = 15$, respectively. By bounded motion, we refer to the acceleration magnitude being below the threshold $a_T|_{r_{min}}$. In fact, when a_T is increased above this threshold, retrograde motion occurs, as can be observed in Fig. 5.10(c). When firing out, periodic orbits are also found; however, since the range of a_T magnitudes valid are smaller (i.e. $0 \leq a_T \leq a_T|_{r_{max}}$, where $a_T|_{r_{max}} = 0.2296$), the algorithm is more numerically sensitive to find the exact value of all the possible periodic orbits. A bounded periodic orbit when

firing out is shown in Fig. 5.10(d). When the acceleration magnitude surpasses the limiting value $a_T|_{r_{max}}$ retrograde motion begins, as can be observed in Fig. 5.10(e)-(f).

The stability of these periodic orbits is studied by computing the eigenvalues of the monodramy matrix. This matrix is defined as the state transition matrix $\mathbf{\Phi}(\tau, 0)$ for one full period $\tau = T_p$. Periodic orbits will always have one unity eigenvalue $\lambda = 1$. Also, the eigenvalues come in reciprocal pairs; therefore, at least two eigenvalues will lie on the real-axis of a unitary circle (real vs. imaginary) at unity. Since we have a four-dimensional state transition matrix, there are a total of four eigenvalues. Therefore, the other two eigenvalues determine the stability of the orbits. All eigenvalues of $\Phi(T, 0)$ for the periodic orbits shown in Fig. 5.10, have unit norm

$$\|\lambda_i\| = 1, \quad i = 1, ..., 4$$

which shows that these orbits are *marginally stable*.

A Poincaré surface of sections is shown in Fig. 5.11. The initial conditions begin on a circular orbit at $\theta = 0$, as given in Eq. (5.49). In order to understand the behavior of the dynamical system, the acceleration magnitude a_T is varied for values of perigee $r_p = [0.1 : 0.1 : 0.9]$ when firing in, and apogee $r_a = [1.1 : .1 : 1.9]$ when firing out. The value of a_T for these radii is found in Eq. (5.31). These trajectories are not periodic in the sense that they do not return to their initial conditions after a full 360^o. However, after many revolutions they return to the initial conditions, to within some tolerance ball.

Table 5.1: Periodic bounded orbit conditions when firing in for $n_{min} \leq n \leq 24$.

n_{odd}	a_T	T_p
6	2.5768	9.7772
7	2.3666	11.8140
8	2.1971	13.9606
9	2.0569	16.2038
10	1.9384	18.5334
11	1.8368	20.9412
12	1.7483	23.4202
13	1.6706	25.9646
14	1.6016	28.5698
15	1.5398	31.2311
16	1.4841	33.9452
17	1.4336	36.7085
18	1.3876	39.5180
19	1.3454	42.3715
20	1.3066	45.2662
21	1.2708	48.2002
22	1.2376	51.1716
23	1.2218	52.6707
24	1.1778	57.2190

A single dot $(x, \dot{x})$ in Fig. 5.11 is plotted, corresponding to $y = 0$ and $\dot{y} > 0$ for 500 revolutions. The crossings at $\dot{x} = 0$ always correspond either to $x = 1$

Table 5.2: Initial conditions for periodic orbits in Fig. 5.10

	Type of Motion	n	a_T	T
(a)	Prograde	6	2.5768	9.7772
(b)	Prograde	15	1.5398	31.2311
(c)	Retrograde	3	3.6828	4.5228
(d)	Prograde	11	-0.2210	87.0066
(e)	Retrograde	5	-0.2999	45.9152
(f)	Retrograde	11	-0.7162	52.7642

or $x = r_p$ when firing in and $x = r_a$ when firing out. The only fixed point occurs at $x = 1$, which corresponds to $a_T = 0$, that is, a coasting trajectory on the initial circle.

5.6 Final Remarks

In this last chapter of the dissertation the motion of spacecraft under the action of constant thrust acceleration in the direction perpendicular to the velocity has been studied. In this system, the energy of the spacecraft remains constant for all time. A spacecraft starting in an initial circular orbit will obtain a minimum (perigee) radius along an *inbound* trajectory. If the thrust is maintained, the spacecraft returns to the initial circular orbit in an outbound trajectory. A maximum (apogee) radius is obtained when starting

in a circular orbit along an *outbound* trajectory, after which the vehicle will return again to the initial circular orbit.

A full analytical solution to this problem has not yet been found; however, an analytical solution to the flight direction angle is found. This solution leads to several insights on the problem, such as obtaining analytical expressions on a valid range of acceleration magnitudes for bounded motion, as well as proving periodicity of the position magnitude in time.

The system exhibits periodic motion in the position magnitude, that is, the spacecraft always returns to the initial circular orbit, but on a different phase location that the initial starting point. Therefore, fully periodic orbits are found which return to the initial location of the spacecraft after a certain number of revolutions. A differential correction procedure is outlined, and their stability is characterized.

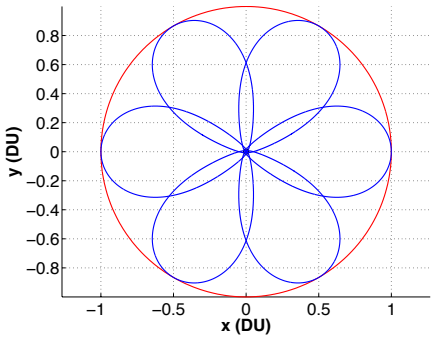

(a) Firing inwards, bounded, $n = 6$

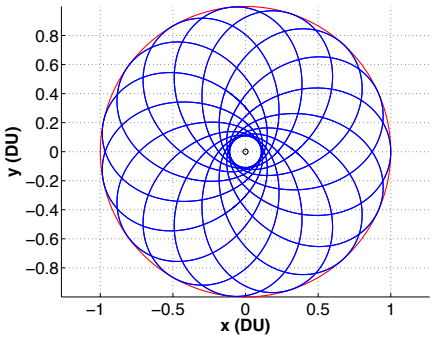

(b) Firing inwards, bounded, $n = 15$

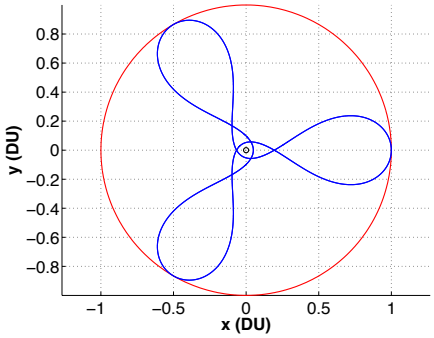

(c) Firing inwards, retrograde motion, $n = 3$

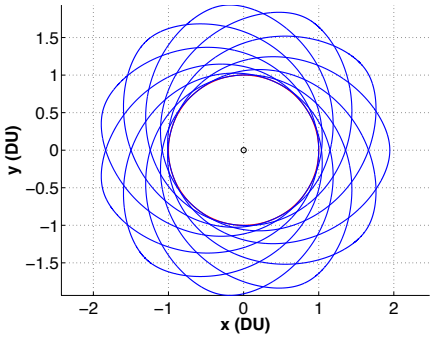

(d) Firing outwards, bounded, $n = 11$

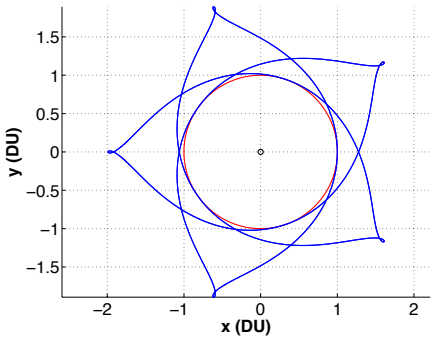

(e) Firing outwards, retrograde motion, $n = 5$

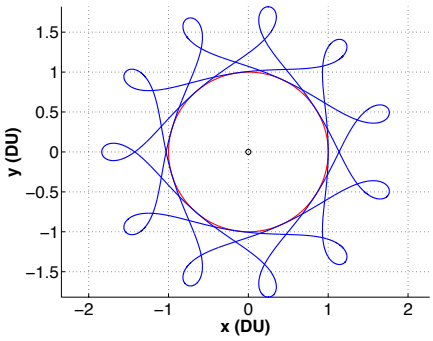

(f) Firing outwards, retrograde motion, $n = 11$

Figure 5.10: Periodic orbits for different a_T values, and n revolutions.

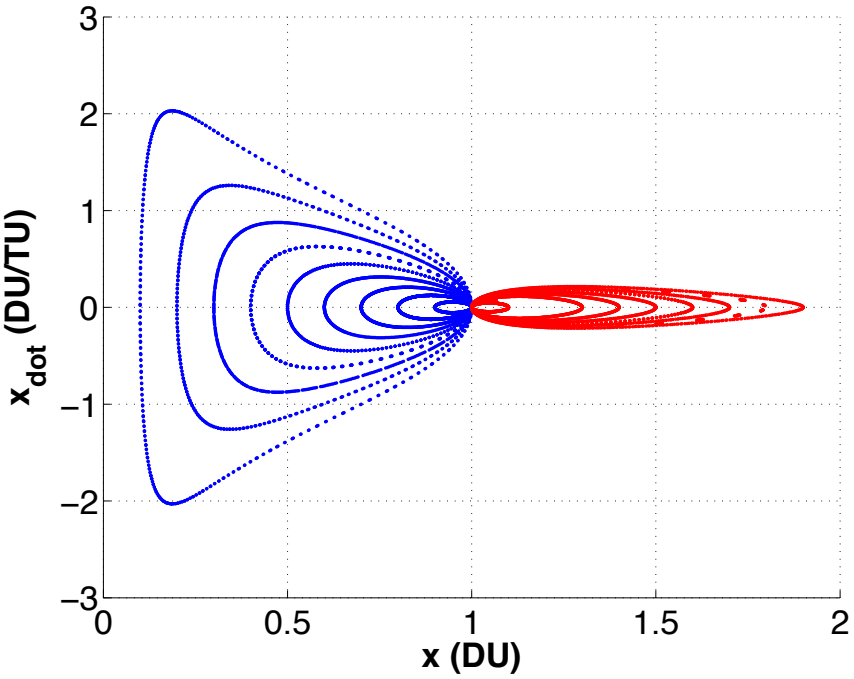

Figure 5.11: Poincare surface of sections corresponding to different a_T values for firing inwards (blue) and outwards (red).

Chapter 6

Dissertation Summary

In this dissertation, several trajectory design problems have been addressed, with the main focus on producing simple algorithms that either admit an analytical solution or require minimal computation time because of their closed-form nature. A perturbed two-body model with continuous thrust is used for all problems, with an emphasis on low-thrust solutions. The three main focuses are: designing Lyapunov-based guidance laws for orbit transfers, finding semi-analytical solutions using a constant magnitude thrust, and using perturbation theory to find approximate analytical solutions. One of the technical qualities that these problems have in common is that they all use, fully or partially, a thrusting model in which the energy of the system remains constant.

The motivation behind using a thrusting model in which energy remains constant, comes from using a regularized two-body model. Originally, the regularization problem was developed in celestial mechanics for collision avoidance-type problems[1, 7], by transforming the singular differential equations into regular ones, such that the model would still be numerically well defined even as $r \rightarrow 0$. One of the remarkable properties of this transformed

model is that the solution to the unperturbed equations of motion is that of a linear harmonic oscillator, where the frequency of oscillation is a function of a, the semi-major axis of the orbit. Therefore, during any coast phase, the analytical solution is explicitly characterized. Also, when the energy of the orbit remains constant, the frequency of oscillation of the harmonic oscillator is also kept constant, which allows for significant simplification in the orbit transfer problems tackled in the dissertation.

In Chapter 2 the problem of designing planar closed-loop guidance for orbit transfers is solved by working in the transformed regularized model. This model is known as the Levi-Civita regularization, valid for planar motion. We design a closed-loop guidance scheme for a coplanar orbit transfer from any initial elliptical orbit to any final specified elliptical orbit utilizing a spacecraft with thrust-coast capabilities. The convergence to the desired formation is performed in two steps. The first step involves converging the spacecraft orbit to the desired semi-major axis a^*, by using a Lyapunov analysis that gives rise to an asymptotically stabilizing control law. Once a^* has been reached to within a specified tolerance, the second step of the algorithm involves matching the other desired orbital parameters, using the same control law as before, but with an added on/off switching mechanism for coasting during certain intervals. The algorithms designed are robust, computationally fast, and can be used for both low- and high-thrust problems. One of the powerful results of this work is that the guidance law is designed based *only* on matching the desired semi-major axis. With the same control law that matches semi-major

axis, we are able to match any desired orbit by adding thrust/coast arcs.

The problem solved in Chapter 2 is generalized to three-dimensional motion in Chapter 3. The equivalent regularized model for out-of-plane motion is known as the Kustaanheimo-Stiefel model, in which the three-dimensional cartesian coordinates are expanded to four-dimensions in order to allow for the regularization to occur. We take advantage of the KS model to design the Lyapunov-based guidance schemes to perform different types of non-coplanar orbit transfers. The solution procedure is implemented in one step, although the design procedure involves two steps. The first step involves converging the spacecraft orbit to the desired semi-major axis (or equivalently, the desired energy). Once the energy has been met, the second step involves converging the remaining subset desired orbital elements (by holding energy constant). We are able to guarantee that any orbital element can be targeted by holding energy constant, which is one of the major contributions of the chapter. The KS model aids in the design of the guidance schemes, but the solutions can be explicitly characterized in the regular cartesian coordinates. No constraint is imposed on the magnitude of the thrust; however, an emphasis is placed on the low-thrust solutions, since they compare well with the optimal ones. One of the main advantages of closed-loop guidance schemes is that they have a low computation time when compared to direct or indirect optimization methods, so they are a good method to obtain an initial guess for mission design purposes. Also they permit for easy onboard implementation, since the control laws are based solely on the current state of the spacecraft.

To find approximate analytical solutions to the guidance schemes derived in Chapter 2, perturbation theory is studied in Chapter 4, by assuming a constant acceleration thrust. The model used is the Levi-Civita model, such that the perturbation is always in the direction perpendicular to the velocity, which ensures constant energy. The analytical expression is solved for spacecraft which are initially in a circular orbit. The approximation is found by performing a Taylor series expansion about the acceleration magnitude, which is assumed to be constant and small, and the time-varying coefficients of the solution are solved by performing the necessary analytical integration. From simulation examples it is clear that the solution is accurate for small acceleration magnitudes, but breaks down for higher magnitudes after several revolutions.

The last chapter of the dissertation, Chapter 5, spacecraft motion under the action of constant thrust acceleration in the direction perpendicular to the velocity is studied, using the normal two-body equations of motion. In this system, the energy of the spacecraft remains constant for all time. A spacecraft starting in an initial circular orbit will obtain a minimum (perigee) radius along an *inbound* trajectory. If the thrust is maintained, the spacecraft returns to the initial circular orbit in an outbound trajectory. A maximum (apogee) radius is obtained when starting in a circular orbit along an *outbound* trajectory, after which the vehicle will return again to the initial circular orbit. A full analytical solution to this problem does not exist; however, an analytical solution to the flight direction angle is found. This solution leads to several insights

on the problem, such as obtaining analytical expressions on a valid range of acceleration magnitudes for bounded motion, as well as proving periodicity of the position magnitude in time.

6.1 Future Work

There are several avenues for future work in the guidance scheme development in both Levi-Civita (Chapter 2) and KS coordinates (Chapter 3). It would be interesting to design control algorithms that do not require the energy of the orbit to be pre-targeted in order to perform an orbit transfer. Another important aspect is to study how to add gains (either time-invariant or time-varying) to explicitly control the rate of convergence of each orbital element (similar to the Q-law algorithm). Some more work needs to be performed in terms of comparing the algorithm presented in this dissertation with other Lyapunov-based approaches as well as optimal solutions. As was mentioned at the beginning of this chapter, solving the rendezvous problem in KS variables was not possible (see Appendix D.2). We plan on further investigating avenues to solve this problem.

The perturbation work in Chapter 4 has only been applied to the planar problem in Levi-Civita coordinates. Further investigation on perturbation theory in the three-dimensional model should be looked at; as well as the possibility of finding a solution when the initial conditions are not circular. A similar study should be done on Chapter 5, to see if semi-analytical solutions exist when starting on an elliptical orbit.

Appendices

Appendix A

Nonlinear Control (Chapters 2 and 3)

The theory in this Appendix is used for Chapters 2 and 3 of this dissertation.

Suppose we have a nonlinear systems and wish to study its behavior and stability. Nonlinear dynamical systems can be modeled as a system of coupled first-ordered differential equations [31]

$$\begin{aligned}
\dot{x}_1 &= f_1(t, x_1, ..., x_N, u_1, ..., u_p) \\
\dot{x}_2 &= f_2(t, x_1, ..., x_N, u_1, ..., u_p) \\
\vdots &\quad\ \vdots \\
\dot{x}_N &= f_N(t, x_1, ..., x_N, u_1, ..., u_p),
\end{aligned}$$

where x_k, $k \in \{1, ..., N\}$, are the state-variables, u_j, $j \in \{1, ..., P\}$, are the control inputs, and t is time. This system of differential equations can be

written in a more compact form. By writing the following vector notation,

$$x = \begin{bmatrix} x_1 \\ x_2 \\ \vdots \\ x_N \end{bmatrix}, \quad u = \begin{bmatrix} u_1 \\ u_2 \\ \vdots \\ u_P \end{bmatrix}, \quad f(t,x,u) = \begin{bmatrix} f_1(t,x,u) \\ f_2(t,x,u) \\ \vdots \\ f_N(t,x,u) \end{bmatrix},$$

we rewrite the system of differential equations as

$$\dot{x} = f(t,x,u),$$

This equation depends explicitly on time and is called non-autonomous or time-varying. Equations that do not depend explicitly on time are called autonomous or time-invariant, and are of the form

$$\dot{x} = f(x,u).$$

The concept of an equilibrium point plays an important role in the stability of dynamical systems. A point $x = x^*$ is an *equilibrium point* of $\dot{x} = f(t,x,u)$ if, whenever the state of the system starts near x^*, it remains near x^* for all time. A system can have one or multiple equilibrium points. Here, an explanation on how to study the stability of equilibrium points for autonomous systems is given. The stability for non-autonomous systems follows similarly, and is explained in detail in [31].

A.1 Stability of Autonomous Systems

Consider the autonomous system

$$\dot{x} = f(x). \tag{A.1}$$

The origin $x^* = 0$ is an equilibrium point of (A.1) if

$$f(x^*) = 0.$$

Definition A.1.1. [31, Definition 4.1] The equilibrium point $x^* = 0$ of model (A.1) is

- stable if all solutions starting at nearby points stay nearby.
- unstable if it is not stable.
- asymptotically stable if it is stable and solutions tend to the equilibrium points as time approaches infinity, i.e., if we can choose an $\epsilon > 0$ such that

$$\text{if } \|x(0)\| < \epsilon, \text{then } \lim_{t\to\infty} x(t) = 0.$$

A depiction of Definition A.1.1 is shown in Figure A.1. The system $\dot{x} = f(x)$ has two equilibrium points. A graphical method to determine the stability of the equilibrium points is to examine the variation in the sign of $f(x)$. We separate the function into segments between equilibrium points, drawing arrows to the left if $f(x)$ is negative and to the right if $f(x)$ is positive.

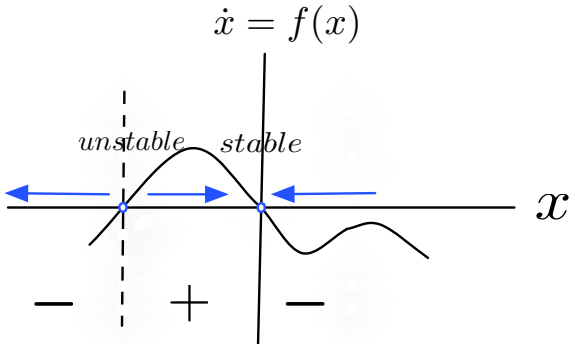

Figure A.1: Example of the stability of an autonomous system.

The equilibrium point is unstable if both arrows face away from the point and stable if both arrows face toward the point.

Another method to determine the stability of an equilibrium point is to use Lyapunov's stability theorem:

Theorem A.1.1. *Lyapunov Stability Theorem [31, Theorem 4.1]. Let* $x^* = 0$ *be an equilibrium point of (A.1) and* $D \in \mathbb{R}^N$ *be a domain containing* $x^* = 0$. *Let* $V : D \to \mathbb{R}$ *be a continuously differentiable function (called potential or*

Lyapunov function) such that

$$V(0) \;=\; 0 \; and \, V(x) > 0 \in D - \{0\}$$

$$\dot{V} \;\leq\; 0 \in D.$$

Then x^* is stable. Also, if

$$\dot{V} < 0 \in D - \{0\},$$

then x^* is asymptotically stable.

Note that the time derivative of V is of the form

$$\dot{V}(x) \;=\; \sum_{i=1}^{N} \frac{\partial V}{\partial x_i}\dot{x}_i = \sum_{i=1}^{N} \frac{\partial V}{\partial x_i} f_i(x) = \begin{bmatrix} & & \\ \frac{\partial V}{\partial x_1} & \cdots & \frac{\partial V}{\partial x_N} \\ & & \end{bmatrix} \begin{bmatrix} f_1(x) \\ \\ \vdots \\ \\ f_N(x) \end{bmatrix}.$$

It is important to keep in mind that Lyapunov functions are not unique. Therefore, failure of a Lyapunov function to satisfy the conditions for stability does not guarantee that an equilibrium point is unstable.

Definition A.1.2. A potential function V is

- Positive definite if $V(0) = 0$ and $V(x) > 0 \; \forall \; x \neq 0$.
- Positive semi-definite if $V(0) = 0$ and $V(x) \geq 0 \; \forall \; x \neq 0$.
- Negative (semi-)definite if $-V(x)$ is positive (semi-)definite

Theorem A.1.1 can also be stated as follows. The equilibrium point $x^* = 0$ is stable if there exits a continuously differentiable positive definite function $V(x)$ such that $\dot{V}(x)$ is negative semi-definite and $x^* = 0$ is asymptotically stable if $\dot{V}(x)$ is negative definite.

Sometimes it is not possible to show that an equilibrium point is asymptotically stable by using Theorem A.1.1 because the potential function $V(x)$ might fail to be negative definite. In these cases, we use LaSalle's Invariance Principle. The following definitions are necessary.

Definition A.1.3. [19] x_0 is a limit point of the set D if there exits a sequence in D which converges to x_0.

Definition A.1.4. [46] p is a positive limit point of $x(t)$, where $x(t)$ is a solution of (A.1), if there exits a sequence $\{t_n\}$, with $t_n \to \infty$ as $n \to \infty$, such

that $x(t_n) \to p$ as $n \to \infty$. The set of all positive limit points of $x(t)$ is called the positive limit set of $x(t)$.

Definition A.1.5. [46] The set M is invariant with respect to $\dot{x} = f(x)$ if, when $x(0) \in M$, $x(t) \in M \; \forall \; t \in \mathbb{R}$.

Theorem A.1.2. *LaSalle's Invariance Principle [31, Theorem 4.4]. Let $\Omega \subset D$ be a compact set that is positive invariant with respect to $\dot{x} = f(x)$. Let $V : D \to \mathbb{R}$ be a continuously differentiable function such that $\dot{V}(x) \leq 0 \in \Omega$. Let E be the set of all points in Ω where $\dot{V} = 0$. Let M be the largest invariant set in E. Then every solution starting in Ω approaches M as $t \to \infty$.*

Note that unlike in Theorem A.1.1, the function V does not have to be positive definite. It is also important to note that the invariance principle applies only to autonomous systems.

Appendix B

Analytical Expression for the Switching Functions (Chapter 2)

The analytical solution of the switching functions S_i, where $i = 1, 2, 3$ in Sections 2.3 and D.2 are solved for here. These functions are of importance because the exact amount of coast time is found by analytically solving for the roots of the function S_i.

B.1 Switching Function S_1 for Circular Orbit Transfers

The switching function S_1 defined in Eq. (2.32) is a function of the product of the position $\mathbf{u}$ (whose analytical solution is given by Eq. (2.18)) and the velocity $\mathbf{u}'$ (whose solution is found by directly taking the derivative of Eq. (2.18)). Assume the frequency of oscillation is given by $\mathcal{W} = \sqrt{-E/2} =$

$\sqrt{(\mu\alpha)/4}$ at some point in time s_0. The roots of S_1 are found by solving

$$\begin{aligned} S_1 &= u_1 u_1' + u_2 u_2' \\ &= C_1 \sin(\mathcal{W}s)\cos(\mathcal{W}s) + C_2\left(\cos^2(\mathcal{W}s) - \sin^2(\mathcal{W}s)\right) = 0 \end{aligned} \quad \text{(B.1)}$$

where

$$C_1 = -\mathcal{W}(u_{1_0}^2 + u_{2_0}^2) + \tfrac{1}{\mathcal{W}}(u_{1_0}'^2 + u_{2_0}'^2)$$

$$C_2 = (u_{1_0}u_{1_0}' + u_{2_0}u_{2_0}')$$

and u_{1_0}, u_{2_0}, u_{1_0}', and u_{2_0}' are the initial conditions at s_0. The roots of the equations are given by

$$s_{cross_1} = \pm\frac{1}{\mathcal{W}}\tan^{-1}\left(\frac{1}{2}\frac{\pm C_1 + \sqrt{C_1^2 + 4C_2^2}}{C_2}\right) \quad \text{(B.2)}$$

which correspond to the times at which the function S_1 changes sign, and therefore gives the time at which the thrusters should be turned on again after a coasting period.

B.2 Switching Function S_2 for General Orbit Transfers

The roots of the switching function S_2 defined in Eq. (2.43) are solved for, again assuming that the frequency of oscillation is given by $\mathcal{W} = \sqrt{(\mu\alpha)/4}$

at some point in time s_0.

$$\begin{aligned} S_2 &= 2(e_x - e_x^*)u_1' u_2' + (e_y - e_y^*)\left(u_2'^2 - u_1'^2\right) \\ &= C_1 \sin(\mathcal{W}s)\cos(\mathcal{W}s) + C_2 \sin^2(\mathcal{W}s) + C_3 \cos^2(\mathcal{W}s) = 0 \end{aligned} \quad \text{(B.3)}$$

where

$$C_1 = 2\left[-(e_x - e_x^*)(u_{1_0}u_{2_0}' + u_{1_0}'u_{2_0}) + (e_y - e_y^*)(u_{1_0}u_{1_0}' - u_{2_0}u_{2_0}')\right]\mathcal{W}$$

$$C_2 = \left[2(e_x - e_x^*)u_{1_0}u_{2_0} + (e_y - e_y^*)(u_{2_0}^2 - u_{1_0}^2)\right]\mathcal{W}^2$$

$$C_3 = \left[2(e_x - e_x^*)u_{1_0}'u_{2_0}' + (e_y - e_y^*)(u_{2_0}'^2 - u_{1_0}'^2)\right]$$

and e_x and e_y are defined in Eq. (2.37) and (2.38). The roots of the equations are given by

$$s_{cross_2} = \pm\frac{1}{\mathcal{W}}\tan^{-1}\left(\frac{1}{2}\frac{\mp C_1 + \sqrt{C_1^2 - 4C_2C_3}}{C_2}\right) \quad \text{(B.4)}$$

which correspond to the times at which the function S_2 changes sign.

Appendix C

Guidance Scheme in Cartesian Coordinates

(Chapter 3)

The guidance schemes presented in this paper have been designed using the KS model. However, it is possible to express the guidance schemes in the normal (more common) cartesian model, where the state to be integrated is position $\mathbf{r}$ and velocity $\dot{\mathbf{r}}$ and the variable of integration is time t.

The equations of motion $\ddot{\mathbf{r}}$ of a spacecraft in a perturbed planar two-body model are defined in Eq. (3.1), where the perturbing acceleration $\mathbf{f}$ is defined in Eq. (3.17) and the mass m varies according to $\dot{m} = -T/c$ where $c = gI_{sp}$, and I_{sp} is the specific impulse of the engine. Note that the unit vector $\hat{\mathbf{r}}'$ expressed in Eq. (3.17), is identical to the norm of velocity direction, i.e. $\hat{\mathbf{r}}' = \dot{\mathbf{r}}/\|\dot{\mathbf{r}}\|$.

We define the following parameters in cartesian coordinates. The inverse of the semi-major axis a is

$$\alpha = \frac{2}{r} - \frac{v^2}{\mu} \tag{C.1}$$

where $r = \|\mathbf{r}\|$ and $v = \|\dot{\mathbf{r}}\|$. The square of the eccentricity can be expressed as

$$e^2 = (1 - r\alpha)^2 + \frac{\alpha}{\mu}(\mathbf{r} \cdot \dot{\mathbf{r}})^2 \tag{C.2}$$

The angular momentum vector

$$\mathbf{h} = [h_1 \; h_2 \; h_3]^T = \mathbf{r} \times \dot{\mathbf{r}} \tag{C.3}$$

and the eccentricity vector

$$\mathbf{e} = [e_1 \; e_2 \; e_3]^T = \frac{1}{\mu}\dot{\mathbf{r}} \times \mathbf{h} - \frac{1}{r}\mathbf{r} \tag{C.4}$$

The following table expresses the guidance schemes in cartesian coordinates:

The following relations are used for the guidance schemes in Table C.1

$$S_e = (\mathbf{r} \cdot \dot{\mathbf{r}})(\mathbf{r} \cdot \hat{\mathbf{p}}) \tag{C.5}$$

$$\mathbf{q}_i = (h_3 - h_3^*)[r_2 \; -r_1 \; 0]^T \tag{C.6}$$

$$\mathbf{q}_h = \begin{bmatrix} -r_3(h_2 - h_2^*) + r_2(h_3 - h_3^*) \\ r_3(h_1 - h_1^*) - r_1(h_3 - h_3^*) \\ -r_2(h_1 - h_1^*) + r_1(h_2 - h_2^*) \end{bmatrix} \tag{C.7}$$

$$\mathbf{q}_o = \mathbf{q}_h - (e_1 - e_1^*)\mathbf{a} - (e_2 - e_2^*)\mathbf{b} \tag{C.8}$$

and

$$\mathbf{a} = \left[\begin{pmatrix} 0 \\ h_3 \\ -h_2 \end{pmatrix} + \begin{pmatrix} -(r_2\dot{r}_2 + r_3\dot{r}_3) \\ r_1\dot{r}_2 \\ r_1\dot{r}_3 \end{pmatrix} \right]$$

$$\mathbf{b} = \left[\begin{pmatrix} -h_3 \\ 0 \\ h_1 \end{pmatrix} + \begin{pmatrix} r_2\dot{r}_1 \\ -(r_1\dot{r}_1 + r_3\dot{r}_3) \\ r_2\dot{r}_3 \end{pmatrix} \right]$$

where r_i and $\dot{r}_i$ for $i = 1, 2, 3$ are the components of the position $\mathbf{r}$ and velocity $\dot{\mathbf{r}}$, respectively.

Table C.1: Summary of guidance schemes in normal cartesian coordinates

	Target Orbital Elements						**Thrust Control Angles**	
	a	**e**	**i**	$\boldsymbol{\omega}$	$\boldsymbol{\Omega}$	$\boldsymbol{\beta}$	$\boldsymbol{\delta}$	**specification**
1	a^*	free	free	free	free	$\sin^{-1}(K_\alpha e_\alpha)$	–	$e_\alpha = \alpha - \alpha^*$
2	a^*	e^*	free	free	free	$\sin^{-1}(K_\alpha e_\alpha)$	$\cos^{-1}\{-\text{sign}\,[(e-e^*)S_e]\}$	S_e in Eq. (C.5)
3	a^*	0	0	n/a	n/a	$\sin^{-1}(K_\alpha e_\alpha)$	$\tan^{-1}\left(\frac{\mathbf{q}_i\cdot\hat{\mathbf{h}}}{\mathbf{q}_i\cdot\hat{\mathbf{p}}}\right)$	$\mathbf{q}_i$ in Eq. (C.6)
4	a^*	e^*	i^*	free	Ω^*	$\sin^{-1}(K_\alpha e_\alpha)$	$\tan^{-1}\left(\frac{\mathbf{q}_h\cdot\hat{\mathbf{h}}}{\mathbf{q}_h\cdot\hat{\mathbf{p}}}\right)$	$\mathbf{q}_h$ in Eq. (C.7)
5	a^*	e^*	i^*	ω^*	Ω^*	$\sin^{-1}(K_\alpha e_\alpha)$	$\tan^{-1}\left(\frac{\mathbf{q}_o\cdot\hat{\mathbf{h}}}{\mathbf{q}_o\cdot\hat{\mathbf{p}}}\right)$	$\mathbf{q}_o$ in Eq. (C.8)

Appendix D

Technical Obstacles with Lyapunov-Based Guidance for Rendezvous

D.1 Rendezvous Using Cartesian Coordinates

The general rendezvous problem, where the goal is to match both position and velocity components of a moving target, using Lyapunov stability theory can be posed in the following way.

Suppose the target spacecraft is governed by the equations of motion in Eq. (3.1) with $\mathbf{f} = \mathbf{0}$, i.e. it is in an unperturbed orbit. The target at some time t has the following position $\mathbf{r}^*(t)$ and velocity $\mathbf{v}^*(t)$ components. The chaser is also governed by Eq. (3.1) and has a state $\mathbf{r}(t)$ and $\mathbf{v}(t)$. The goal is to design $\mathbf{f}$ such that both the position and velocity errors between chaser and target go to zero as time goes to infinity. Defining the following error functions

$$\mathbf{e}_r = \mathbf{r} - \mathbf{r}^* \tag{D.1}$$

$$\mathbf{e}_v = \mathbf{v} - \mathbf{v}^* \tag{D.2}$$

we design the following Lyapunov-candidate function

$$V(\mathbf{e}_r, \mathbf{e}_v) = \frac{1}{2} K_1 \mathbf{e}_r^T \mathbf{e}_r + \frac{1}{2} K_2 \mathbf{e}_v^T \mathbf{e}_v \tag{D.3}$$

where $K_1 > 0$ and $K_2 > 0$ are gains to be designed by the user. The function V is quadratic and minimum at our desired state.

The time-derivative of Eq. (D.3) is

$$\begin{aligned} \dot{V}(\mathbf{e}_r, \mathbf{e}_v) &= K_1 \mathbf{e}_r^T \mathbf{e}_v + K_2 \mathbf{e}_v^T \left(\ddot{\mathbf{r}} - \ddot{\mathbf{r}}^* \right) & \text{(D.4)} \\ &= K_1 \mathbf{e}_r^T \mathbf{e}_v + K_2 \mathbf{e}_v^T \left[-\mu \left(\frac{\mathbf{r}}{r^3} - \frac{\mathbf{r}^*}{r^{*^3}} \right) + \mathbf{f} \right] & \text{(D.5)} \end{aligned}$$

If we had no restriction on the magnitude of $\mathbf{f}$, choosing

$$\mathbf{f} = \mu \left(\frac{\mathbf{r}}{r^3} - \frac{\mathbf{r}^*}{r^{*^3}} \right) - \frac{K_1}{K_2} \mathbf{e}_r - K_3 \mathbf{e}_v \tag{D.6}$$

would result in

$$\dot{V} = -K_2 K_3 \mathbf{e}_v^T \mathbf{e}_v \leq 0 \tag{D.7}$$

The problem is that we have to cancel out two terms that do not depend on the thrust magnitude, and therefore, we have no control over the magnitude of $\mathbf{f}$. In cartesian coordinates, it is nonviable to design feedback control algorithm to ensure convergence to a target with a fixed thrust magnitude.

D.2 Rendezvous Design in Fictitious Time Using KS Variables: Equivalent to an Orbit Transfer

Since it is impossible to design a guidance scheme using a Lyapunov approach in cartesian coordinates, we will now attempt to solve the problem using the KS variables in time τ, which is the fictitious time related to the chaser spacecraft. The notation used in this section is coincident with the notation in Chapter 3.

No restrictions are placed on the initial separation between the chaser and the target. We define the candidate Lyapunov function to minimize the error difference in both position and velocity between the chaser and the target

$$Z(\tau) = \frac{\mu}{2}\alpha^* \mathbf{e}_{\mathbf{u}}^T \mathbf{e}_{\mathbf{u}} + 2\mathbf{e}_{\mathbf{u}'}^T \mathbf{e}_{\mathbf{u}'} \tag{D.8}$$

where the target parameter $\alpha^* = 1/a^*$, and the errors in position, velocity, and acceleration are defined as

$$\begin{aligned} \mathbf{e}_{\mathbf{u}}(\tau) &= \mathbf{u}(\tau) - \mathbf{u}^*(\tau) \\ \mathbf{e}_{\mathbf{u}'}(\tau) &= \mathbf{u}'(\tau) - \mathbf{u}'^*(\tau) \\ \mathbf{e}_{\mathbf{u}''}(\tau) &= \mathbf{u}''(\tau) - \mathbf{u}''^*(\tau) \end{aligned} \tag{D.9}$$

where the target's state is $\mathbf{u}^* = [u_1^* \; u_2^* \; u_3^* \; u_4^*]^T$ and $\mathbf{u}'^* = [u_1'^* \; u_2'^* \; u_3'^* \; u_4'^*]^T$ and it's equation of motion $\mathbf{u}''^*$ is governed by the unperturbed equations of motion in Eq. (3.14). Note Eq. (D.8) is in fact a measure of the total energy for the harmonic oscillator describing the target's trajectory expressed in KS variables.

Note that the quadratic function in Eq. (D.8), minimizes the error between the position and velocity coordinates of the chaser and spacecraft in time τ. However, for the same τ of the chaser and target, corresponds to different values of real time t for each spacecraft, since the time t and τ are related by the position magnitude r of each spacecraft.

$$\frac{dt}{d\tau} = r \tag{D.10}$$

$$\frac{dt^*}{d\tau} = r^* \tag{D.11}$$

Therefore, it is clear to see that what is considered a rendezvous in time τ does not correspond to a rendezvous in real time t. In fact, it corresponds to the chaser getting on the same orbit as the target. So a *rendezvous in time τ corresponds to an orbit transfer in time t.*

The time derivative (in τ coordinates) of Z is

$$\begin{aligned} Z' &= \mu\alpha^* \mathbf{e}_{\mathbf{u}}^T \mathbf{e}_{\mathbf{u}'} + 4\mathbf{e}_{\mathbf{u}'}^T \mathbf{e}_{\mathbf{u}''} \\ &= \mu\alpha^* \mathbf{e}_{\mathbf{u}}^T \mathbf{e}_{\mathbf{u}'} + 4\mathbf{e}_{\mathbf{u}'}^T \left[-\frac{\mu}{4}\alpha\mathbf{u} + \frac{1}{2}r\mathcal{L}(\mathbf{u})^T\mathbf{F} + \frac{\mu}{4}\alpha^*\mathbf{u}^* \right] + \frac{\mu}{4}(\alpha^* - \alpha^*)\mathbf{u} \\ &= \mu\alpha^* \mathbf{e}_{\mathbf{u}}^T \mathbf{e}_{\mathbf{u}'} + 4\mathbf{e}_{\mathbf{u}'}^T \left[-\frac{\mu}{4}\alpha^*\mathbf{e}_{\mathbf{u}} - \frac{\mu}{4}e_\alpha\mathbf{u} + \frac{1}{2}r\mathcal{L}(\mathbf{u})^T\mathbf{F} \right] \\ &= \mu e_\alpha(\mathbf{e}_{\mathbf{u}'} \cdot \mathbf{u}) + 2r\left[\mathbf{e}_{\mathbf{u}'} \cdot \mathcal{L}(\mathbf{u})^T\mathbf{F}\right] \end{aligned} \tag{D.12}$$

If we assume that the semi-major axis of the chaser has been previously matched to be that of the target (to within some specified tolerance) by using the control $\mathbf{F}$ in Eq. (2.23), $e_\alpha = \alpha - \alpha^* \approx 0$. Choosing this same control law

$\mathbf{F}$ and β in Eq. (3.22), the time derivative of the potential becomes

$$\begin{aligned} Z' &\approx 2r\left[\mathbf{e}_{\mathbf{u}'}\cdot\mathcal{L}(\mathbf{u})^T\mathbf{F}\right] \\ &= 2r\left[\mathcal{L}(\mathbf{u})\mathbf{e}_{\mathbf{u}'}\right]^T\mathbf{F} \\ &= 2r\frac{T}{m}\left[\mathcal{L}(\mathbf{u})(\mathbf{u}'-\mathbf{u}'^*)\right]^T\left[\frac{\mathbf{R}'}{\|\mathbf{R}'\|}\sin\beta+\hat{\mathbf{L}}\cos\beta\cos\delta+\hat{\mathbf{e}}\cos\beta\sin\delta\right] \\ &= 2r\frac{T}{m}\left[\frac{1}{2}\mathbf{R}'-\mathcal{L}(\mathbf{u})\mathbf{u}'^*\right]^T\left[\frac{\mathbf{R}'}{\|\mathbf{R}'\|}\sin\beta+\hat{\mathbf{L}}\cos\beta\cos\delta+\hat{\mathbf{e}}\cos\beta\sin\delta\right] \end{aligned} \tag{D.13}$$

Note that since $e_\alpha \approx 0$, $\sin\beta \approx 0$ and $\cos\beta \approx 1$. Also recall, $\mathbf{R}'\cdot\hat{\mathbf{L}} = \mathbf{0}$ and $\mathbf{R}'\cdot\hat{\mathbf{e}} = \mathbf{0}$. Therefore,

$$Z' = -2r\frac{T}{m}\left[\mathcal{L}(\mathbf{u})\mathbf{u}'^*\right]^T\left[\cos\delta\hat{\mathbf{P}}+\sin\delta\hat{\mathbf{H}}\right] \tag{D.14}$$

We define δ to make $\left[\cos\delta\hat{\mathbf{P}}+\sin\delta\hat{\mathbf{H}}\right]$ in Eq. (D.14) lie in the same direction as $Q_r = \mathcal{L}(\mathbf{u})\mathbf{u}'^*$, which will result in $Z' \leq 0$. Defining

$$\mathbf{Q}_r = \mathcal{L}(\mathbf{u})\mathbf{u}'^* \tag{D.15}$$

the time-derivative of Z' looks equivalent to V_i' in Eq. (3.42), therefore, the exact same theoretical solution follows and δ is designed as

$$\delta = \tan^{-1}\left(\frac{\mathbf{Q}_r\cdot\hat{\mathbf{H}}}{\mathbf{Q}_r\cdot\hat{\mathbf{P}}}\right) \tag{D.16}$$

where $\mathbf{Q}_r$ is defined in Eq. (D.15). This ensures $Z' \leq 0$.

Proposition D.2.1. ***Targeting*** $\mathbf{u}^*$ ***and*** $\mathbf{u}'^*$ ***in time*** $\tau \rightarrow$ ***Orbit transfer in time*** t***:*** *Let a spacecraft with a constant available thrust T and initial mass m_0 be on any closed orbit. All solutions governed by the force model*

in Eq. (3.12) with thrust vector in Eq. (3.18) and mass varying according to Eq. (3.16), converge to an orbit with prescribed semi-major axis a^*, eccentricity e^*, inclination i^*, right ascension of the ascending node Ω^*, and argument of periapsis ω^* when the control angles β and δ are chosen as in Eq. (3.22) and Eq. (3.70), respectively, and $\mathbf{Q}_z$ is defined in Eq. (D.15).

Proof. The proof follows equivalently to the proof in Proposition 3.4.1. □

The algorithm proposed in Proposition D.2.1 performs an orbit transfer to any general closed orbit. Therefore, it has the same outcome as the orbit transfer algorithm derived in Chapter 3, Proposition 3.4.3. However, it is less optimal in terms of both time and fuel, since in the algorithm in this appendix targets right elements, four components of target position $\mathbf{u}^*$ and four components of target velocity $\mathbf{u}'^*$. On the other hand, the algorithm in Chapter 3 only targets five elements, and still performs the same task.

D.3 Rendezvous Design in Real Time Using KS Variables

Since the algorithm in the previous section only allows for an orbit transfer, and not a full rendezvous, we now look at the possibility of designing a slightly different candidate function, in which the independent variable is

now real time t.

$$V(t) = \frac{\mu}{2}\alpha^* \mathbf{e}_{\mathbf{u}}^T(t)\mathbf{e}_{\mathbf{u}}(t) + 2\mathbf{e}_{\mathbf{u}'}^T(t)\mathbf{e}_{\mathbf{u}'}(t) \tag{D.17}$$

where the errors in position, velocity, and acceleration are defined as

$$\begin{aligned}
\mathbf{e}_{\mathbf{u}}(t) &= \mathbf{u}(t) - \mathbf{u}^*(t) = \mathbf{u}(\tau) - \mathbf{u}^*(\tau^*) \\
\mathbf{e}_{\mathbf{u}'}(t) &= \mathbf{u}'(t) - \mathbf{u}'^*(t) = \mathbf{u}'(\tau) - \mathbf{u}'^*(\tau^*) \\
\mathbf{e}_{\mathbf{u}''}(t) &= \mathbf{u}''(t) - \mathbf{u}''^*(t) = \mathbf{u}''(\tau) - \mathbf{u}''^*(\tau^*)
\end{aligned} \tag{D.18}$$

where time t and the fictitious time for the chaser τ and target τ^* are related with the following

$$\frac{d\tau}{dt} = \frac{1}{r} \tag{D.19}$$

$$\frac{d\tau^*}{dt} = \frac{1}{r^*} \tag{D.20}$$

The time-derivative

$$\begin{aligned}
\frac{dV}{dt} &= \mu\alpha^* \mathbf{e}_{\mathbf{u}}^T(t)\left(\frac{d\mathbf{u}}{dt} - \frac{d\mathbf{u}^*}{dt}\right) + 4\mathbf{e}_{\mathbf{u}'}^T(t)\left(\frac{d\mathbf{u}'}{dt} - \frac{d\mathbf{u}^{*'}}{dt}\right) \\
&= \mu\alpha^* \left(\mathbf{u} - \mathbf{u}^*\right)^T \left(\frac{d\mathbf{u}}{d\tau}\frac{d\tau}{dt} - \frac{d\mathbf{u}^*}{d\tau^*}\frac{d\tau^*}{dt}\right) + 4\left(\mathbf{u}' - \mathbf{u}'^*\right)^T \left(\frac{d\mathbf{u}'}{d\tau}\frac{d\tau}{dt} - \frac{d\mathbf{u}^{*'}}{d\tau^*}\frac{d\tau^*}{dt}\right) \\
&= \mu\alpha^* \left(\mathbf{u} - \mathbf{u}^*\right)^T \left(\frac{1}{r}\mathbf{u}' - \frac{1}{r^*}\mathbf{u}'^*\right) + 4\left(\mathbf{u}' - \mathbf{u}'^*\right)^T \left(\frac{1}{r}\mathbf{u}'' - \frac{1}{r^*}\mathbf{u}''^*\right) \\
&= \frac{1}{rr^*}\left[\mu\alpha^* \left(\mathbf{u} - \mathbf{u}^*\right)^T \left(r^*\mathbf{u}' - r\mathbf{u}'^*\right) + 4\left(\mathbf{u}' - \mathbf{u}'^*\right)^T \left(r^*\mathbf{u}'' - r\mathbf{u}''^*\right)\right]
\end{aligned}$$

Substituting for the acceleration of the chaser $\mathbf{u}''$ and target $\mathbf{u}''^*$,

$$\begin{aligned}
\frac{dV}{dt} = & \frac{1}{rr^*}\Big[\mu\alpha^*\left(\mathbf{u}-\mathbf{u}^*\right)^T\left(r^*\mathbf{u}'-r\mathbf{u}'^*\right) \\
& +4\left(\mathbf{u}'-\mathbf{u}'^*\right)^T\left(-\frac{\mu\alpha}{4}r^*\mathbf{u}+\frac{1}{2}rr^*\mathcal{L}^T(\mathbf{u})\mathbf{F}+\frac{\mu}{\alpha^*}4r\mathbf{u}^*\right)\Big] \\
= & \frac{1}{rr^*}\Big[\mu\alpha^*\left(\mathbf{u}-\mathbf{u}^*\right)^T\left(r^*\mathbf{u}'-r\mathbf{u}'^*\right)+2rr^*\left(\mathbf{u}'-\mathbf{u}'^*\right)^T\mathcal{L}^T(\mathbf{u})\mathbf{F}\ldots \\
& \qquad \cdots+\mu\left(\mathbf{u}'-\mathbf{u}'^*\right)^T\left(-\alpha r^*\mathbf{u}+\alpha^* r\mathbf{u}^*+r^*(\alpha^*-\alpha^*)\mathbf{u}\right)\Big] \\
= & \frac{1}{rr^*}\Big[\mu\alpha^*\left\{\left(\mathbf{u}-\mathbf{u}^*\right)^T\left(r^*\mathbf{u}'-r\mathbf{u}'^*\right)-\left(\mathbf{u}'-\mathbf{u}'^*\right)^T\left(r^*\mathbf{u}-r\mathbf{u}^*\right)\right\}\ldots \\
& \qquad \cdots+2rr^*\left(\mathbf{u}'-\mathbf{u}'^*\right)^T\mathcal{L}^T(\mathbf{u})\mathbf{F}-\mu r^*(\alpha-\alpha^*)\left(\mathbf{u}'-\mathbf{u}^{*\prime}\right)^T\mathbf{u}\Big] \\
= & \frac{\mu}{r}\left[\frac{\alpha^*}{r^*}\left(r-r^*\right)\left(\mathbf{u}^*\cdot\mathbf{u}'-\mathbf{u}\cdot\mathbf{u}'^*\right)-(\alpha-\alpha^*)\left(\mathbf{u}'-\mathbf{u}^{*\prime}\right)^T\mathbf{u}\right] \\
& +2\left(\mathbf{u}'-\mathbf{u}'^*\right)^T\mathcal{L}^T(\mathbf{u})\mathbf{F}
\end{aligned} \tag{D.21}$$

Recall that we only have freedom to choose the thrust vector $\mathbf{F}$; therefore we have no control over the first terms in Eq. (D.21). However, if $\alpha=\alpha^*$ and $r=r^*$, the time-derivative simplifies to

$$\frac{dV}{dt}=2\left(\mathbf{u}'-\mathbf{u}'^*\right)^T\mathcal{L}^T(\mathbf{u})\mathbf{F} \tag{D.22}$$

Defining the 4-dimensional vector

$$\mathbf{Q}_{rend}=\mathcal{L}(\mathbf{u})\left(\mathbf{u}'-\mathbf{u}'^*\right)^T \tag{D.23}$$

the time-derivative dV/dt looks equivalent to V_i' in Eq. (3.42), with the exception of $\mathbf{Q}_{rend}$ term versus $\mathbf{Q}_i$. Therefore, the exact same theoretical solution follows and δ is designed as

$$\delta=\tan^{-1}\left(\frac{\mathbf{Q}_{rend}\cdot\hat{\mathbf{H}}}{\mathbf{Q}_{rend}\cdot\hat{\mathbf{P}}}\right) \tag{D.24}$$

where $\mathbf{Q}_{rend}$ is in Eq. (D.23). This ensures $dV/dt \leq 0$.

However, note that we have made a fairly big assumption here: $r = r^* \; \forall \; t$, implies that both $\alpha = \alpha^*$ and $e = e^*$, so the chaser and target are in the same circular orbit, but can have different inclinations. The problem needs to be restated as follows:

Suppose a target spacecraft is in a circular orbit with parameters α^*, $e^* = 0$, and any inclination i^*. By transferring the chaser spacecraft to the same target α^* and eccentricity $e^* = 0$ by the guidance scheme in Proposition 3.3.1, can the guidance scheme in Eq. (D.24) be used to rendezvous with a target, by maintaining both $\alpha = \alpha^*$ and $e = e^*$?

As it turns out, after implementation, it was seen that the rendezvous with the proposed guidance scheme is not possible. The target orbit represents an invariant manifold to the system; therefore, the chaser spacecraft reaches the target orbit, but with a phase a difference, therefore stays in the target orbit.

Appendix E

Perturbation Theory (Chapter 4)

Because nonlinear differential equations tend to be fairly complex, exact analytical solutions are generally, not possible to find. In general, we use numerical solution methods to solve the differential equations. In Chapter 4, we explore what is known as *asymptotic methods* to find approximate analytical solutions [31]. The mathematical background on perturbation theory is explained here.

Suppose we are given the differential equation

$$\dot{x} = f(t, x, \varepsilon), \quad x(t_0) = \eta_0 \tag{E.1}$$

where ε is a "small" scalar parameter. Under certain conditions, the equation can have an exact solution $x(t, \varepsilon)$. The goal of an asymptotic method is to obtain an approximate solution $\tilde{x}(t, \varepsilon)$, such that $\tilde{x}(t, \varepsilon) - x(t, \varepsilon)$ is small. In this case we will use a finite Taylor expansion to come up with an approximate solution to our problem at hand.

Of course, the simplest approximation results by setting $\varepsilon = 0$ in

Eq. (E.1) to find the solution to the unperturbed problem $x(t,0)$

$$\dot{x} = (t, x, 0), \quad x(t_0) = \eta_0 \tag{E.2}$$

To obtain a higher order approximation of $x(t,\epsilon)$, we construct a finite Taylor series

$$x(t,\varepsilon) = \sum_{k=0}^{n-1} x_k(t)\varepsilon^k + \varepsilon^n R_x(t,\varepsilon) \tag{E.3}$$

By Taylor's theorem, the smoothness requirement on the initial state $\eta(\varepsilon)$ guarantees the existence of a finite Taylor series for $\eta(\varepsilon)$; that is

$$\eta(\varepsilon) = \sum_{k=0}^{n-1} \eta_k\varepsilon^k + \varepsilon^n R_\eta(\varepsilon) \tag{E.4}$$

Therefore,

$$x_k(t_0) = \eta_k, \quad k = 0, 1, ..., n-1 \tag{E.5}$$

Substituting Eq. (E.3) into Eq. (E.1) yields

$$\begin{aligned} \sum_{k=0}^{n-1} \dot{x}_k(t)\varepsilon^k + \varepsilon^n \dot{R}_x(t,\varepsilon) &= f(t, x(t,\varepsilon), \varepsilon) \equiv h(t,\varepsilon) \\ &= \sum_{k=0}^{n-1} h_k(t)\varepsilon^k + \varepsilon^n R_h(t,\varepsilon) \end{aligned} \tag{E.6}$$

where the coefficients of the Taylor series of $h(t,\varepsilon)$ are functions of the coefficients of the Taylor series of $x(t,\varepsilon)$. Since Eq. (E.6) holds for all sufficiently small ε, it holds as an identity in ε. Therefore, coefficients of like powers of ε must be equal. By matching those coefficients, we can derive the equations that must be satisfied by x_0, x_1, etc.

The coefficients of the Taylor series of $h(t, \varepsilon)$ need to be found. For example, the zeroth-order term $h_0(t)$ is given by

$$h_0(t) = f(t, x_0(t), 0) \tag{E.7}$$

The differential equation of the zeroth term must satisfy (by Eq. (E.6))

$$\dot{x}_0 = f(t, x_0, 0), \quad x_0(t_0) = \eta_0 \tag{E.8}$$

Similarly, the first-order term is

$$\begin{aligned} h_1(t) &= \frac{\partial}{\partial \varepsilon} f(t, x(t, \varepsilon), \varepsilon)\Big|_{\varepsilon=0} \\ &= \frac{\partial f}{\partial x}(t, x_0(t), 0) x_1(t) + \frac{\partial f}{\partial \varepsilon}(t, x_0(t), 0) \end{aligned} \tag{E.9}$$

Matching coefficients of ϵ in Eq. (E.6), $x_1(t)$ must satisfy

$$\dot{x}_1 = \frac{\partial f}{\partial x}(t, x_0(t), 0) x_1 + \frac{\partial f}{\partial \varepsilon}(t, x_0(t), 0), \quad x_1(t_0) = \eta_1 \tag{E.10}$$

Defining

$$A(t) = \frac{\partial f}{\partial x}(t, x_0(t), 0), \quad g_1(t, x_0(t)) = \frac{\partial f}{\partial \varepsilon}(t, x_0(t), 0) \tag{E.11}$$

we can rewrite x_1 as

$$\dot{x}_1 = A(t) x_1 + g_1(t, x_0(t)), \quad x_1(t_0) = \eta_1 \tag{E.12}$$

which is now a linear equation.

The same process can be continued to find the differential equation for x_2, x_3, and so on. In summary the Taylor series coefficients x_0, x_1, ..., x_{n-1}

are obtained by solving the following set of linear differential equations

$$\dot{x}_0 = f(t, x_0, 0), \quad x_0(t_0) = \eta_0 \tag{E.13}$$

$$\dot{x}_k = A(t)x_k + g_k(t, x_0(t), ..., x_{k-1}(t)), \quad x_k(t_0) = \eta_k \tag{E.14}$$

for $k = 1, 2, ..., n-1$, where $A(t)$ is the Jacobian $\partial f/\partial x$ evaluated at $x = x_0(t)$ and $\epsilon = 0$. The term $g_k(t, x_0(t), x_1(t), ..., x_{k-1}(t))$ is a polynomial in $x_1, ..., x_{k-1}$ with coefficients depending continuously on t and $x_0(t)$.

Several examples are given in [31] for a better understanding on how to apply perturbation theory.

Appendix F

Time-Varying Coefficients (Chapter 4)

F.1 Coefficients of the example in Section 4.3.1

The time-varying coefficients of the solution in Eq. (4.44) have been written up to order ε^2 in Section 4.3. To not boggle the reader, we have decided to write the coefficients of ε^3, ε^4, and ε^5 here. The solution is written with the independent variable $t = \tau$.

- Third Order Terms: ε^3

$$\begin{aligned} x_{1_3} &= \frac{1}{786432}\left[-36\left(4t^2+3\right)\cos(t) + 8t\sin(t)\left(-2t^2+18\cos(2t)+51\right)\right. \\ &\qquad \left. +111\cos(3t) - 3\cos(5t)\right] \\ x_{2_3} &= \frac{1}{393216}\left[-4t\cos(t)\left(-2t^2+18\cos(2t)+75\right)\right. \\ &\qquad \left. -3\sin(t)\left(32t^2-34\cos(2t)+\cos(4t)-91\right)\right] \end{aligned}$$

$$
\begin{aligned}
x_{3_3} &= \frac{1}{393216}\left[4t\cos(t)\left(-2t^2+54\cos(2t)-21\right)\right. \\
&\qquad \left.+3\sin(t)\left(16t^2-82\cos(2t)+5\cos(4t)+33\right)\right] \\
x_{4_3} &= \frac{1}{786432}\left[8t\sin(t)\left(-2t^2+54\cos(2t)+63\right)\right. \\
&\qquad \left.-6\cos(t)\left(24t^2-86\cos(2t)+5\cos(4t)+81\right)\right]
\end{aligned}
$$

- Fourth Order Terms: ε^4

$$
\begin{aligned}
x_{1_4} &= \frac{1}{25165824}\left[36\left(25-6t^2\right)\cos(3t)+12t\sin(t)\left(-12t^2+142\cos(2t)\right.\right. \\
&\qquad \left.-5\cos(4t)+231\right)+\left(8t^4-912t^2-873\right)\cos(t)-28\cos(5t) \\
&\qquad \left.+\cos(7t)\right] \\
x_{2_4} &= \frac{1}{25165824}\left[2t\left(8\left(11t^2-261\right)\cos(t)+4t\sin(t)\left(t^2-54\cos(2t)-201\right)\right.\right. \\
&\qquad \left.-423\cos(3t)+15\cos(5t)\right)+2649\sin(t)+822\sin(3t) \\
&\qquad \left.-26\sin(5t)+\sin(7t)\right] \\
x_{3_4} &= \frac{1}{25165824}\left[2t\left(-4t\left(t^2-60\right)\sin(t)+8\left(6-7t^2\right)\cos(t)+324t\sin(3t)\right.\right. \\
&\qquad \left.+1107\cos(3t)-75\cos(5t)\right)+2793\sin(t)-1818\sin(3t) \\
&\qquad \left.+110\sin(5t)-7\sin(7t)\right] \\
x_{4_4} &= \frac{1}{25165824}\left[324\left(5-2t^2\right)\cos(3t)+12t\sin(t)\left(-12t^2+326\cos(2t)-25\cos(4t)\right.\right. \\
&\qquad \left.\left.+279\right)+\left(8t^4-864t^2-1527\right)\cos(t)-100\cos(5t)+7\cos(7t)\right]
\end{aligned}
$$

- Fifth Order Terms: ε^5

$$
\begin{aligned}
x_{1_5} &= \frac{1}{32212254720}\left[24\left(40t^2\left(4t^2-259\right)-11531\right)\cos(t)+8\left(45\left(791-366t^2\right)\cos(3t)\right.\right.\\
&\quad +2t\left(\left(8\left(t^2-355\right)t^2+30210\right)\sin(t)+45\left(467-24t^2\right)\sin(3t)\right.\\
&\quad \left.-925\sin(5t)+35\sin(7t)+375t\cos(5t)\right))-8440\cos(5t)+445\cos(7t)\\
&\quad \left.-21\cos(9t)\right]\\
x_{2_5} &= \frac{1}{32212254720}\left[80t\left(27\left(8t^2-145\right)\cos(3t)+2t\sin(t)\left(28t^2-1518\cos(2t)\right.\right.\right.\\
&\quad \left.+75\cos(4t)-3273\right)+175\cos(5t)-7\cos(7t))-64t\left(2t^4-970t^2\right.\\
&\quad \left.+17235\right)\cos(t)+3(225848\sin(t)+84200\sin(3t)-2360\sin(5t)\\
&\quad \left.+145\sin(7t)-7\sin(9t))\right]\\
x_{3_5} &= \frac{1}{32212254720}\left[80t\left(81\left(115-8t^2\right)\cos(3t)+2t\sin(t)\left(-20t^2+3918\cos(2t)\right.\right.\right.\\
&\quad \left.-375\cos(4t)+2661\right)-775\cos(5t)+49\cos(7t))+32t\left(4t^4-940t^2\right.\\
&\quad \left.-435\right)\cos(t)+760104\sin(t)-518040\sin(3t)+27400\sin(5t)\\
&\quad \left.-2555\sin(7t)+189\sin(9t)\right]\\
x_{4_5} &= \frac{1}{32212254720}\left[360\left(1235-918t^2\right)\cos(3t)+24\left(160t^4-9000t^2-17729\right)\cos(t)\right.\\
&\quad +8\left(270t\left(317-24t^2\right)\sin(3t)+25\left(150t^2-107\right)\cos(5t)+8t\left(2t^4-690t^2\right.\right.\\
&\quad \left.\left.+4665\right)\sin(t)-7250t\sin(5t)+490t\sin(7t))+7(355\cos(7t)-27\cos(9t))\right]
\end{aligned}
$$

F.2 Coefficients for any initial condition on the circle

For any general initial condition on the circle from Eq. (4.43), and as shown by the blue diamonds in Figure 4.1, the analytical approximate solution

has also been found. The results are shown below for order of ε^2 to show that an analytical expression does exists.

- Zeroth Order Terms: ε^0

$$x_{1_0} = \texttt{eta10 Cos[t] - eta20 Sin[t]}$$

$$x_{2_0} = \texttt{eta20 Cos[t] + eta10 Sin[t]}$$

$$x_{3_0} = \texttt{-eta20 Cos[t] - eta10 Sin[t]}$$

$$x_{4_0} = \texttt{eta10 Cos[t] - eta20 Sin[t]}$$

Figure F.1: ε^0 analytical results for any initial location.

- First Order Terms: ε^1

$$x_{1_1} = \frac{\left(\texttt{eta10}^2 + \texttt{eta20}^2\right)\ \texttt{(eta20 t Cos[t] + (-eta20 + eta10 t) Sin[t])}}{4\sqrt{-\texttt{b} + \frac{\texttt{a}}{\texttt{eta10}^2+\texttt{eta20}^2}}}$$

$$x_{2_1} = -\frac{\left(\texttt{eta10}^2 + \texttt{eta20}^2\right)\ \texttt{(eta10 t Cos[t] - (eta10 + eta20 t) Sin[t])}}{4\sqrt{-\texttt{b} + \frac{\texttt{a}}{\texttt{eta10}^2+\texttt{eta20}^2}}}$$

$$x_{3_1} = \frac{\left(\texttt{eta10}^2 + \texttt{eta20}^2\right)\ \texttt{(eta10 t Cos[t] + (eta10 - eta20 t) Sin[t])}}{4\sqrt{-\texttt{b} + \frac{\texttt{a}}{\texttt{eta10}^2+\texttt{eta20}^2}}}$$

$$x_{4_1} = \frac{\left(\texttt{eta10}^2 + \texttt{eta20}^2\right)\ \texttt{(eta20 t Cos[t] + (eta20 + eta10 t) Sin[t])}}{4\sqrt{-\texttt{b} + \frac{\texttt{a}}{\texttt{eta10}^2+\texttt{eta20}^2}}}$$

Figure F.2: ε^1 analytical results for any initial location.

- Second Order Terms: ε^2

$$x_{1_2} = \frac{1}{256\left(a - b\left(\text{eta10}^2 + \text{eta20}^2\right)\right)^2}\left(\text{eta10}^2 + \text{eta20}^2\right)^3$$
$$\left(\left(a\left(-3\,\text{eta10} + 28\,\text{eta20}\,t - 8\,\text{eta10}\,t^2\right) + 2\,b\left(\text{eta10}^2 + \text{eta20}^2\right)\left(\text{eta10} - 8\,\text{eta20}\,t + 4\,\text{eta10}\,t^2\right)\right)\text{Cos}[t] + \text{eta10}\left(3\,a - 2\,b\left(\text{eta10}^2 + \text{eta20}^2\right)\right)\text{Cos}[3\,t] + \left(-2\,b\left(\text{eta10}^2 + \text{eta20}^2\right)\left(-5\,\text{eta20} + 8\,\text{eta10}\,t + 4\,\text{eta20}\,t^2\right) + a\left(-19\,\text{eta20} + 20\,\text{eta10}\,t + 8\,\text{eta20}\,t^2\right)\right)\text{Sin}[t] + \text{eta20}\left(-3\,a + 2\,b\left(\text{eta10}^2 + \text{eta20}^2\right)\right)\text{Sin}[3\,t]\right)$$

$$x_{2_2} = \frac{1}{256\left(a - b\left(\text{eta10}^2 + \text{eta20}^2\right)\right)^2}$$
$$\left(\text{eta10}^2 + \text{eta20}^2\right)^3\left(\left(2\,b\left(\text{eta10}^2 + \text{eta20}^2\right)\left(\text{eta20} + 8\,\text{eta10}\,t + 4\,\text{eta20}\,t^2\right) - a\left(3\,\text{eta20} + 28\,\text{eta10}\,t + 8\,\text{eta20}\,t^2\right)\right)\text{Cos}[t] + \text{eta20}\left(3\,a - 2\,b\left(\text{eta10}^2 + \text{eta20}^2\right)\right)\text{Cos}[3\,t] + \left(a\left(19\,\text{eta10} + 20\,\text{eta20}\,t - 8\,\text{eta10}\,t^2\right) + 2\,b\left(\text{eta10}^2 + \text{eta20}^2\right)\left(-5\,\text{eta10} - 8\,\text{eta20}\,t + 4\,\text{eta10}\,t^2\right)\right)\text{Sin}[t] + \text{eta10}\left(3\,a - 2\,b\left(\text{eta10}^2 + \text{eta20}^2\right)\right)\text{Sin}[3\,t]\right)$$

$$x_{3_2} = \frac{1}{256\left(a - b\left(\text{eta10}^2 + \text{eta20}^2\right)\right)^2}$$
$$\left(\text{eta10}^2 + \text{eta20}^2\right)^3\left(\left(-2\,b\,\text{eta20}\left(\text{eta10}^2 + \text{eta20}^2\right)\left(3 + 4\,t^2\right) + a\left(9\,\text{eta20} + 4\,\text{eta10}\,t + 8\,\text{eta20}\,t^2\right)\right)\text{Cos}[t] + 3\,\text{eta20}\left(-3\,a + 2\,b\left(\text{eta10}^2 + \text{eta20}^2\right)\right)\text{Cos}[3\,t] + \left(-2\,b\,\text{eta10}\left(\text{eta10}^2 + \text{eta20}^2\right)\left(9 + 4\,t^2\right) + a\left(23\,\text{eta10} - 12\,\text{eta20}\,t + 8\,\text{eta10}\,t^2\right)\right)\text{Sin}[t] + 3\,\text{eta10}\left(-3\,a + 2\,b\left(\text{eta10}^2 + \text{eta20}^2\right)\right)\text{Sin}[3\,t]\right)$$

$$x_{4_2} = \frac{1}{256\left(a - b\left(\text{eta10}^2 + \text{eta20}^2\right)\right)^2}$$
$$\left(\text{eta10}^2 + \text{eta20}^2\right)^3\left(\left(2\,b\,\text{eta10}\left(\text{eta10}^2 + \text{eta20}^2\right)\left(3 + 4\,t^2\right) + a\left(4\,\text{eta20}\,t - \text{eta10}\left(9 + 8\,t^2\right)\right)\right)\text{Cos}[t] - 3\,\text{eta10}\left(-3\,a + 2\,b\left(\text{eta10}^2 + \text{eta20}^2\right)\right)\text{Cos}[3\,t] + 2\left(-2\,b\,\text{eta20}\left(\text{eta10}^2 + \text{eta20}^2\right)\left(3 + 2\,t^2\right) + a\left(7\,\text{eta20} + 6\,\text{eta10}\,t + 4\,\text{eta20}\,t^2\right) + \left(-9\,a\,\text{eta20} + 6\,b\,\text{eta20}\left(\text{eta10}^2 + \text{eta20}^2\right)\right)\text{Cos}[2\,t]\right)\text{Sin}[t]\right)$$

Figure F.3: ε^2 analytical results for any initial location.

References

[1] Sverre J. Aarseth. *Gravitational N-Body Simulations*. Cambridge University Press, 2003. pp. 51–55.

[2] M. R. Akella. On low radial thrust spacecraft motion. *The Journal of the Astronautical Sciences*, 48(2–3):149–161, April–Spetember 2000.

[3] M. R. Akella and R. A. Broucke. Anatomy of the constant radial thrust problem. *AIAA Journal of Guidance, Control, and Dynamics*, 25(3):563–570, 2002.

[4] R. R. Bate, D. D. Mueller, and J. E. White. *Fundamentals of Astrodynamics*. Dover Publications, Inc., 1971.

[5] R. H. Battin. *An Introduction to the Mathematics and Methods of Astrodynamics*. AIAA Education Series, 1999. p. 182.

[6] M. M. Berry and L. M. Healy. The generalized sundman transformation for propagation of high-eccentricity elliptical orbits. In AAS, AIAA *Space Flight Mechanics Meeting, AAS 02-109*, San Antonio, Texas, January 2002.

[7] D. G. Bettis and V. Szebehely. Treatment of close approaches in the numerical implementation integration of the gravitational problem of n bodies. *Astrophysics and Space Science*, 14(1), 1971. pp. 133–150.

[8] F. W. Boltz. Orbital motion under continuous radial thrust. *AIAA Journal of Guidance, Control, and Dynamics*, 14(3):667–670, 1991.

[9] F. W. Boltz. Orbital motion under continuous tangential thrust. *AIAA Journal of Guidance, Control, and Dynamics*, 15(6):1503–1507, 1992.

[10] V. R. Bond. A recursive formulation for computing the coefficients of the time-dependent f and g series solutions to the two-body problem. *Journal of Astronomy*, 71(1):7–8, 1966.

[11] B. Bonnard and J. B. Caillau. Riemannian metric of the averaged energy minimization problem in orbital transfer with low thrust. *In Annales de l'Institut Henri Poincare (C) Non Linear Analysis*, 24(3):395–411, 2007.

[12] T. Carter and M. Humi. Fuel-optimal rendezvous near a point in general keplerian orbit. *AIAA Journal of Guidance, Control, and Dynamics*, 10(6):567–573, 1987. DOI: 10.2514/3.20257.

[13] A. Celletti. Basics of regularization theory. In *Chaotic Worlds: From Order to Disorder in Gravitational N-Body Dynamical Systems*, pages 203–230. Springer, 2006.

[14] D. E. Chang, D. F. Chichka, and J. E. Marsden. Lyapunov-based transfer between elliptic keplerian orbits. *Discrete and Continuous Dynamical Systems-Series B*, 2(1):57–67, 2002.

[15] T. N. Edelbaum. Optimum power-limited orbit transfer in strong gravity fields. *AIAA Journal*, 3(5):921–925, 1965.

[16] T. N. Edelbaum. Optimum low-thrust rendezvous and station-keeping. *AIAA Journal of Spacecraft and Rockets*, 40(6):960–965, 2003.

[17] J. A. Englander, B. A. Conway, and T. Williams. Automated interplanetary trajectory planning. In AIAA/AAS *Astrodynamics Specialist Conference, AIAA 2012-4517*, Minneapolis, Minnesota, August 2012.

[18] P. J. Enright and B. A. Conway. Optimal finite-thrust spacecraft trajectories using collocation and nonlinear programming. *AIAA Journal of Guidance, Control, and Dynamics*, 14(5):981–985, 1991. doi: 10.2514/3.20739.

[19] P. Fitzpatrick. *Advanced Calculus*. Thomson Corportation, 2nd edition, 2006.

[20] Y. Gao and C. A. Kluever. Analytic orbital averaging technique for computing tangential-thrust trajectories. *Journal of Guidance, Control, and Dynamics*, 28(6):1320–1323, November–December 2005.

[21] C. E. Garner, M. M. Rayman, G. J. Whiffen, J. R. Brophy, and S. C. Mikes. Ion propulsion: An enabling technology for the dawn mission. In

AIAA/AAS *Space Flight Mechanics Meeting, AAS 13-342*, Kauai, Hawaii, February 2013.

[22] S. Geffroy and R. Epenoy. Optimal low-thrust transfers with constraints – generalization of averaging techniques. *Acta Astronautica*, 41(3):133–149, 1997.

[23] N. A. Hatten. A critical evaluation of modern low-thrust feedback-driven spacecraft control laws. Master's thesis, The University of Texas at Austin, Austin, TX, December 2012.

[24] S. Hernandez and M. R. Akella. Energy conserved planar spacecraft motion with constant thrust acceleration. AIAA *Journal of Guidance, Control, and Dynamics*, 2014. Submitted.

[25] S. Hernandez and M. R. Akella. Lyapunov-based guidance for orbit transfers and rendezvous in levi-civita coordinates. AIAA *Journal of Guidance, Control, and Dynamics*, 37(4):1170–1181, 2014. doi: 10.2514/1.62305.

[26] S. Hernandez and M. R. Akella. Lyapunov-based low-thrust guidance for orbit transfers in ks variables. *Celestial Mechanics and Dynamical Astronomy*, 2014. Submitted.

[27] J. M. Hudson and D. J. Scheeres. Reduction of low thrust continuous controls for trajectory dynamics. *Journal of Guidance, Control, and Dynamics*, 32(3):780–787, 2009.

[28] J. M. Hudson and D. J. Scheeres. Fourier coefficient selection for low-thrust control shaping. *Journal of Guidance, Control and Dynamics*, 36(6):1783–1786, 2013.

[29] M. R. Ilgen. Low thrust otv guidance using lyapunov optimal feedback control techniques. *Advances in the Astronautical Sciences*, 85(2):1527–1545, 1993.

[30] J. A. Kechichian. Optimal low-thrust rendezvous using equinoctial orbital elements. *Acta Astronautica*, 38(1):1–14, 1996.

[31] H. K. Khalil. *Nonlinear Systems*. Prentice Hall, third edition, 2002.

[32] C. A. Kluever. Low-thrust orbit transfer guidance using an inverse dynamics approach. *AIAA Journal of Guidance, Control, and Dynamics*, 18(1):187–189, 1995.

[33] H.S. Ko and D.J. Scheeres. Essential thrust fourier coefficient set of averaged gauss equations for orbital mechanics. *Journal of Guidance, Control and Dynamics*, 2013. In Press.

[34] P. Kustaanheimo and E. Stiefel. Perturbation theory of kepler motion based on spinor regularization. *Journal of Mathematics*, 1965(218):204–219, 1965.

[35] D. F. Lawden. Optimal trajectories for space navigation. *Butter-worths, London*, pages 79–94, 1963.

[36] D. F. Lawden. Optimal transfers between coplanar elliptical orbits. *AIAA Journal of Guidance, Control, and Dynamics*, 15(3):788–791, 1992.

[37] S. Lee, A. E. Petropoulos, and P. von Allmen. Low-thrust orbit transfer optimization with refined q-law and multi-objective genetic algorithm. In AAS, AIAA *Astrodynamics Specialist Conference, AAS 05-393*, Lake Tahoe, California, August 2005.

[38] T. Levi-Civita. Traietoorie singular ed urti nel problema ristretto dei tre corpi. *Ann. Math*, 3, 1904.

[39] I. Lopez and C. R. McInnes. Autonomous rendezvous using artificial potential function guidance. *AIAA Journal of Guidance, Control, and Dynamics*, 18(2):237–241, 1995.

[40] B. J. Naasz. Classical element feedback for spacecraft orbital maneuvers. Master's thesis, Virginia Polytechnic Institute and State University, Blacksburg, Virginia, May 2002.

[41] H. J. Oberle and K. Taubert. Existence and multiple solutions of the minimum-fuel orbit transfer problem. *Journal of Optimization Theory and Applications*, 95(2):243–262, 1997.

[42] C. A. Ocampo. Finite burn maneuver modeling for a generalized spacecraft trajectory design and optimization system. *Astrodynamics, Space Missions, and Chaos, Annals of the New York Academy of Sciences*, 1017(1):210–233, 2004.

[43] C. Park, V. Guibout, and D. J. Scheeres. Solving optimal continuous thrust rendezvous problems with generating functions. *AIAA Journal of Guidance, Control, and Dynamics*, 29(2):321–331, 2006. DOI: 10.2514/1.14580.

[44] D. Pastrone, L. Casalino, and G. Colasurdo. Indirect optimization for round-trip mars trajectories. *Advances in the Astronautical Sciences*, 90(1):85–99, 1995.

[45] E. Pellegrini, R. P. Russell, and V. Vittaldev. F and g taylor series solutions to the stark and kepler problems with sundman transformations. *Celestial Mechanics and Dynamical Astronomy*, 118(4):355–378, april 2014.

[46] Lawrence Perko. *Differential Equations and Dynamical Systems*. Springer, 3rd edition, 2000.

[47] A. E. Petropoulos. Low-thrust orbit transfers using candidate lyapunov functions with a mechanism for coasting. In AIAA/AAS *Astrodynamics Specialist Conference, AIAA 2004-5089*, Providence, Rhode Island, August 2004.

[48] A. E. Petropoulos and J. A. Sims. A review of some exact solutions to the planar equations of motion of a thrusting spacecraft. In *In Proceedings 2nd International Symposium Low Thrust Trajectories*, Toulouse, France, June 2002.

[49] J. E. Prussing and V. Coverstone-Carroll. Constant radial thrust acceleration redux. *AIAA Journal of Guidance, Control, and Dynamics*, 21(3):516–518, 1998.

[50] G. D. Racca and et. al. Smart-1 mission description and development status. *Planetary and Space Science*, 50(14–15), December 2002. pp. 1323–1337.

[51] C. L. Ranieri and C. A. Ocampo. Optimization of roundtrip, time-constrained, finite burn trajectories via an indirect method. *AIAA Journal of Guidance, Control, and Dynamics*, 28(2):306–314, 2005. doi: 10.2514/1.5540.

[52] R. P. Russell. Primer vector theory applied to global low-thrust trade studies. *AIAA Journal of Guidance, Control, and Dynamics*, 30(2):460–472, 2007. DOI: 10.2514/1.22984.

[53] P. Sconzo, A. LeSchack, and R. Tobey. Symbolic computation of f and g series by computer. *The Astronomical Journal*, 70(4):269–270, 1965.

[54] J. Senent and C. A. Ocampo. Low-thrust variable-specific-impulse transfers and guidance to unstable periodic orbits. *AIAA Journal of Guidance, Control, and Dynamics*, 28(2):280–290, 2005. doi: 10.2514/1.6398.

[55] P. Sengupta and S. R. Vadali. Satellite orbit transfer and formation reconfiguration via an attitude control analogy. *AIAA Journal of Guidance, Control, and Dynamics*, 28(6):1200–1209, 2005.

[56] H. Seywald, C. M. Troitmayr, and P. A. Troutman. Fuel-optimal orbital transfers for variable specific impulse power spacecraft. *Advances in the Astronautical Sciences*, 114:347–364, 2003.

[57] E. L. Stiefel and G. Scheifele. *Linear and Regular Celestial Mechanics*. Springer-Verlag, Berlin, 1971.

[58] O. Stryk and R. Bulirsch. Direct and indirect methods for trajectory optimization. *Annals of Operations Reserach*, 37(1):357–373, 1992.

[59] K. F. Sundman. Mémpire sur le problme des trois corps. *Acta Mathematica*, 36(1):105–179, 1913.

[60] B. D. Tapely, B. E. Schutz, and G. H. Born. *Statistical Orbit Determination*. Elsevier Academic Press, 2004. pp. 50–54.

[61] D. Thakur, S. Hernandez, and M. R. Akella. Spacecraft swarm finite-thrust cooperative control for common orbit convergence. In AIAA/AAS *Space Flight Mechanics Meeting*, Santa Fe, New Mexico, January 2014.

[62] D. Thakur, S. Hernandez, and M. R. Akella. Spacecraft swarm finite-thrust cooperative control for common orbit convergence. AIAA *Journal of Guidance, Control, and Dynamics,*, 2014. Accepted for publication.

[63] C. Thomas and H. Mayer. Fuel-optimal rendezvous near a point in general keplerian orbit. *AIAA Journal of Guidance, Control, and Dynamics*, 10(6):567–573, 1987.

[64] J. D. Thorne and C. D. Hall. Minimum-thrust orbit transfers using the kustaanheimo-stiefel transformation. *AIAA Journal of Guidance, Control, and Dynamics*, 20(4):836–838, 1997.

[65] H. S. Tsien. Take-off from satellite orbit. *Journal of the American Rocket Society*, 23(4):233–236, July–August 1953.

[66] S. R. Vadali, R. Nah, E. Braden, and I. L. Johnson. Fuel-optimal planar interplanetary trajectories using low-thrust exhuast-modulated propulsion. *Advances in the Astronautical Sciences*, 102(1):431–441, 1999.

[67] W. E. Wiesel and S. Alfano. Optimal many-revolution orbit transfer. *AIAA Journal of Guidance, Control, and Dynamics*, 8(1):155–157, 1985.

[68] B. Zhou, Z. Lin, and G. Duan. Lyapunov differential equation approach to elliptical orbital rendezvous with constrained controls. *AIAA Journal of Guidance, Control, and Dynamics*, 34(2):345–358, 2011.

Vita

Sonia Hernandez was born and raised in Madrid, Spain. She studied Aerospace Engineering at St. Louis University (in Madrid 03-05 and in St. Louis 05-07), where she received her B.S. Her Master's degree was obtained at the University of Maryland in the same field, where she specialized in cooperative control of unmanned vehicles. She is currently a Ph.D. candidate at The University of Texas at Austin in the Aerospace Engineering department. Her research interests include Lyapunov-based guidance laws for low-thrust problems, as well as trajectory design and optimization for Near-Earth asteroid missions. She has been a Co-op at NASA Goddard and an Amelia Earhart Fellow.

Contact email: *sonia.hernandez@utexas.edu*

This dissertation was typeset with LaTeX[†] by the author.

[†]LaTeX is a document preparation system developed by Leslie Lamport as a special version of Donald Knuth's TeX Program.